UiT
THE ARCTIC UNIVERSITY OF NORWAY

Faculty of Science and Technology
Department of Geology

Heinrich events of the late Pleistocene; evidence from a sediment core west of Jan Mayen. An analogue to present day ice sheet collapse?

William Copeland
Master thesis in Marine Geology and Geophysics (GEO-3900)
May 2017

UNIVERSITY OF TROMSØ

Front page photo credit – (Reuters news agency) A large iceberg drifting past the New Foundland town of Ferryland in April 2017

Abstract

A thorough lithological investigation of deep sea sediment core HH13-100GC has been undertaken, in order to investigate the climate and oceanographic fluctuations of the last glacial epoch. The cause of Heinrich events has remained an enigma ever since the discovery of Heinrich layers in the North Atlantic in the 1980s. Through a combination of XRF and X-ray imagery, geotechnical property investigation, ice rafted debris counts, grain size analysis, foraminiferal counts and isotopic analysis; it is possible to investigate the claims put forward so far. Here we build on others work in combination with data from HH13-100GC in order to resolve some of the questions surrounding the process of Heinrich event initiation and evolution. HH13-100GC offers a comprehensive record of climate fluctuations of the past 130, 000 cal. BP. Not only Heinrich events are represented, but also a very clear record of marine isotope stage 5, including the last interglacial, the Eemian.

Six Heinrich events spanning several thousand years were found within the 130,000 cal. BP record of HH13-100GC. Lithological investigation of ice rafted debris grains, suggests that each Heinrich event has its own IRD signature, meaning differing source regions for each event. The defining sequence of features for every Heinrich event investigated was a warm sub-surface prior to the event, indicated by a prevalence of temperate foraminifera, followed by a collapse in foraminiferal fluxes and a reduction in the efficiency of the Atlantic meridional overturning circulation, as indicated by fining of sortable silt. Sub surface warming has been used as a causative argument for present day ice sheet collapse in both Greenland and Antarctica. The author feels that investigation of Heinrich events is vital in the quest to understand the conditions we may expect from anthropogenically induced warming of the oceans, and subsequent ice sheet collapse in the present day.

Acknowledgements

First thanks go to my supervisor Professor Tine Lander Rasmussen for giving me the opportunity to take part in this research. The preceeding course (Reconstructing Quaternary Climates) was well run and layed a perfect foundation for further study into this field of research. Thanks also to Juho Junttila who was a lifeline for the sortable silt aspect of this paper.

Thanks to the laboratory staff Trine Dahl, Ingvild Hald and Karina Monsen for their patience and helpfulness as I carried out my lab work. Without them it would have been a struggle.

The move to Norway from the UK was difficult, with different standards expected and cultural differences a challenge. However my time at UiT has brought me closer to realising what a great country Norway is, I'm sure to stay and work here in the future. Tusen takk!

Thanks go to my parents for offering all they could to make my time in Norway as good as it could be!

My final thanks go to my good friend May Baker. Through all the ups and downs of the past 2 years she was there with a reassuring aura. Something priceless in what has been a challenging 2 years for both of us.

William Copeland

May 2017

Aims of this study.

- To reconstruct the palaeo-environment of the eastern section of the East Greenland Current based on lithostratigraphic and foraminiferal proxies back to Marine Isotope Stage (MIS) 6. This will include variations in the influence of Atlantic Water inflow into this region during the late Quaternary stadial-interstadial regime.

- Special emphasis will be put on the identification of Heinrich Events from MIS2 through to MIS4 looking at the planktic foraminiferal isotopic proxies, IRD and sortable silt analysis in particular to determine oceanographic change prior, during and post Heinrich events.

- To compare and contrast data obtained in this study to that of studies carried out in adjacent regions, along with climatic proxies provided from the NGRIP ice core.

- To discuss the effect of the changing influence of Atlantic Water on ice sheet stability with regard to Heinrich event modulation, drawing comparisons to the modern day setting of coastal Greenland and in particular the West Antarctic Ice Sheet.

Contents

Continued overleaf.

Contents (continued)

Chapter 1 - Introduction

1.1 Study area location

A deep sea gravity sediment core (HH13-100GC) was taken from west of Jan Mayen (71 00.02 N, 010 55.77 W) on the morning of July 4th 2013 along with CTD (conductivity, temperature and density) deployment (figure 1). The core was taken by the research vessel R/V Helmer Hansen, previously named R/V Jan Mayen with a core length measured at 447cm long taken at a water depth of 1372m. The core location is situated ~70km WNW from Jan Mayens southern tip, a volcanic island which marks the rough boundary between the colder East Greenland Current (EGC) to the east and warmer north flowing Atlantic water to the west. During the winter the island is surrounded by pack ice which retreats west during summer, while glaciers are present on the island all year round (Orheim, 1993).

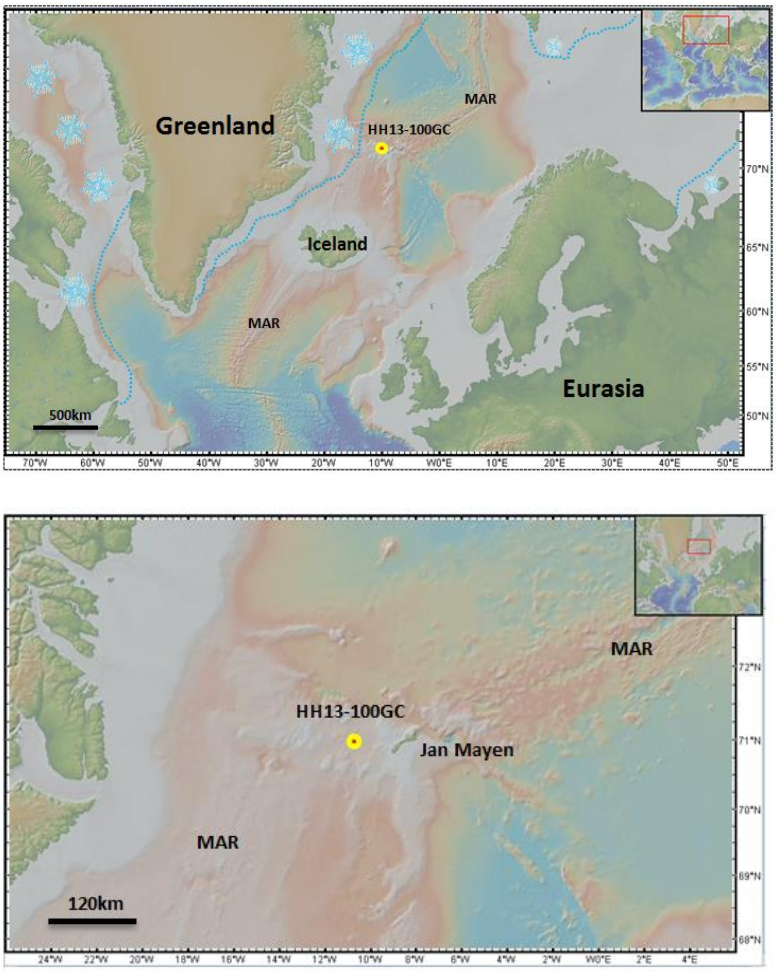

Figure 1 (Maps taken from GeoMapApp)

A north Atlantic view (top) and close up view (bottom) of the core site location. Note the proximity to the small Norwegian volcanic Island Jan Mayen.

Blue dotted lines are included in the top image to represent maximum winter sea ice extent in the present day

1.2 Oceanographical setting and history of study area

The environmental setting of this study is located within the eastern branch of the East Greenland Current (EGC), the main transfer pathway of Arctic waters into the Atlantic Ocean (Figure 2a) (Bond et al, 1997). According to Rudels et al, (2012) the EGC is composed of three main water masses. These are summed up in figure 2b.

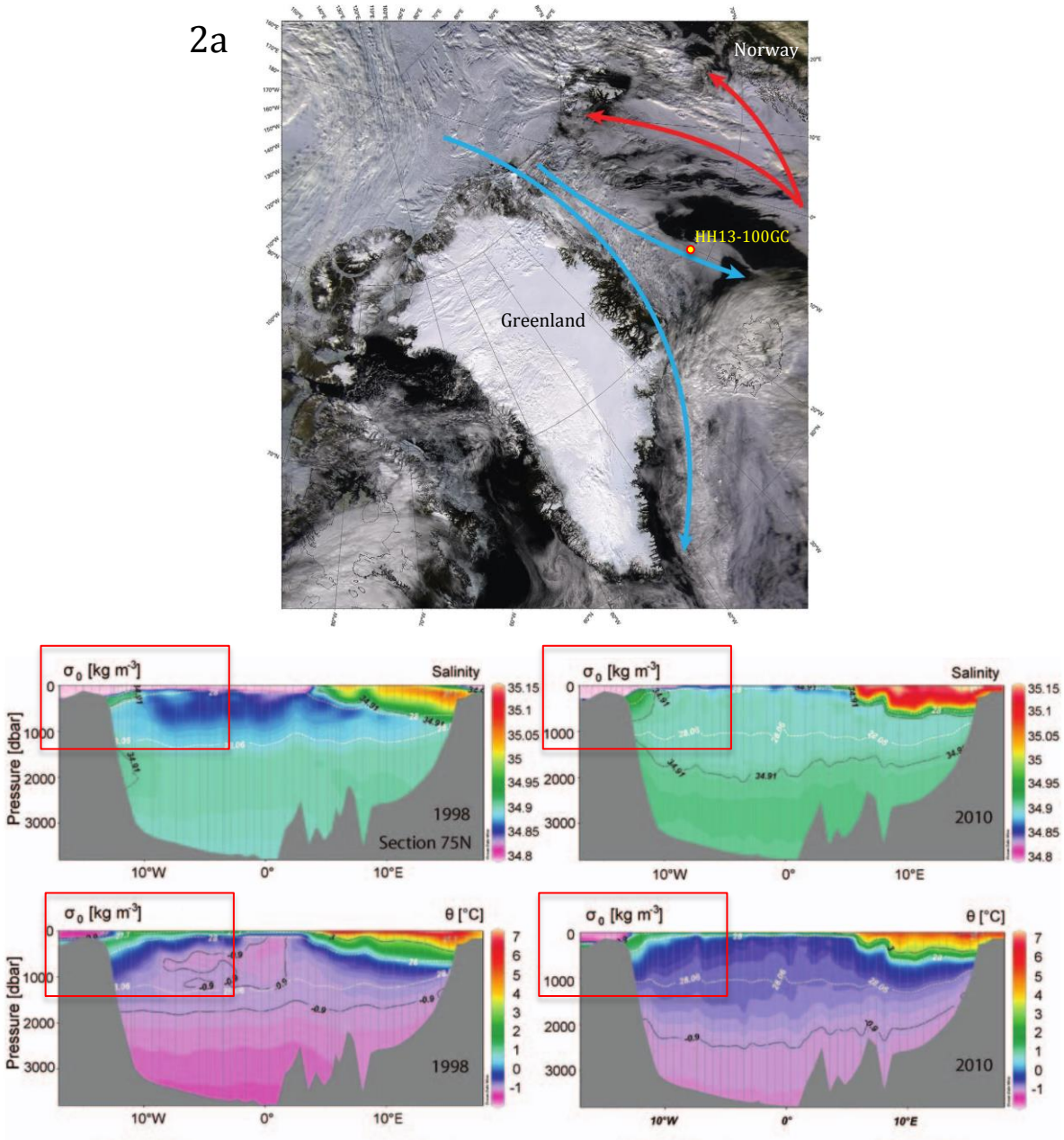

Figures 2a (Modis rapid response image of Greenland, NASA) and **2b** from Rudels et al, 1997. Figure 2a shows a satellite image of Greenland with ocean current directions overlain. The blue arrows represent the East Greenland Current while the red arrows signify the norward flowing Norwegian current. Figure 2b shows cross sections from Greenland to the norwegian continental shelf showing water masses in detail in the years 1998 and 2010. In the west (within the red box) 3 water masses can be observed making up the EGC. The surface polar waters with salinity ~34.8 and temperature at or below 0, intermediate water with salinity ~34.95 and temperature between 1-3^{0}C and finally bottom waters with salinites of ~34.9 and temperatures below 0.

These water masses and their movements have changed considerably over the past millennia. Emiliani (1955) was the first to number major swings in the δ18O from sediment cores around the Caribbean. These shifts came to be known as the Oxygen Isotope Stages (OIS) or Marine Isotope Stages (MIS) (Railsback et al, 2015) are defined by borders of significant shifts in the isotopic record indicating significant climate shifts. Further assignment of sub-stages to the main MIS boundaries have been made since Shackleton, (1969) who divided marine isotope stage 5 into a series of sub-stages. Since this time numerous authors have assigned sub-stages to different sections of the marine oxygen isotope record which had a lack of consistency (Railsback et al, 2015). Therefore a standard MIS and substage record has been developed using a standard δ18O bethic stack record (figure 3) (Lisiecki and Raymo, 2005; Railsback et al, 2015). For means of conciseness the record of this area will discussed only in relation to the last 6 MISs which are believed to be represented in the upcoming results section.

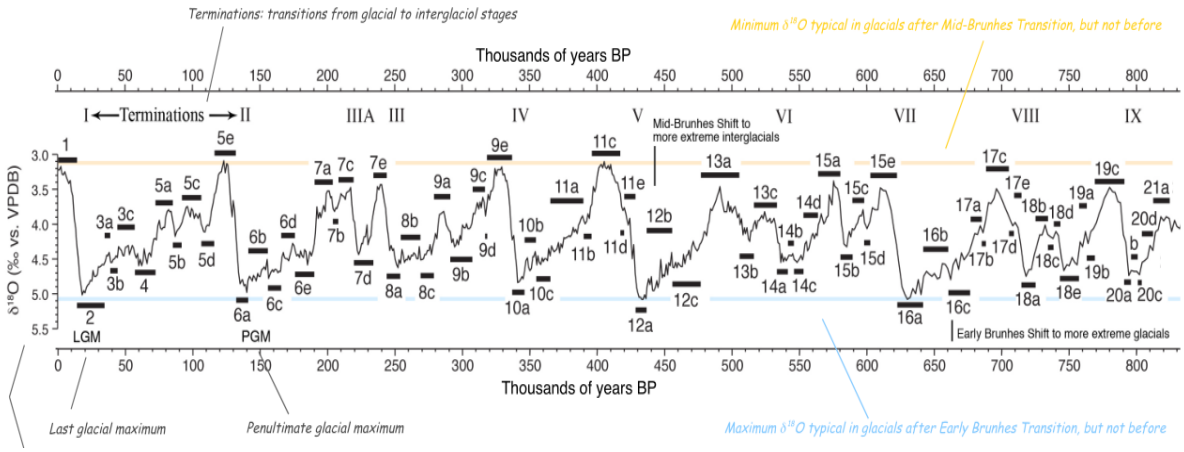

Figure 3 – (From Railsback et al, 2015) Here is presented the benthic stack of Lisiecki and Raymo (2005) overlain with substages defined by Railsback et al (2015) In this study we concentrate only on marine isotope stages 6 and younger, but it is clear climate fluctuations have been occuring for millenia, a timeframe out of the contstraints of deep sea sediment cores.

During MIS6 the Saalian glaciation took place (130-188ka) resulting in what Alley et al, (2010) describes as Greenland's most extensive ice period. Work by Funder et al (1998) estimated that at Jameson Land in East Greenland ice during MIS6 was ~1000m thick, an area now ice free. Paleoclimate reconstruction from marine cores off the Spitsbergen coast also show that during MIS 6 ice extent was large with ice out to the shelf edge (Mangerud et al, 1998). There is then a sharp transition at the MIS 5/6 boundary, or more specifically the boundary between MIS6 and sub-stage 5e. During this interglacial episode, orbital forcing as part of the Milakovitch cycling resulted in a greater axial tilt of Earth (Berger, 1978; Toscano et al, 1999). This change in tilt resulted in much stronger insolation at higher latitudes. Further to this, orbital eccentricity was higher and precession was more intense during the boundary time of ~130-126ka (figure 4) (Crucifix and Loutre, 2002). Extensive collapse of the Greenland, Laurentide, Eurasian and Antarctic ice sheets are indicated by a marked sea level rise of 4-5m seen in the positioning of fossil reefs along stable continental margins such as the Florida coastline and western Australia (Muhs, 2002; Kopp et al, 2009). Work by Jansen et al, (2007) modelled a 5 degree Celsius temperature anomaly compared to the present day, while Cuffey and Marshall, (2000) looked at ice core records and modelled a complete melt of the southern ice dome in Greenland. Kopp et al, (2009) argues that 2.5 metres of the sea level rise seen was from the Greenland ice sheet. This would have resulted in a massive and sudden input of meltwater at the MIS 5e/6 boundary to the Fram Strait, which resulted in a large negative $\delta 18O$ spike in the foraminifera record which can be seen in multiple records (e.g. Stein et al, 1996 and Fronval et al, 1996).

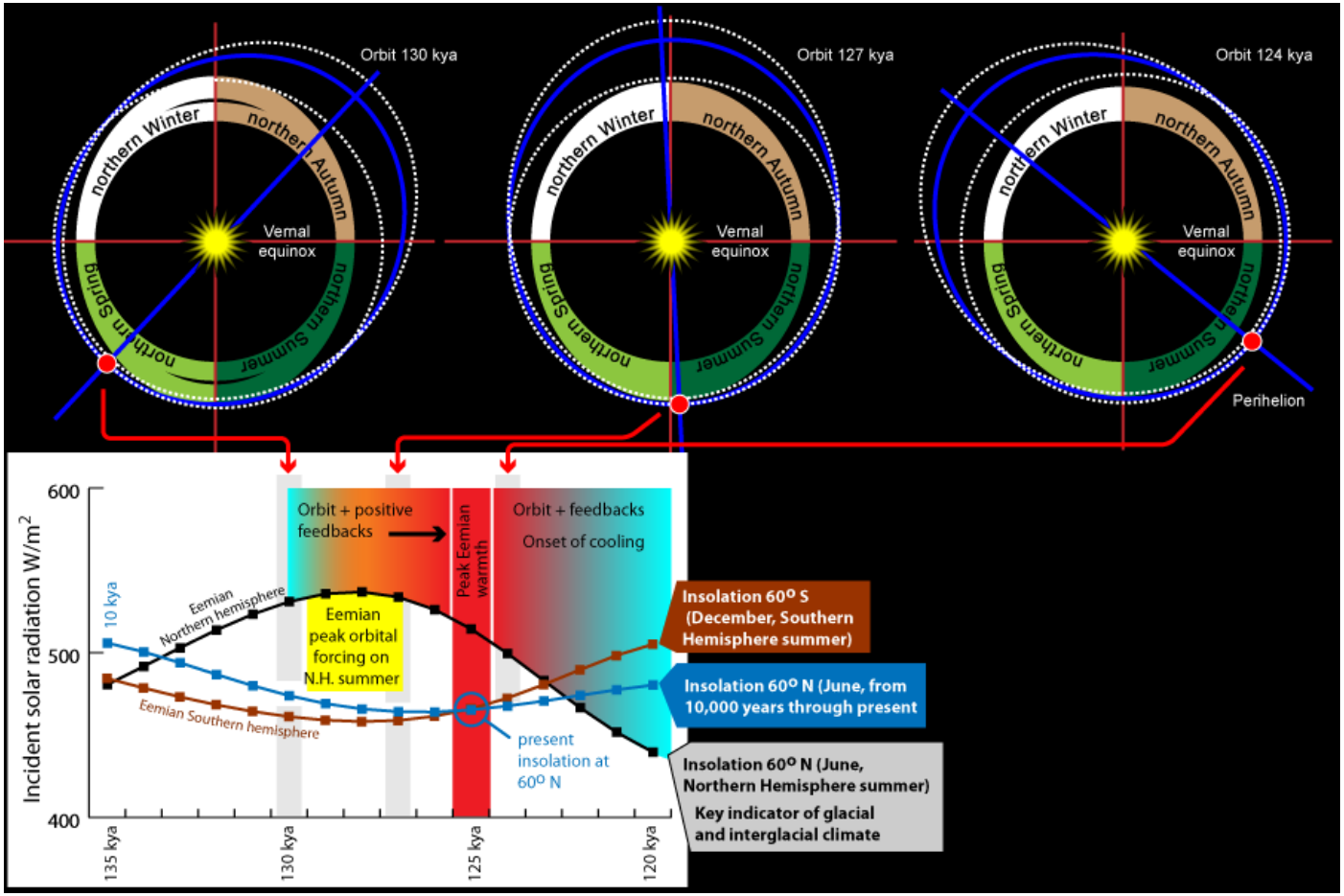

Figure 4 – (From brightstarwildomar.com) Here is presented the orbital forcing mechanisms behind the Eemian warming period. The Eemian occured during peak insolation in the northern hemisphere resulting in a rapid rise in temperatures and assumed mass ice loss post the Saalian glaical of MIS6.

The transition between substage 5e and 5d is marked by an average increase in $\delta^{18}O$ by an order of ~1.5‰ which is consistent with a change to colder conditions (Stoner et al, 1995). From this point until the present day, temperature minima are recorded at MIS substage 5b, 5d, MIS 4 and MIS 2, while maxima are recorded in MIS substage 5a, 5c and MIS 3 (figure 5) (Alley et al, 2010). Within this general trend there are also much faster changes in temperature recorded in both the marine and ice record. Rapid temperature increases (Dansgaard-Oeschger events) and rapid cooling events (Heinrich events) are dispersed throughout the period from MIS 4 through into MIS2 and are purported to be linked to changes in the behaviour of the Atlantic Meridional Overturning Circulation (AMOC) (Alley et al, 2007). An increase in wintertime ice during colder periods affecting deep water formation in the far North Atlantic is one hypothesis for a decrease in strength of the world conveyor belt circulatory system (Denton et al, 2005).

During MIS 2, more well-dated climate shifts occurred in response to a variety of factors including meltwater outbursts from the Laurentide ice sheet to volcanic activity in response to isostatic uplift (Gornitz, 2012; Praetorius et al, 2016). These events include the Bølling-Allerød (BA) warm period of 14.7Ka-12.7ka, the sudden cooling event named the Younger Dryas peaking ~12.8ka and finally a small cooling event at 8ka attributed to a ice sheet outburst event (Alley and Ágústsdóttir, 2005; Andrews and Denhill, 2004; Van der Plicht et al, 2004).

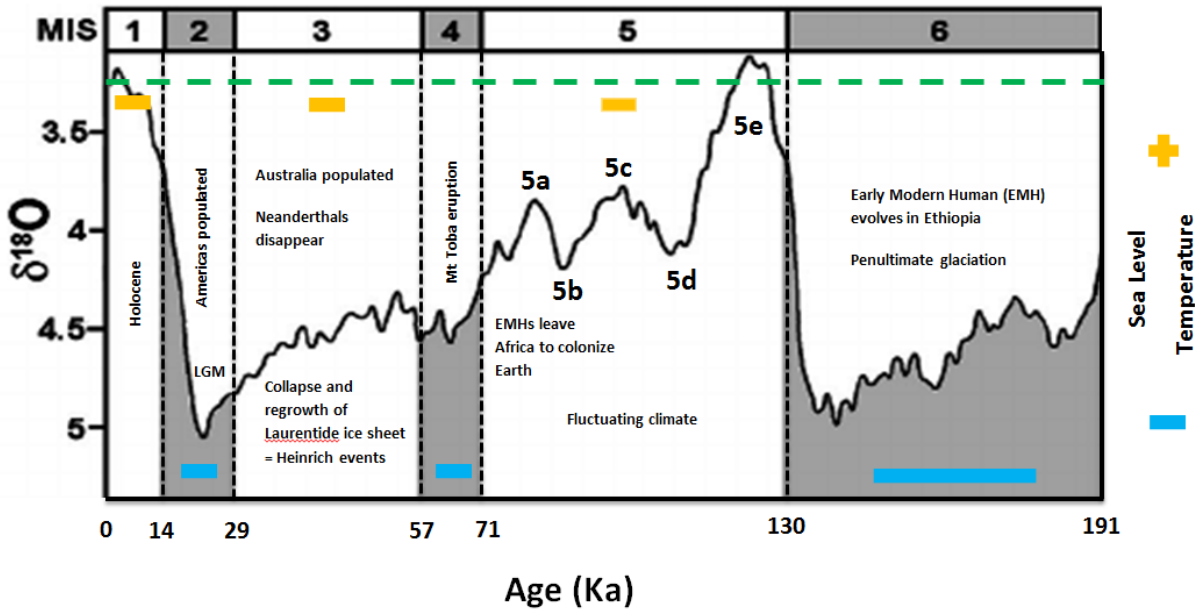

Figure 5 – Taken and adapted from Lopes et al, 2014. Marine isotope stages are defined along with the substages of MIS6. To put into context the timescales involved, human evolutionary events have been included from (Hirst, 2017).

1.3 Heinrich Events

The link between 6 or more layers of anomalously lithic rich sediment in the North Atlantic and past climatic change were first noted by Heinrich et al. (1988). Since that time, numerous studies have built upon an ever growing database of marine sediment records in the north Atlantic region (Bond et al, 1993). Massive wasting events from the Laurentide ice sheet and the adjoining Greenland ice sheet are said to have released mass iceberg armadas into the Atlantic and Fram Strait regions respectively (figure 6) (Bond et al, 1993; Bassis et al, 2017). Models developed by Bagniewski et al. (2017) estimate sea level rise of between 4-11m due to input of water into the oceans from the melting ice. While Hemming et al, (2004) notes that there was not just a local effect, these mass influxes of freshwater influenced the thermohaline circulation affecting climate on a global scale (Figure 7).

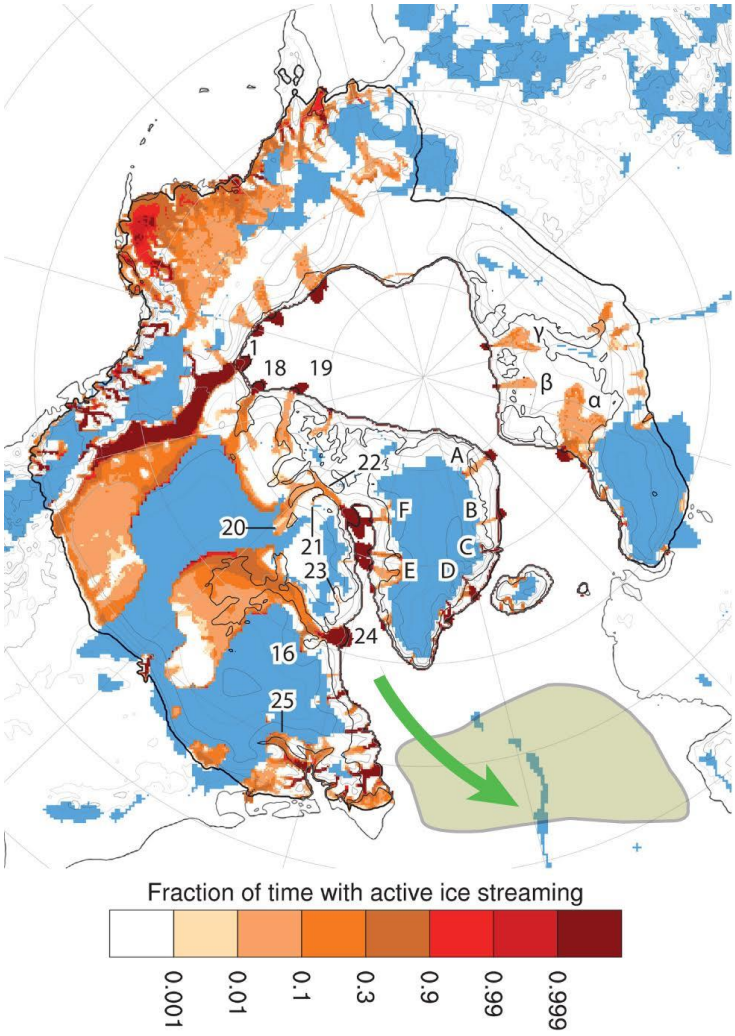

Figure 6 - (From Ziemen et al, 2014) Using an atmospheric – ocean coupling model, active ice streams of the last glacial period were defined. Aa can be seen, ice streaming was very active in the Hudson Bay region leading to Ruddimans, (1977) IRD 'belt' in the North Atlantic. Meanwhile active ice streaming on the Greenland coastlines was also present which if of major interest in this study into the effects of Heinrich events to the north of the IRD belt in the Greenland Sea sector.

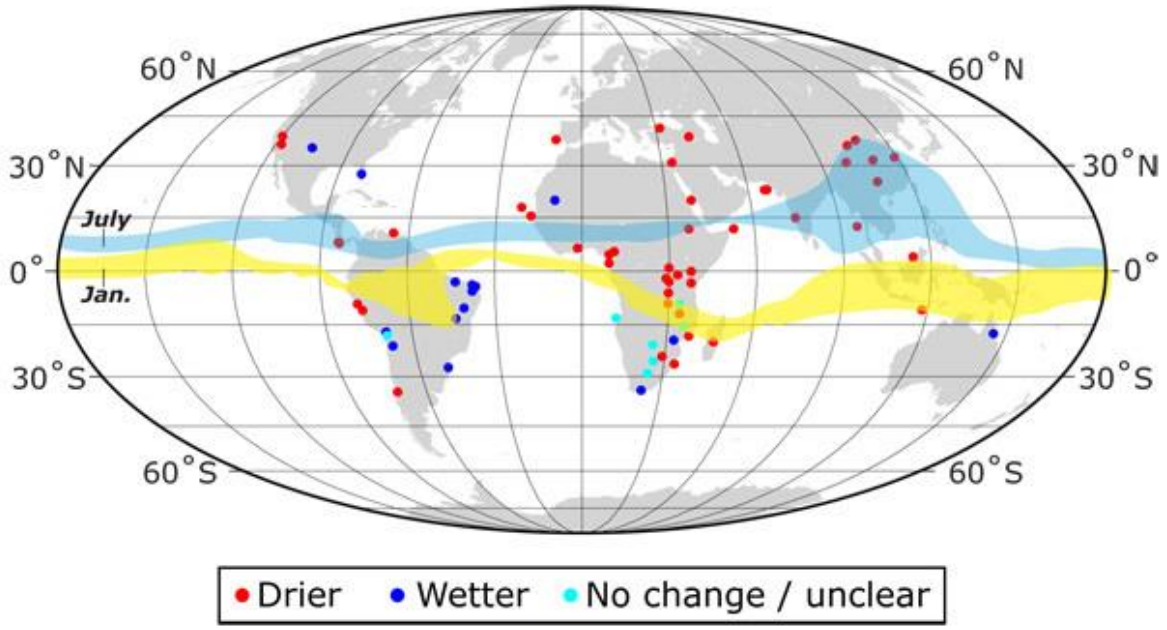

Figure 7 – (From Oppo et al, 2012) A compilation of many studies is presented here from Heinrich event 1. One can see that to the north of the Inter Tropical Convergence Zone (ITCZ) significant indication of dryer climates if evident. However, to the south of the ITCZ a wetter environment is present.

The exact mechanism behind the forcing of such large ice sheet collapse episodes is still heavily debated (Hemming et al, 2004; Barker et al, 2015 and Bassis et al, 2017). Stein et al, (1996) notes that Heinrich events do not follow Milankovitch cycling ruling this out as a factor for ice sheet destabilisation, meanwhile Bassis et al, (2017) notes that Heinrich events occurred during the cold portion of millennial scale Dansgaard-Oeschger cycles. This would suggest a sub ocean surface mechanism for Heinrich events as it rules out surface temperature increase as a causing factor. A binge-purge scenario of ice growth and collapse has also been suggested as a causative factor, where ice builds until critical mass is reached causing high basal slip and therefore rapid acceleration of ice streams until mass reduces again (MacAyeal, 1993). However, these coarse grained layers are not evident in sediments of past glacial episodes, which weakens support for this model (Hemming, 2004).

The GRIP ice core revels that Heinrich events were simultaneous with cooling of air temperatures (Stein et al, 1996), with abrupt warmings following named Dansgaard Oeschger events (Dansgaard et al, 1993; Bond et al, 1993, 99). An ocean forced basal melt system of collapse is a theory gaining reputability, with an influx of warmer Atlantic modified water causing basal melting of ice shelves and marine terminating glaciers resulting in ice sheet collapse (Bassis et al, 2017). This resembles closely the present situation of the marine ice sheet instability worries surrounding the Western Antarctic Ice Sheet, more especially within the Amundsen Sea Embayment (Turner et al, 2017).

Meanwhile in the Antarctic ice cores such as the Byrd core, fluctuations in isotopes show a distinct polarity to those of GRIP (Stenni et al, 2011). This is known as the Bipolar Seesaw theory, where asymmetric temperature fluctuation against poles are created by fluctuations in the production of deep water as a result of changing surface conditions at each pole (Manabe and Stouffer 1988; Broecker, 1998; Pedro et al, 2011; Barker et al, 2009).

1.4 Anthropocene ice loss trends

It is now a generally accepted truth that our current state of climate is significantly altered by the influence of human activity in the form of greenhouse gas release to the atmosphere (Crutzen, 2006). In the period 1993-2010 a sum of ice loss from the Greenland and Antarctic ice sheets was -133 Gt a year equivalent to 0.4mm sea level rise a year (Bamber et al, 2012). Greenland especially has suffered major ice sheet losses with a deficit of 90 to 220 cubic kilometres per year over the period 1996-2006 (Rignot and Kanagaratnam, 2006). Some have related present day conditions to those of marine isotope stage 5, sub-stage 5e, the Eemian (McIntyre and Ruddiman, 1972). However, the effect of insolation on millennia time scales is a very different situation to the exponential increase in greenhouse gasses we see today, regardless of insolation effects (Berger and Loutre, 2002).

Present day conditions are warmer than the glacial period in which Heinrich events occurred, however, the process of subsurface ice shelf warming and collapse of ice sheets is still one of great importance in the present day. The Western Antarctic Ice sheet it most susceptible to inflow of subsurface warm water as it is mostly below sea

level and has landward dipping bed topography (Turner et al, 2017). Meanwhile in Greenland, seaward dipping base topography limits the effect of subsurface melting today, but in the glacial period ice shelves protruding from the Greenland ice sheet would have been significantly at risk to changes in oceanic conditions, especially those affected by isostatic 'push down' (Bassis et al, 2017).

By understanding ice sheet collapse mechanisms and the effect they have had on climates in the past, we can look at today's situation and make predictions on what we can expect in the following decades, centuries and millennia (Bassis et al, 2017). This makes investigation of Heinrich events very relevant in a time of mass wasting from ice sheets, especially in the the Antarctic and modern day Greenland.

1.5 Background to deep sediment cores and their proxies

Marine sediment cores and their proxies within have been used to reconstruct Quaternary palaeoclimate since the Swedish Deep Sea Expedition of the late 1940s (Pfleger, 1948). Sediment cores act as time capsules with proxies such as ice rafted debris, lithostratigraphic analysis, foraminiferal and their assemblages, including calcite isotopic signatures being used to interpret changing environments.

1.5 1, Foraminifera as proxies

In the case of this study, identification of planktonic foraminifera was used in an attempt to look at the changing environment. With elaborate calcite tests these heterotrophic protists are unique in that their eukaryotic unicellular bodies are characterised by a fibrillar structure, a potential buoyancy aid, helping them stay upright in the water column (figure 8) (Kucera, 2007; Hemleben et al, 1989). The faunal record of planktic foraminifera is fairly consistent from the late Cenozoic to the present day making them a good microfossil to use when comparing data on scales of thousands of years, although one must be wary when looking at millennial scale change due to the noise created from genetic divergence influencing what is known as the stationary principle (figure 9) (Kucera, 2007; Kucera and Darling, 2002). The principle states that the environments, properties and relationships between/of organisms must have remained constant through the time of proxy application.

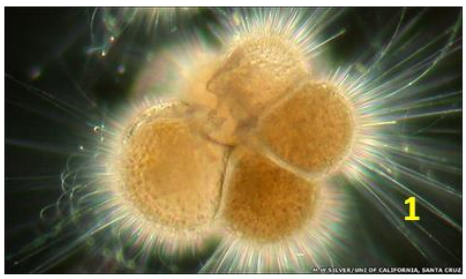

Neogloboquadrina Pachyderma, SEM

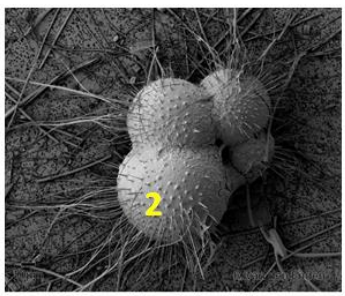

Neogloboquadrina pachyderma, SEM.

Figure 8 – (In order taken, from left to right - scienceblogs.com, taxonomic.add.gov.au) The top left image shows a live *N.pachyderma* with extending axopoda indicated by the number 1. The right hand image shows a recently dead *N.pachyderma* with axopodia shedding from the formainiferal calcite test. Small spines on the surface indicate the fusule pore region of axopodia connection.

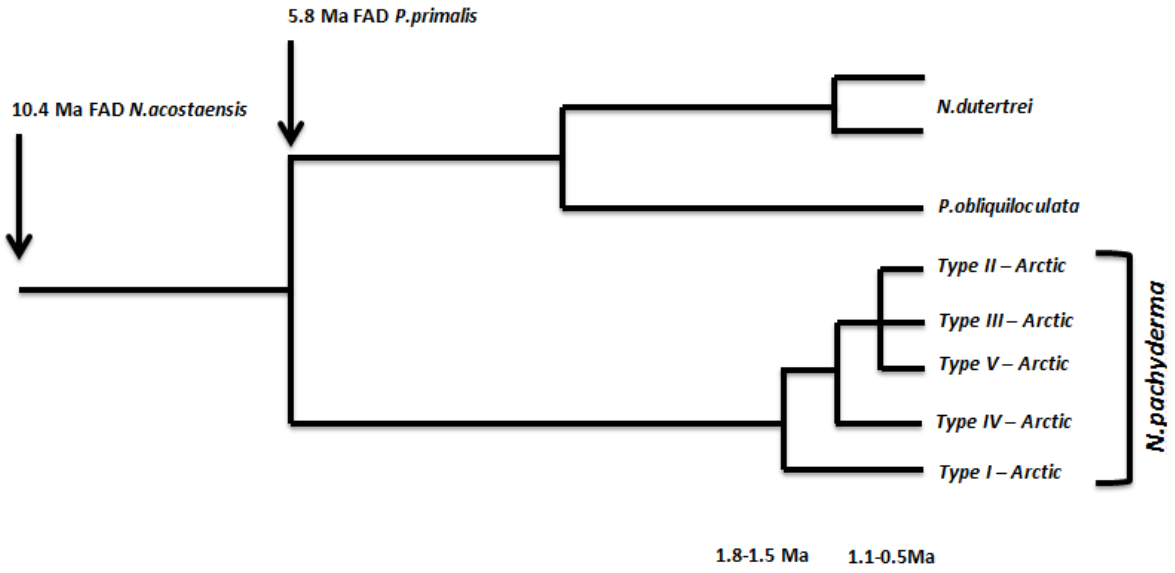

Figure 9 – (Adapted from Kucera, 2007) A taxonomic tree showing the changing genetic makeup of planktic foraminifera leading to the development of the modern day *N.pachyderma*. Pre-1.1-0.5Ma is the upper limit at which this formainifera can be used as a proxy for climate studies as specimens older than this may breach the stationary principle.

Morey et al. (2005) identified sea surface temperatures as the most controlling factor for assemblage composition. Towards the poles, where this study is based, the main polar water planktic foraminifera *Neogloboquadrina pachyderma* (Ehrenberg 1861) is present in abundance whereas in sub-polar regions *Turborotalita quinqueloba* (Natland, 1938) and *Globigerina bulloides* (d'Orbigny, 1826) are more likely found (Figure 10) (Schiebel and Hemleben, 2005). These 'niches' are often defined by the strengths of specific gradients in the oceans

From the calcite tests of these foraminifera, the isotopic compositions can be taken. for example, $\delta^{18}O$ proxies to look at fluctuating climate,$\delta^{13}C$ values to look at ventilation in the water column and ^{14}C radiocarbon AMS dating (Kucera et al, 2007; Henderson, 2002). A combination of species identification and isotopic measurements can give a wealth of resources when deciphering the past climate not just locally but also on a global scale when used in conjunction with multiple studies.

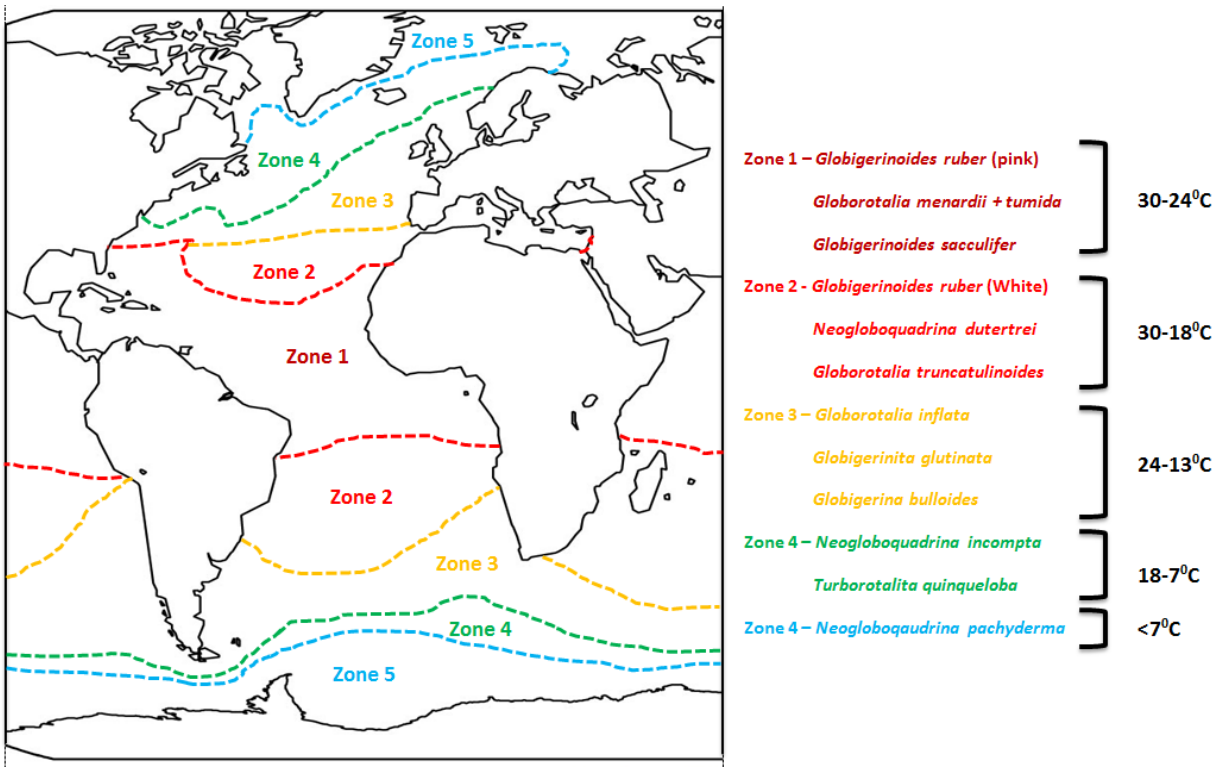

Figure 10 – (Adapted from Kucera, 2007) Names of the most commonly found formainiferal forms with zonation in the Atlantic Ocean with regards to differing temperature environments.

1.5 2, Ice Rafted Debris as a proxy

Along with foraminiferal analysis, ice rafted debris counts and grain size analysis were carried out. Looking at the grain size fraction of sortable silt (10-63μm) we can make assumptions on the strength of bottom current activity (McCave, 2008). This is something of special interest in this study with regard to the fluctuating strength of the East Greenland Current. North Atlantic sediment cores have identifiable thin layers of larger grain sizes and ice rafted debris (IRD), with sand sized particles also considered part of the IRD (Jessen and Rasmussen, 2015). As the name suggests these layers occur due to the melting and subsequent fall out of material from icebergs moving away from ice shelves or marine terminating glaciers and are known as Heinrich events (Heinrich et al, 1989). The source origins of IRD may be interpreted from changes in lithology related to changes in iceberg source over time (Hebbeln et al, 1998).

1.5 3, Magnetic Susceptibility

Magnetic susceptibility has been used since the 1980s to determine past oceanographic changes from sediment cores (Robinson et al, 1995). Sediments contain a variety of magnetic minerals from the highly magnetised ferromagnetic to the less positively magnetised paramagnetic minerals. You then have diamagnetic minerals such as halite or calcite which result in a more negative magnetic susceptibility (Dearing, 1999).
The loop sensor recorders have an oscillator which creates a small magnetic field pulsing with a frequency of ~0.565kHz. When the loop moves over an area of highly magnetised material the frequency will change and this can be recorded giving a magnetic susceptibility record along a whole core section. Work carried out by Rasmussen et al, 2006 found that more positive magnetic susceptibilities were recorded with the grain sizes 63μm to 1mm (coarser material) than with more clay and silt dominated sediment. This is important and has been used by Moros et al, 2002 and Kissel et al, 1997 to look into changes in the deep water formation and bottom current strength near the Iceland Faroe Ridge.

1.5 4, Stable Isotopes as proxies

In order to investigate stable isotope values we run samples through a mass spectrometer. Put simply, the mass spectrometer sorts a charged molecular mix according to mass by using the motions created by initiation of a magnetic or electric field (figure 11). Shackleton and Opdyke, (1973) were the first to demonstrate the relationship between δ18O signals and changes in global ice volume change and secondly the relationship to temperature fluctuations which they built upon from Eptein et al, 1953). It was also Shackleton (1977) who deciphered the relationship between δ13C and palaeo-productivity/ water mass movement and age. The use of these stable isotopes (δ18O and δ13O), both of which can be found within the tests of foraminifera, is essential with regards to reconstruction of paleo-oceanography and paleo-climate.

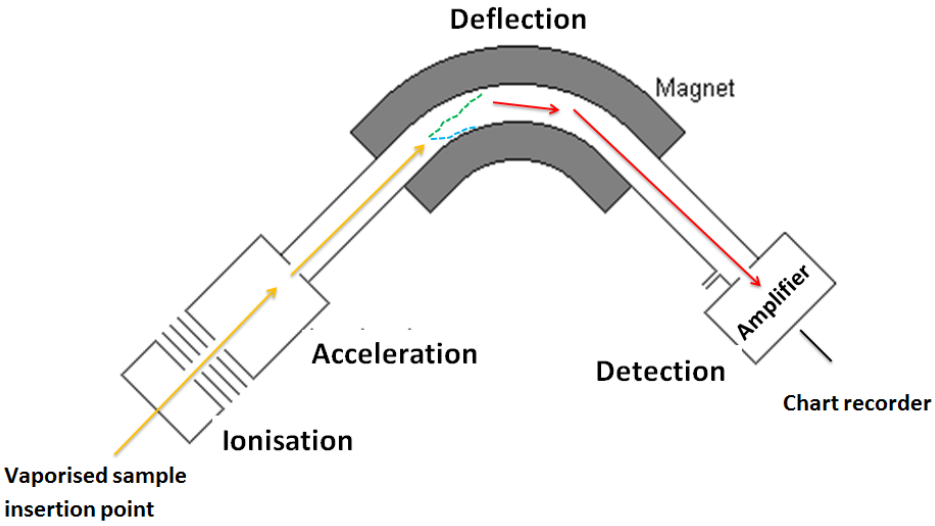

Figure 11 – (Adapted from sustainability.sellafieldsites.com) A basic mass spectrometer diagram showing the basic process of isotope seperation. The dashed blue line represents light isotopes being filtered out while the green line represents the heavier isotopes being filtered. This leaves the red arrows of pre-defined isotopic weight that want to be investigated.

A set of pre-set parameters are present for comparison of δ18O/δ13C against the mean. These are the Vienna Pee Dee Belemnite (PDB) and the Vienna Standard Mean Ocean Water (SMOW) (Coplen, 1996). Delta isotope values are all presented as being part per thousand (‰).

Oxygen consists of the stable isotopes (^{16}O, ^{17}O and ^{18}O). During evaporation of the sea surface the Rayleigh distillation process results in the heavier isotope (^{18}O) being removed from the system (through precipitation) more favourably than its lighter counterpart ^{16}O which can be transported further to the colder polar regions (Figure 12). Therefore higher recorded levels of $\delta^{18}O$ (ratio of $^{16}O/^{18}O$) in foraminifera tests for example, correspond to more storage of $H2^{16}O$ in the ice in the polar regions (Lowe and Walker 2014). This is because the increased storage of $H2^{16}O$ means an enrichment of ^{18}O in the seawater.

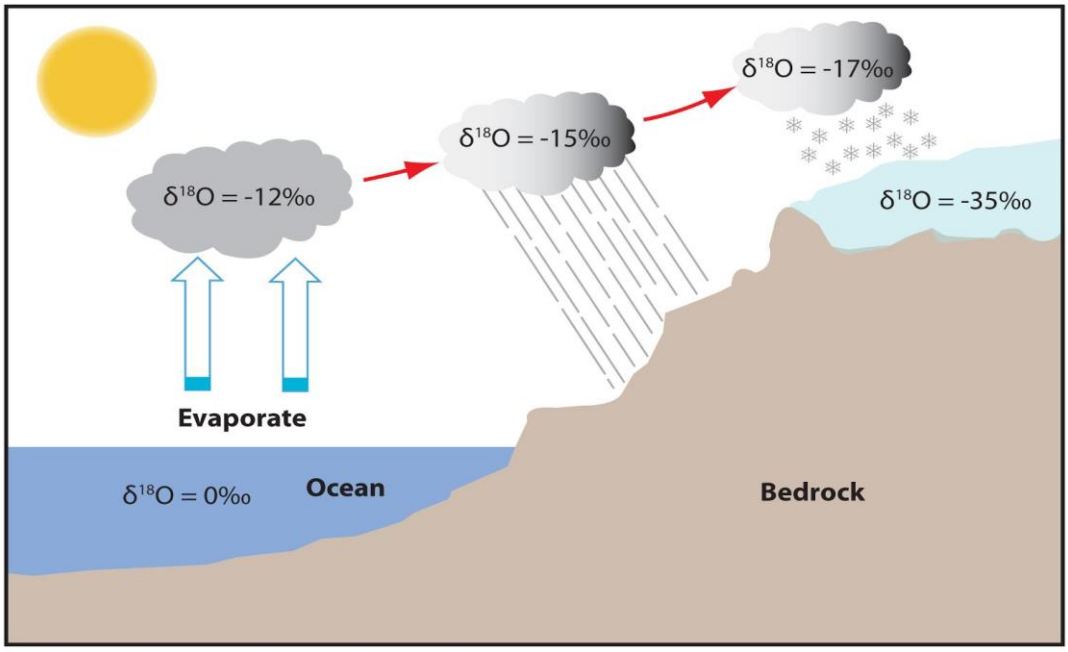

Figure 12 – A schematic diagram to show the Rayleigh fractionation process in action. Preferential evaporation of ^{16}O results in a base line of negative $\delta^{18}O$ in the clouds formed. The $\delta^{18}O$ that has been evaporated is then preferentially removed in precipitation. Northward movement of water vapour to the polar regions following climate cell systems results in severely negative $\delta^{18}O$ values once the vapour reaches the polar regions. This means ice formed from precipitation falling onto the ice will freeze and leave a negative $\delta^{18}O$ signature. During large ice melting events, such as Heinrich events, ^{16}O enriched water flows into the oceans causing the $\delta^{18}O$ signal to be more negative in the oceans, while during glacial episodes large lock up of ^{16}O in the ice results in a higher $\delta^{18}O$ signal in the oceans.

For example, Rozanski et al, (1993) who looked at the isotopic composition of global precipitation found that the δ18o signature for Antarctic rainfall was as low as -57‰ which is an extremely low amount compared to the mean ocean level stated by Katz et al, (2010) of 0‰. We can conclude form this that during stadials ocean water was enriched in ^{18}O and less enriched during interstadials. This is something that can be recorded in the calcium carbonate tests of foraminifera through the equilibrium fractionation process (temperature dependent). Researchers as far back as Epstein et al, (1953) were using $^{18}O/^{16}O$ ratios to calculate palaeo-temperature. While building their tests, foraminifera utilise the minerals in the surrounding seawater which gives us a record of the environmental conditions at the time of calcite building. However, one must take into account the effects of local fluvial input, surface mixing (storms) and the depth at which a foraminifera develops (Katz et al, 2010). This is why a global standard is often chosen to keep global data synchronous e.g. the use of *N.pachyderma* in Polar Regions (Simstitch et al, 2003).

Carbon consists of the stable isotopes ^{12}C and ^{13}C. Preferential usage of ^{12}C in photosynthesis results in euphotic layer enrichment of dissolved ^{13}C and depletion of ^{12}C. Death of organisms such as foraminifera results in sinking of the ^{12}C rich tests to deeper waters where they undergo remineralisation and biogenic decomposition. This results in the release of ^{12}C into the deep ocean. A gradient between the ^{13}C enriched surface and the ^{12}C deep waters is established, upwelling zones of deep water release the carbon in the form of CO2 back into the atmosphere, this is known as the biological pump (Figure 13) (Sigman and Boyle, 2000). Therefore we can conclude that waters with high δ13C values indicate a relatively young, well oxygenated water mass with nutrient poor bottom waters whilst low $\delta^{13}C$ indicates a less oxygenated, higher nutrient baring bottom water mass of 'older' age.

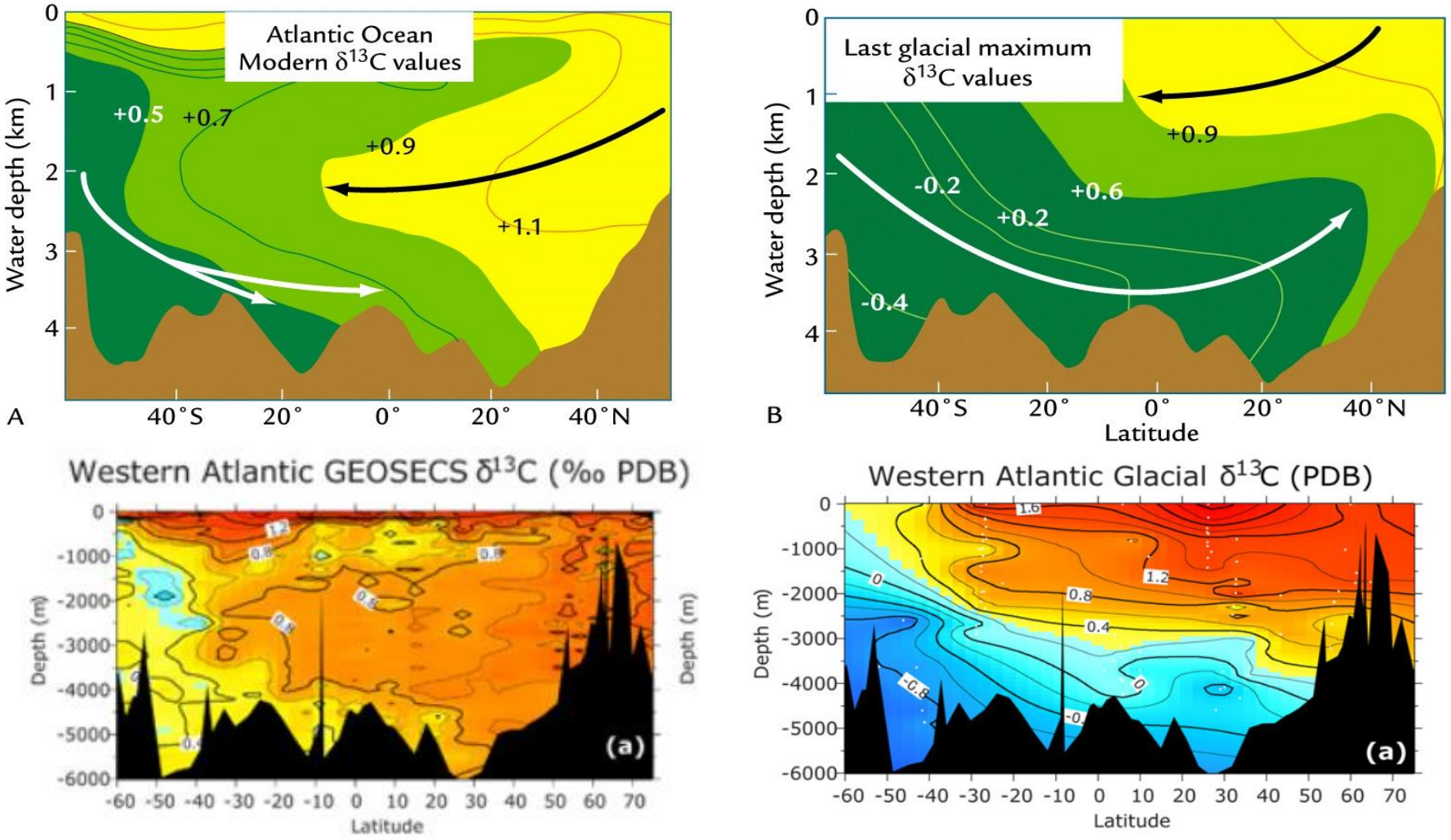

Figure 13 – (Top 2 images taken from Brovkin et al, 2007, bottom 2 images taken from Oppo et al, 2012). The top images show the distribution of $\delta^{13}C$ in a southern to northern hemisphere transect. In the modern day incomplete photosynthesis in the Antarctic results in less input of ^{12}C to the deep water with therefore lower $\delta^{13}C$ surface waters. In the North Atlantic complete photosynthesis results in high ^{12}C delivery to the deep water with high $\delta^{13}C$ surface waters. During glacials an enhanced Antarctic overturning delivers more nutrient waters to the surface increasing the biological pump and therefore deepwater projection into the Atlantic. In the North Atlantic North Atlantic deep water penetration is greatly reduced. These diagrams have been modelled as can be seen in the bottom right image confirming the hypothesis and observations.

Menviel et al, (2016) modelled this organic pump in the present day Atlantic v conditions during the last glacial maximum. During stadials, much larger areas of the ocean are ice covered, resulting in reduced oceanic ventilation with an increase in carbon supply due to the death of many terrestrial carbon sources e.g. plant life. This enhances the carbon pump process, resulting in a build-up of respired carbon in the deeper waters (Tschumi et al, (2011). A weakening and apparent shallowing of North Atlantic Deep water (NADW) are ascribed to reduced ventilation of waters from the north resulting in a negative δ13C value. Meanwhile a more positive δ13C value and highly ventilated North Atlantic Intermediate waters (NAIW) is ascribed to increased δ13C fractionation resulting from lower sea surface temperatures and a longer residence time of the water mass at the surface flowing above 2km depth (Menviel et al, 2016). Therefore during the glacial periods there is an increase in the efficiency of the biological pump leading to a decrease in the δ13C of deep waters and reduced NADW formation resulting in less upwelling and increased carbon storage within the ocean (figure 14). The exact reason for why reduced upwelling occurs is still heavily debated (Watson and Garabato, 2005).

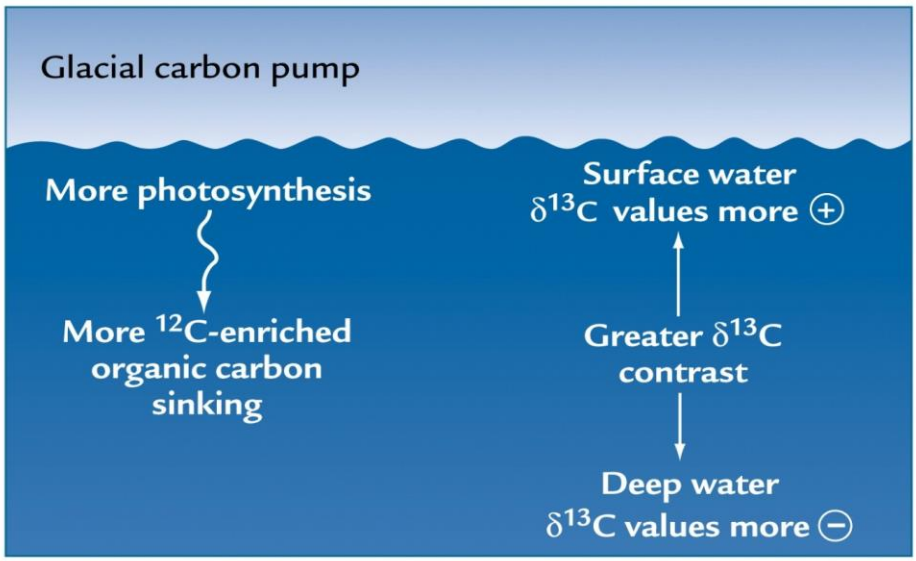

Figure 14 – (Taken from aos.wisc.edu) A simplified view of the processes involved with transport of ^{12}C to the deep ocean and it's effects of $\delta^{13}C$ values at the surface and base of the water clomun.

In terms of foraminiferal δ13C, you would expect an increase to suggest decreased stratification and increased primary production. So in the case of Heinrich events for example, large inputs of freshwater into the ocean system would likely result in temporary increased stratification and reduced productivity leading to lower δ13C values (Spielhagen and Erlenkeuser, 1994).

1.5 5, Sortable silt as a proxy

Increasing sea floor flow rates have been associated with changes in the coarseness of material on the sea floor (Hass et al, 2002). Grain sizes between 10μm and 63μm are most likely to be affected by changes in flow rates and are therefore used as a proxy for changing behaviour of major ocean currents such as those in the north Atlantic region (Hass et al, 2002; Jessen and Rasmussen, 2015). With increased flow less finer material would be able to settle to the sea floor, while more coarse grains could settle out of the water column creating an anomalously high level of coarser grains in the sediment record. Meanwhile the opposite can be said for decreased current flow. This has been used to investigate major climate perturbations such as Heinrich events and their effect on the ocean current behaviour (Jessen and Rasmussen, 2015).

During Heinrich events the effect of increased coarse sedimentation from ice-berg rafted debris can create error in interpretation of this record. Therefore, IRD corrected sortable silt must be carried out using regression analysis between the wt% sand and median size of sortable silt (Jessen and Rasmussen, 2015).

1.5 6, Accelerator Mass Spectrometer (AMS) C^{14} dating

There are three natural carbon isotopes present in the Earth System, ^{12}C, ^{13}C and ^{14}C. Unlike ^{12}C and ^{13}C, ^{14}C is not a stable isotope and is radioactive with a half-life of 5570±40 years. Carbon 14 filters into our atmosphere due to bombardment from cosmic rays and is ingested by most organisms on Earth. While the organism is alive the levels of ^{14}C remain constant due to continued ingestion, however on death the radiocarbon decay count down begins. By detecting ^{14}C levels in a sample, age can be estimated, however due to carbon 14s half-life, the maximum age at which a sample can de dated is to ~50,000 years.

An accelerator mass spectrometer (AMS) is used to work out counts of ^{14}C in order to work out an age Kyr (age is age from ~AD1950). The process involves converting a sample to graphite and mounting it on an ion source. The sample is then accelerated through a magnetic field, deflecting atoms of different masses onto pre-set 'targets'. One of these targets is for the detection of ^{14}C.

Previously it was thought the radiocarbon decay process was constant but we now know changes in our magnetic field e.g. Vries effects, can result in changes in decay rate. Therefore calibration curves must be used as a correction e.g. the program CALIB 4.0. Correction for the reservoir effect must also be carried out. The reservoir effect occurs due to storage of ^{14}C within the deep oceans which is upwelled and taken up by organisms. As a result, marine organisms are depleted in C14 and this must be corrected for with a standard of ~405 years, although this can change based on location. Normalization for isotopic fractionation (preferential uptake of ^{13}C as opposed to ^{14}C) must also be applied with the assumption that $\delta^{13}C$ had an original value of -25‰.

Chapter 2 - Materials and Methods

2.1 Materials

A gravity sediment core (HH13-100GC) was taken from west of Jan Mayen (71 00.02 N, 010 55.77 W) on the morning of July 4th 2013 along with CTD (conductivity, temperature and density) deployment.

The R/V Helmer Hansen has a steel barrelled 6m long gravity corer with an 11cm inner diameter. A 1600kg weight acts to push the core into the sediments using the force of gravity. The corer is attached to a 3000m long wire allowing deep coring of some of the oceans deeper locations. A core cutter at the base of the corer acts a trap preventing sediment from falling out while the core is being retrieved. While the closure of a valve on top of the device allows for a vacuum to initiate, again, stopping sediment 'falling' out on its ascent to the surface. Once on the ship the core is sawed into 1m sections, capped both sides and labelled top-bottom.

2.2 Lithological and geotechnical properties

Each 1m section on board the R/V Helmer Hansen was passed through a Bartington MS2 loop sensor measuring every 1cm for 10 second intervals. This was done before the author of this paper had access to the core. On retrieval of the core sections from storage the cores were placed within the Geotek MSCL-XCT x-ray machine at Tromsø University (UiT). Sections were then cut lengthwise into two halves and prised open using an osmotic knife. One half for archive and the other for sample extraction with the archive section being placed within plastic wrapping and kept in the cooler. On opening of the first section it was noted that the section had been labelled wrongly by the cruise participants with regards to top-bottom orientation. This was corrected for by relabelling and reversal of pre-taken X-ray imaging and magnetic susceptibility.
The archive sections were used to take colour x-ray fluorescence images of each section for reference using the Jai L-107CC CCD RBG Line Scan Camera installed on the Avaatch XRF core scanner at UiT. The working half of the core was logged with sediment structures, grain size and colour (Munsell soil colour chart) all noted.

Every centimetre of the working core (4-5cm, 9-10cm and so on) was cut out using an osmotic knife and placed in pre-weighed bags before being weighed itself. At the end of the core the material was crumbly and difficult to remove so the material was grouped into larger (437-442cm and 442-447cm) samples. The bags were placed in the freezer for several days before being placed in a freeze dryer (Christ alpha 1-4). Within the freeze dryer the sample material is dried by vaporisation of water without melting. This is a less destructive process for foraminifera preservation than if the samples were placed within the oven. After 3-4 days the samples were removed and weighed again, water content, porosity and dry bulk density (DBD) (g cm^{-3}) of each sample were calculated using the following equations.

Porosity = Water content / Volume
Wet Bulk Density (WBD) = Wet weight/ Volume ($\pi r^2 h$) (r=5cm; h=1cm)
DBD = Wet Bulk Density – (1.026 x (Porosity/100))

2.3 Accelerator Mass Spectrometry (AMS) dating

Based on foraminifera counts, 3 samples of ~1200 *N.pachyderma* were sent for dating at the ^{14}CHRONO centre, Queens University, Belfast, Northern Ireland. Calibrated ages were calculated from AMS C14 radiocarbon ages using the programme Calib 7.0.4 using the calibration setting Marine 13.14C (Stuvier and Reimer, 1993; Reimer et al, 2013). A standard marine reservoir correction of -405 years is applied (Reimer et al, 2009). From the newly calibrated ages (Cal yr BP) an assumed linear sedimentation rate model was developed to look at ages throughout the core. AMS C14 dates between data points were also calculated in order to decipher Heinrich events within HH13-100GC as much of the literature states the event ages as C14 dates.

2.4 Stable Isotope Investigation

From 87 of the 94 100µm samples, 23 good condition, 4 chambered *N.pachyderma* were selected for δ18O and δ13C isotopic analysis. The 7 samples omitted from isotopic analysis were due to under 15 *N.pachyderma* being present within the whole sample. Analysis took place at UiT with the use of the mass spectrometer (Thermo-Fisher MAT253 IRMS with Gasbench II) which allows for the investigation of isotopic composition of carbonates (foraminifera tests for example). Isotope values are presented in the form per mill (‰).

2.5 Foraminiferal Investigation

For each 5cm interval, stacked sieving took place with size fractions of 63πm, 100πm, 500πm and 1mm taken and placed within labelled filter paper which was then transferred to the oven to dry. Once dried, the weights of each size fraction were taken and the samples placed within labelled glass jars for further investigation. The 100πm-1mm size fractions were investigated for foraminifera through the microscope model (Leica CLS150X – MZ12s). Each sample was placed on a counting tray and squares were counted until 300 planktics had been recorded. Benthics were also counted but it became apparent that there were simply too few to be used in reliable species level investigation (under 50 per sample). Planktic and Benthic counts were calculated by dividing by the total dry weight of the original bag sample which gave the number of foraminifera per gram.

Species level identification of all planktic foraminifera was carried out with special emphasis placed on the counts of *N.pachyderma, Neogloboquadrina incompta* (Cifelli, 1961) and *T. Quinqueloba.* All other species were counted together as 'other'. The relative percentage abundance of each species were calculated and plotted in relation to the total number counted. Meanwhile fluxes (no. $cm^{-2}ka^{-1}$) were calculated using the following equations.

Mass accumulation rate (MAR) (g cm^{-2} ka^{-1}) = Linear sedimentation rate (cm ka^{-1}) x DBD (g cm^{-3})

Flux = Foraminifera Concentration (no. g^{-1}) x MAR

2.6 Ice Rafted Debris

Grain sizes 500µm-1mm along with 1mm+ are used to count lithic material from which IRD per gram could be calculated. Material and lithology present in each sample were also noted down to look at potential changes in source location. This was expanded upon by calculating the percentage of dark to light material to look at distal-proximal source regions.

2.7 Sortable Silt Analysis

Due to complete usage of material from the sample ranges (4-5cm, 9-10cm and so on) unused bagged material was used from the adjacent cm (5-6cm, 10-11cm and so on). The sample 442-447cm had to be taken from the archive section. Lab coat and latex gloves were worn throughout the following outlined procedure. This procedure is after Hass, (2002).

Approximately 2g of dry material was taken and placed within a labelled test tube, covered with 20% Hydrochloric Acid (HCL) and left within a fume hood for at least 24 hours. After 24 hours the sample was placed in a centrifuge for 4 minutes at 4000 rpm cementing the material at the bottom of the test tube. The 20% HCL was then decanted, replaced with distilled water and centrifuged again for 4 minutes, this process is repeated twice. To make sure all the sediment was being 'washed' each refill of distilled water involved shaking the tube a little to entrain the material into the water.
Each sample was then covered again with 20% HCL, had aluminium foil placed on top of the test tube and is then placed within a thermal bath (~85 degrees for 2 hours). A hole was placed in the top of the aluminium foil to allow escaping gas a pathway. In some cases a strong chemical reaction took place and the sample had to be removed to calm down for a few minutes before being placed back into the bath. All this was carried out under the fume hood.

After 2 hours the samples were removed from the thermal bath and the centrifuge/washing cycle as outlined previously was repeated. However this time, once washed, the material was removed from the test tube into labelled plastic cups by entraining the sediment within the smallest amount of distilled water and pouring it out.

The cups are then left to dry under the fume hood for ~48 hours depending on how much water is present within the cup.

Once dried, ~0.2g was taken from the each sample and placed within the same labelled cup while the remaining material was placed within a labelled plastic bag. Around 20ml of distilled water was added and then the samples were placed on a shaking table for one and a half days. After this time the cups are removed, 2 drops of Calgon were applied and then the cups were placed within an ultrasonic bath for 5 minutes. The samples could then be analysed by the Beckman Coulter LS 13 320 Particle Size Analyser (LDPSA).

Three runs for each sample were carried out and stored within excel files on the connected computer. The 3 runs had to be collated into one excel file where averages were calculated and used within the GRADISTAT software (Blot and Pye 2001). From this percentages of clay, silt and sand were calculated. Using the raw data from the LDPSA, median values were taken from the sortable silt grain size fraction (10-63μm) to account for the multimodal grain size distribution attributed to IRD fallout (Hass, 2002; Jessen et al, 2015). Regression analysis of Wt% sand plotted against the median sortable silt fraction (10-63μm) was used. IRD (SSIRD) is considered the distance between data points in the plot versus the regression line allowing for the use of the following equation.

ΔSS (Corrected sortable silt) = $SS - SS_{IRD}$

This attenuates for the effect of IRD on the sortable silt analysis and can be plotted as such.

Chapter 3 - Planktic Foraminiferal Assemblages

Differing species of foraminifera have distinct environmental conditions under which they can thrive. Therefore identification of foraminifera is of vital importance to the understanding of changing environmental conditions over time in any given area (Kucera et al, 2005). Benthic foraminifera were of too low abundance with HH13-100GC to be considered of reliable use in this study with regards to assemblage assignment. In this section the dominating and sub-dominating planktic species are described in terms of their environmental living conditions and morphological features (figure 15a and 15b).

3.1 Dominating species

3.1 1, *Neogloboquadrina pachyderma* (Ehrenberg, 1861)

N. pachyderma is the dominant polar species found north of the Atlantic Front, representing polar waters at the surface (Carstens, 1997; Duprat et al, 1996). Living between around 25-200m water depth, the sinistrally coiling *N.pachyderma* are able to record a large ocean section of ambient water properties (Simstich et al, 2003). Not to be confused with the newly named dextrally coiling *Neogloboquadrina incompta* (Cifelli, 1961) (Darling et al, 2006).

3.2 Sub-dominating species

3.2 1, *Neogloboquadrina incompta* (Cifelli, 1961)

N. incompta is the dextrally coiling version of the morphologically similar *N. pachyderma,* with the suggested renaming to *N. incompta* by Darling et al (2006) on the grounds of genetic divergence *studies.* Unlike its polar counterpart, *N*. *incompta* is associated with warmer waters (~12^0C) according to Schmidt et al (2004).

3.2 2, *Turborotalita quinqueloba* (Natland, 1938)

Described as a subpolar species by Bauch (1994), *T. quinqueloba* is associated with transitional waters and more importantly as an indicator for the approach of the Arctic and/ or polar fronts (Johannessen et al, 1994). Studies by Carsten and Wefer (1992) on modern day appearance of *T. quinqueloba* in Arctic waters found the foraminifera living within the top 500m of the water column in the basal Atlantic Intermediate waters as far north as the Nansen Basin, high Arctic.

3.2 3, *Globigerina bulloides* (d'Orbigny, 1826)

G. bulloides are a species covering a range of transitional water masses and are commonly associated with upwelling regions and have a preference for productive environments (Brock et al, 1992; Kennet and Srinivasan, 1983). This makes them a good indicator for the encroachment of warmer Atlantic waters (Kennet and Srinivasan, 1983).

3.2 4, *Globigerinita Uvula* (Ehrenberg 1861)

G. Uvula is a subpolar to tropical species found commonly in temperate waters, distinguished by it's characteristically microperforate surface ultrastructure (Kennett and Srinivasan, 1983).

3.2 5, *Globigerinita glutinata* (Egger, 1895)

Subpolar to tropical species common in temperate waters and again an indicator for influx of more temperate waters to the Greenland, Arctic or Norwegian seas respectively (Kennett and Srinivasan, 1983).

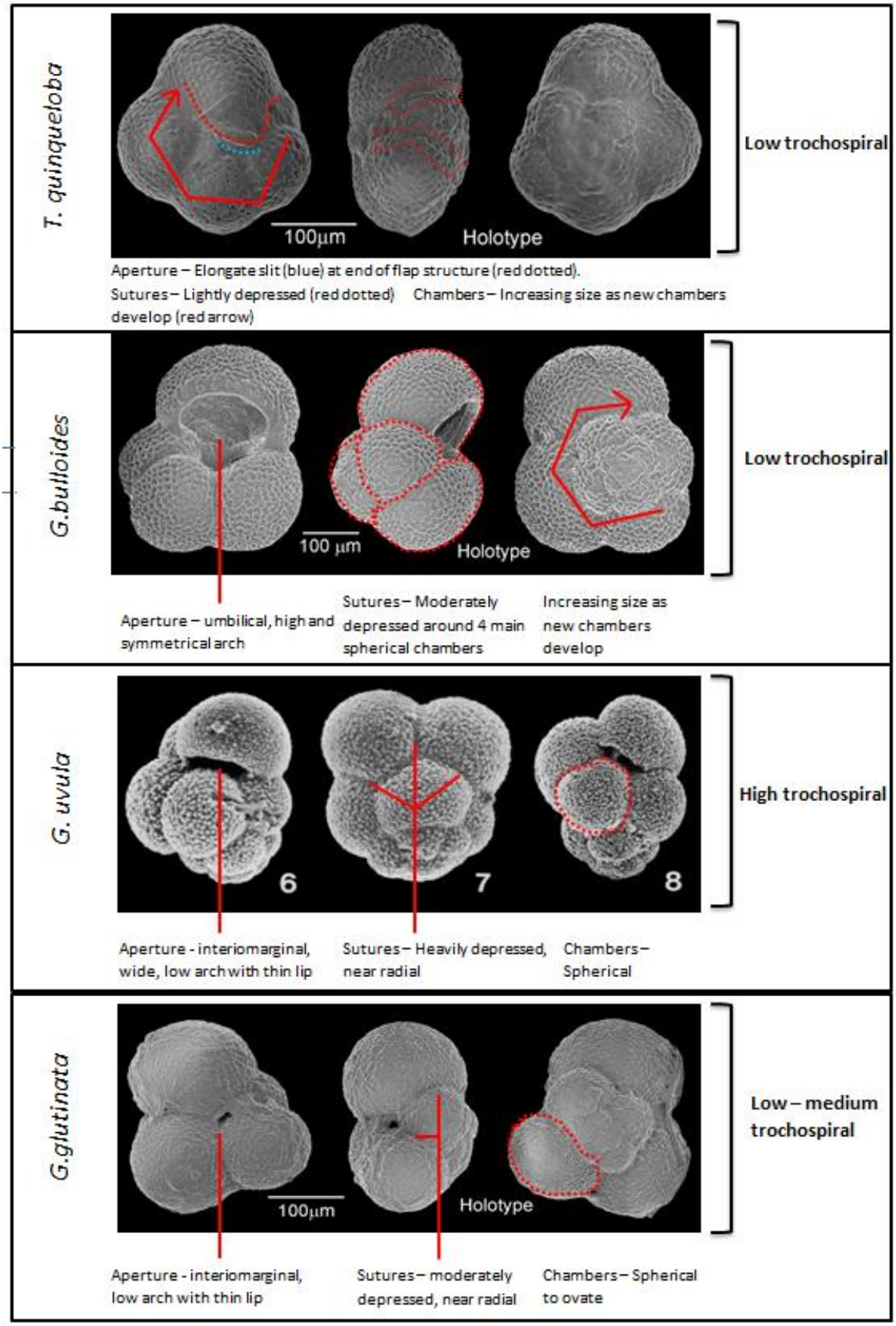

Figure 15a – (All images taken from miktrotax.org) SEM images labelled for diagnostic features used in the identification of stated foraminiferal forms.

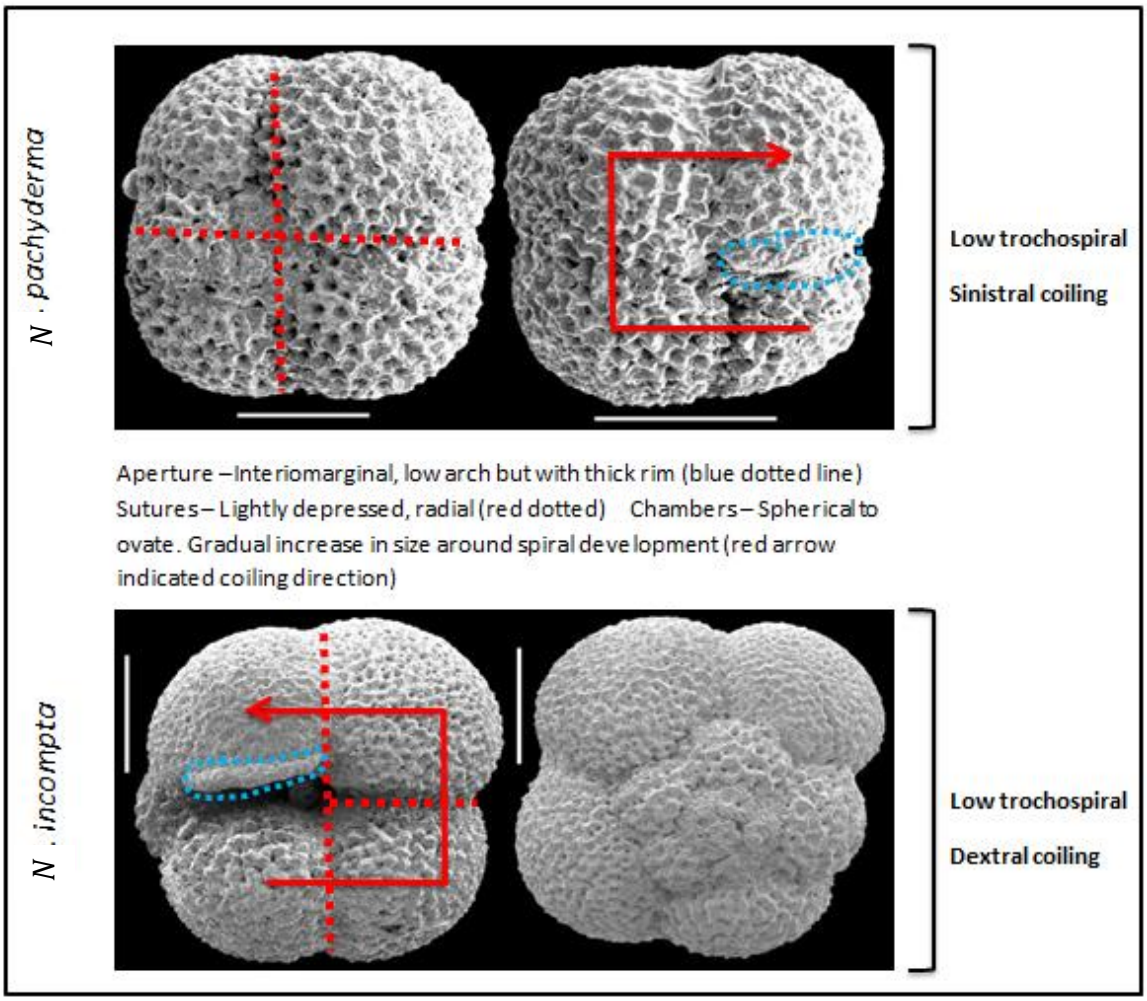

Figure 15b – (Both images taken from miktrotax.org) SEM images labelled for diagnostic features used in the identification of the morphologically similar *N.incompta* (dextrally coiling) and *N.pachyderma* (sinistrally coiling).

Chapter 4 - Results

4.1 Lithological units

Lithological units (U1-U6 up-core from base) have been decided upon based on sediment grain size investigation, magnetic susceptibility, sortable silt variations, the IRD record and lithological properties including sediment log. A constant throughout HH13-100GC was the presence of a light grey carbonate and quartz mix in the <500µm grain size fraction, any deviations from this are noted in the unit descriptions below. The accumulation rate mean across the whole unit is stated in the title of each section. Please refer to figure 16 for lithological IRD analysis, figure 17 showing the defined boundaires of each subsequent unit description, figure 18 showing various lithological properties of the sediment and finally figure 19 showing IRD corrected sortable silt results.

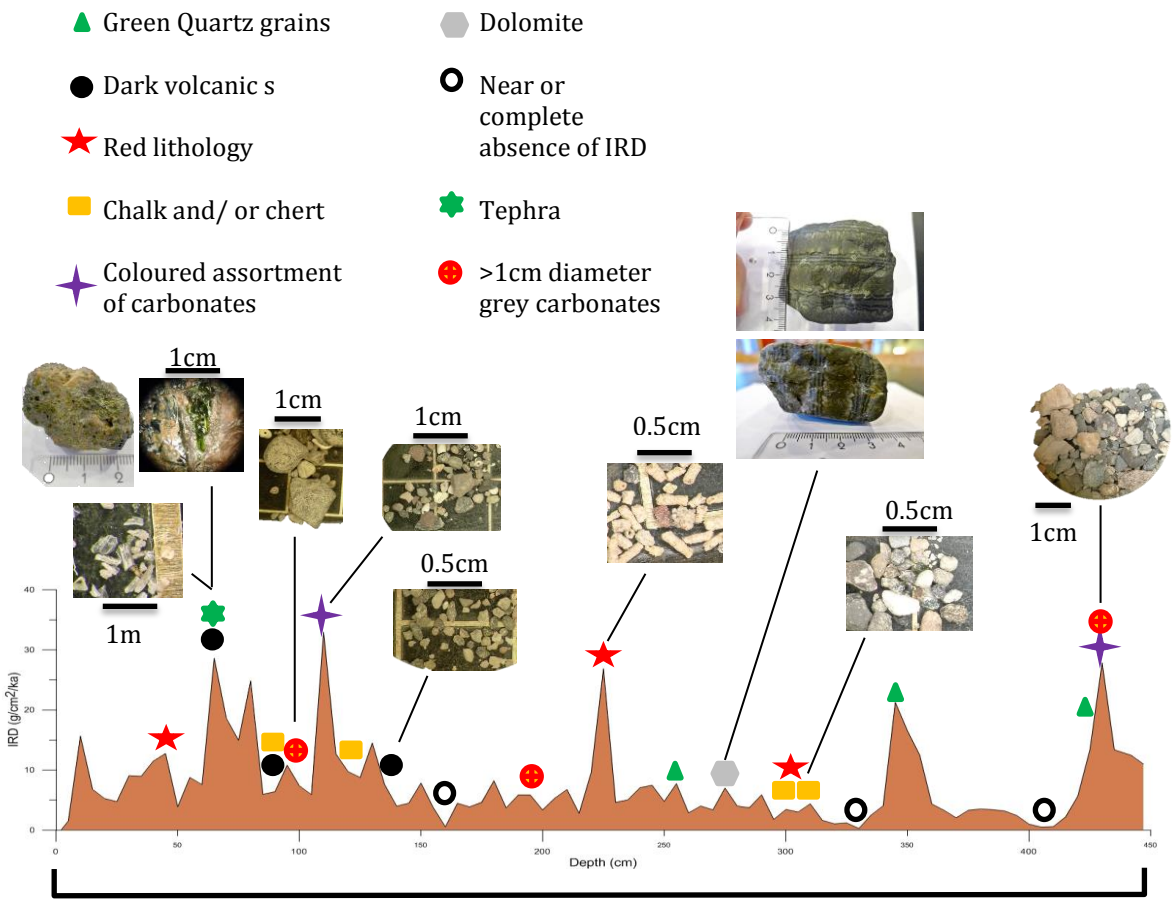

Figure 16 - Lithological investigation of HH13-100GC IRD through microscope analysis of the 500->1mm grain size fraction. Larger rock fragments within the core are also included along with the tephra layer at 65-70cm which was identified from the 100µm fraction.

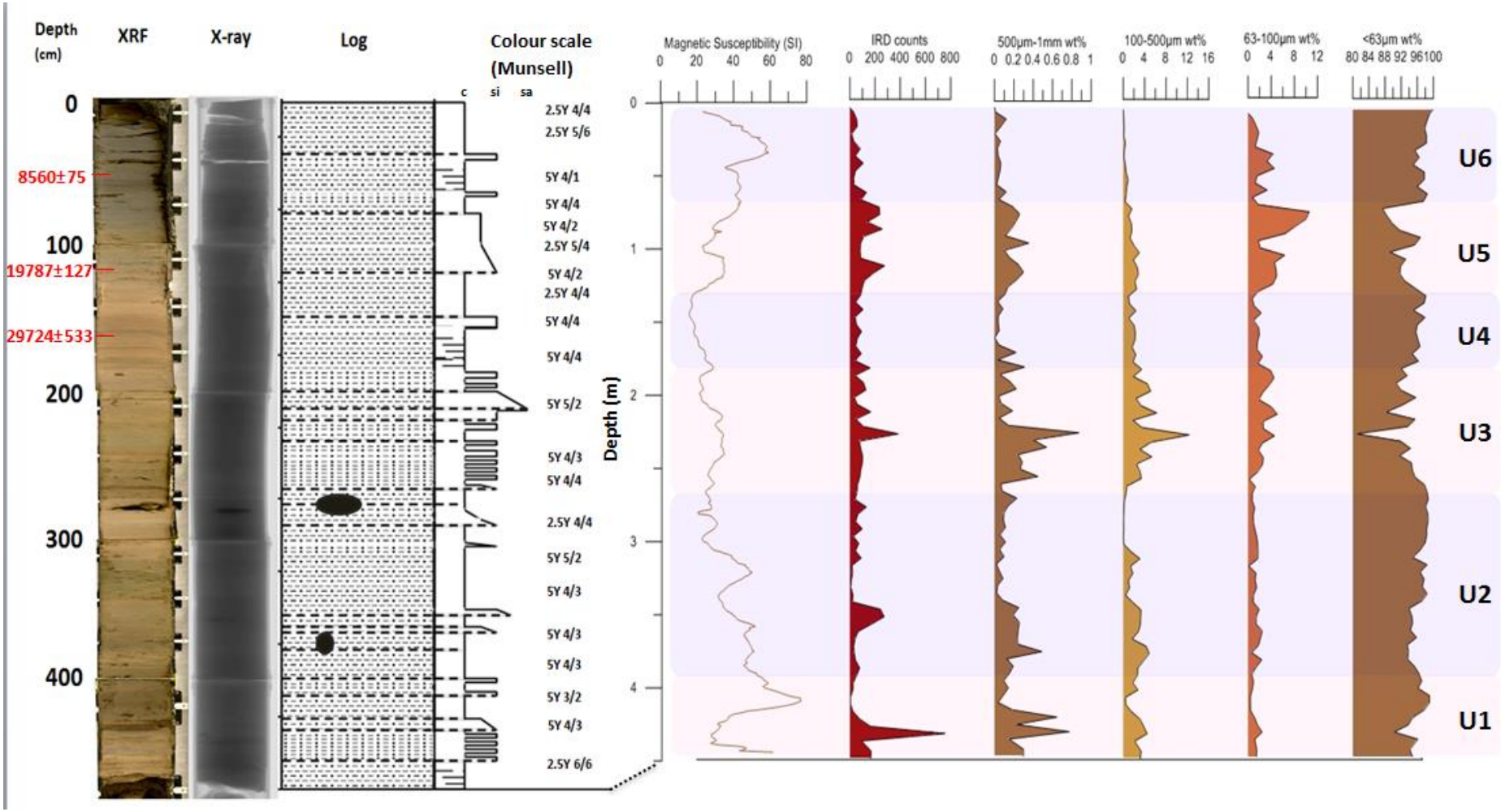

Figure 17 – A representation of the lithostratigraphic XRF imagery, X-ray images, log section, magnetic susceptibility and the differing grain size fractions. Units were defined based on a culmination of factos including changes in colour in the XRF imagery and grain size distributions.

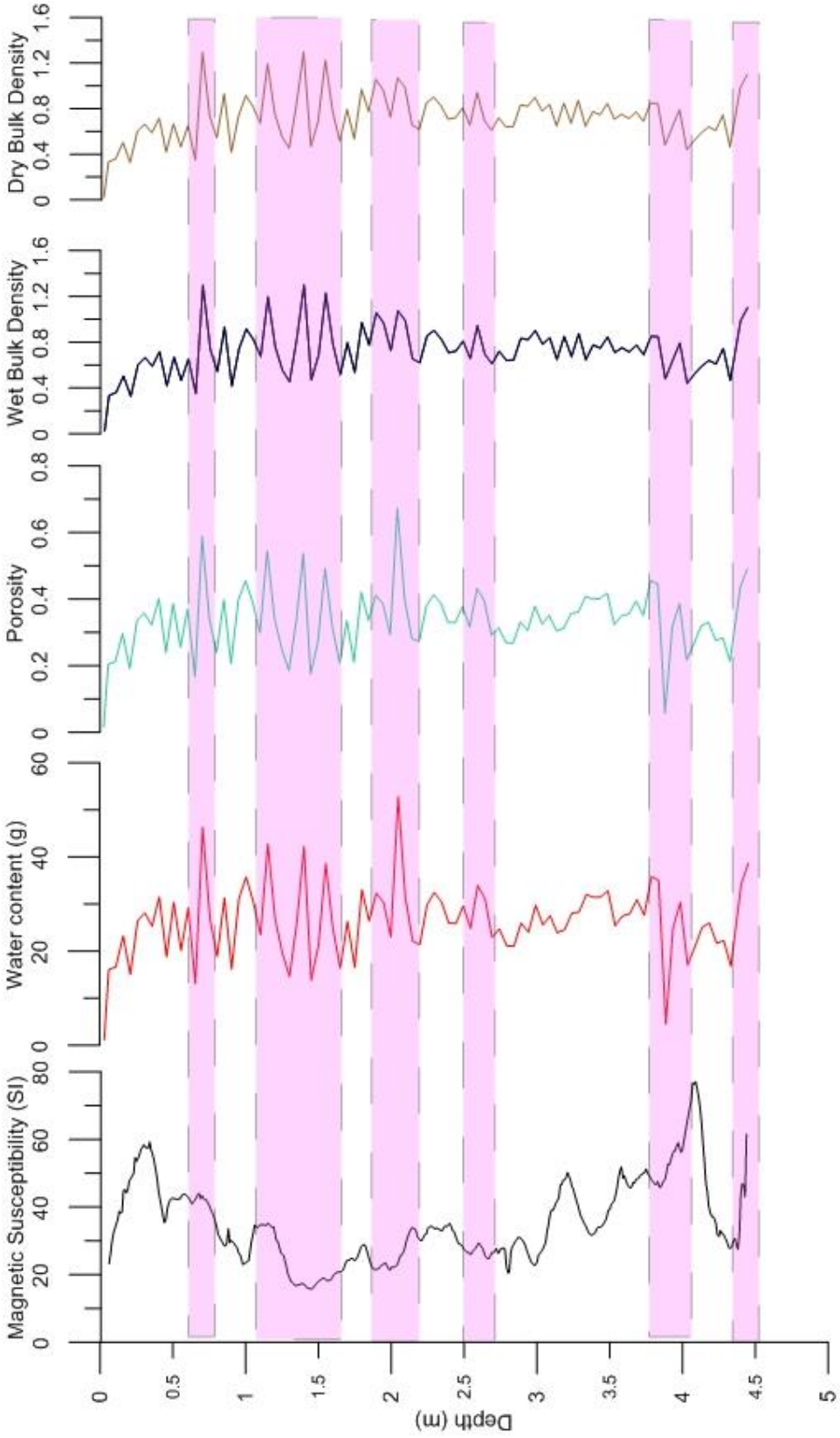

Figure 18 – Lithological properties of the sediment, calculated from pre and post drying of the sediments (see chapter 2.2 . Pink shaded boxes define the peaks in the record.

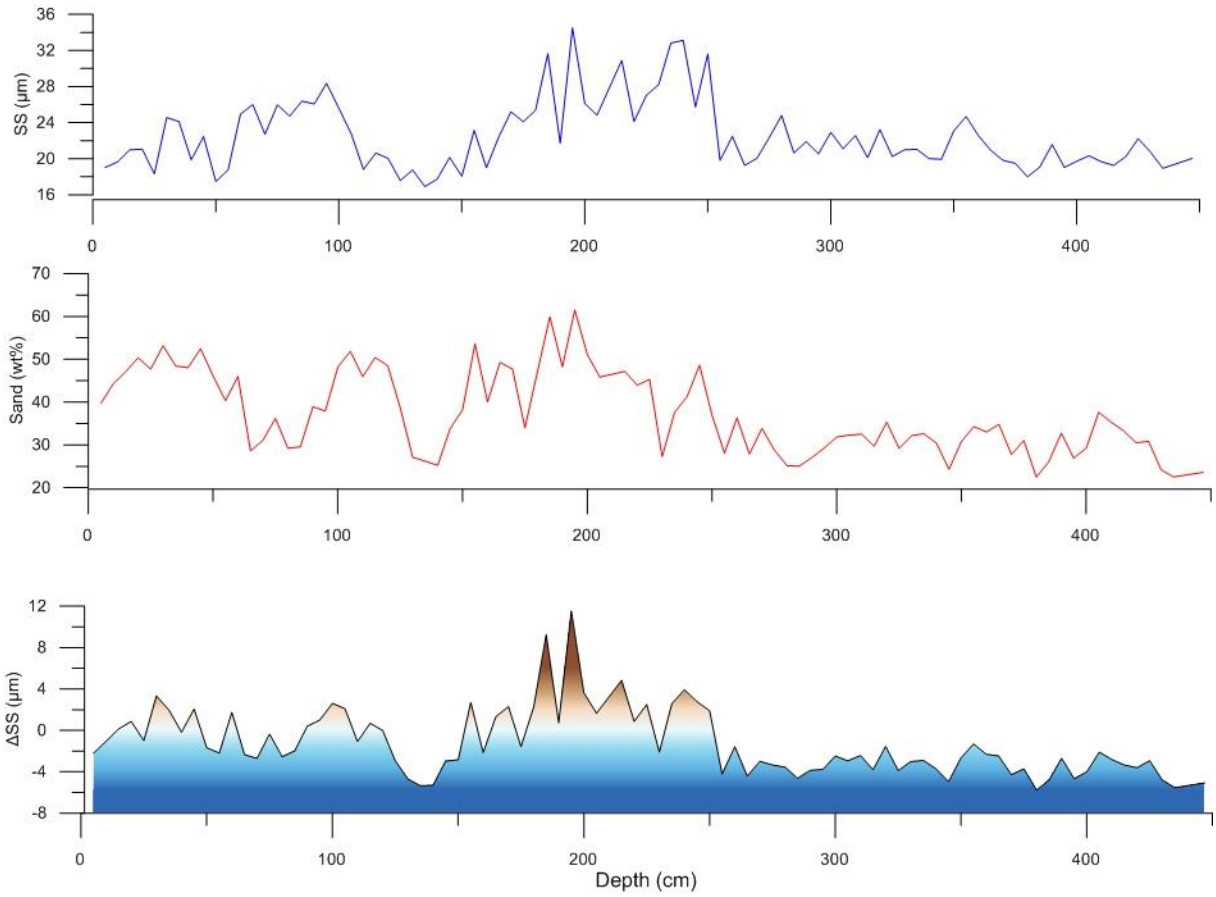

Figure 19 – Figure showing median sortable silt (top) wt% sand (middle) and (ΔSS) (bottom). ΔSS gives an indication of the fining or coarsening of the sediment, with more positive values you would expect a higher flow rate (removing the finer sediment) while with a finer (less positive) values you would expect a lower flow rate (settling out of finer material).

4.1 1, Unit 1 (447-395cm; Accumulation rate – 2.9cm/kyr)

Unit 1 has a large peak in IRD and sand content 430cm which corresponds with a low value of ~30 SI 10^{-5} for magnetic susceptibility (MS). A maximum IRD flux occurs at 430cm (27.9 (no/cm^2/ka). From 447cm to 420cm there is significant lamination evident with colour variations from 5Y 4/3 to 2.5Y 6/6 (olive to olive yellow). There is then a rapid switch to an MS reading of ~80 SI 10^{-5} by 410cm which coincides with a switch from more sandy to more clay-silt dominated sediment. Between ~395cm and ~420cm there is a more uniform sediment colour, 5Y 3/2 (dark olive grey).
Four medium sized (1mm diameter) green quartz minerals are noted in the IRD investigation at 425cm.

IRD corrected sortable silt results show generally negative values throughout the unit.

Unit 1 has a water content peak of 38.62g at 447cm with low point at 435cm of 16.75g; porosity peaks at 0.49 at 447cm with low point at 435cm of 0.21 while; dry bulk density peaks at 447cm with a low point at 405cm of 0.44.

4.1 2, Unit 2 (395-265cm; Accumulation rate – 2.9cm/kyr)

Unit 2 has fine-medium sand peaks at 375cm and 350cm compared to an overall clay and silt signal which is especially prevalent between 265cm and 310cm. There is a staggered decrease in magnetic susceptibility up-core from a peak of 50 SI 10^{-5} at ~395cm with another peak of 50 SI 10^{-5} at 355cm. The low point of MS comes at 300cm with a value of 50 SI 10^{-5} coinciding with clay and silt grain signature. There is a lower 'spike' at 280cm in the record, however, this is attributed to a large drop-stone present in the core and is therefore disregarded as a representative value. A colour change can be noted from 5Y 4/3 (olive), 5Y 5/2 (olive gray) at 310cm to 2.5Y 4/4 (olive brown) at 290cm.

IRD contents vary widely throughout this section from the grey carbonate and quartz constant. A distinct absence of IRD grains has been noted at 330cm. Volcanic glass is noted at 290cm, 300cm, 340cm, 360cm, 385cm and 395cm. A red unknown lithology is noted at both 295cm and 310cm while white chalk grains are noted at 300cm, 315cm and 320cm. Abundant dolomite is noted at 275 and 280cm with larger than average

quartz grains (1cm diameter) noted at 375-380cm. Shell fragments are present at 290cm and 295cm. At between 270-280cm a large rock (5cm width, 2cm height) is present. The patterns on the rock consist of parallel lines with apparent crystal or biogenic growth, lithology unknown.

IRD corrected sortable silt results show a consistent negative trait with the most negative ΔSS at 380 cm (-5.8μm) and most positive at 320cm (-1.6μm).
Unit 2 has a water content peak of 35.78g at 380cm with low point at 390cm of 4.51; porosity peaks at 0.46 at 380cm with low point at 390cm of 0.06 while; dry bulk density peaks 0.90 at 300cm with a low point at 390cm of 0.48.

4.1 3, Unit 3 (265-170cm; Accumulation rate – 2.9cm/kyr)

Unit 3 starts with high clay and silt levels at the unit 2/3 boundary but then rapidly moves into a chaotic peak – trough system up-core right up to the unit 3/4 boundary. The largest IRD and sand peak occurs at 225cm where there is almost a complete lack of clay and silt grains. This peak also coincides with a small negative deviation in magnetic susceptibility values of ~30 SI 10^{-5}. Fluctuations in grain size continue up to the unit 3/4 boundary with a drop in magnetic susceptibility to a lowest value of ~20 SI 10^{-5} at 200cm. Sediments are laminated throughout unit 3 as can be seen on both the XRF and X-ray images. Colour change from 5Y 4/4 (olive) to 5Y 4/2 (olive grey) can be seen up-core alternating between lamentation. IRD anomalies present in Unit 3 include grey vesicular volcanic material at 265cm, angular carbonates at 255cm, dolomite appearance at 215cm and an unknown red lithology at 225 and 200cm.

IRD corrected sortable silt results show the same chaotic nature to the plots as is seen for the larger grain sizes. Nearly the whole unit has positive values with high peaks at 195cm (+11.4μm) and 185cm (+9.3μm) and low peaks of (-4.22μm) at 255cm and -2.1 μm at 190cm.

Unit 3 has a water content peak of 52.82g at 205cm with low point at 175cm of 16.52; porosity peaks at 0.67 at 205cm with low point at 175cm of 0.21 while; dry bulk density peaks 1.07 at 205cm with a low point at 175cm of 0.53.

4.1 4, Unit 4 (170-130cm; Accumulation rates, 170-155cm – 2.9cm/kyr; 155-130cm – 5.05cm/kyr)

Unit 4 has a far more stable sediment size record with dominance for clay and silt grain sizes. The magnetic susceptibility decreases from ~30 SI 10^{-5} at 170cm to ~18 SI 10^{-5} at 145cm with a general decrease up the whole section. Lamination is still present in the XRF and X-ray imagery, however, the colour change is far less distinct (5Y 4/4 (olive-grey); 2.5Y 4/4 (olive brown)) compared to Unit 3 and the lower section of Unit 1. IRD anomalies include volcanic glass at 145cm, a volcanic grey lithology with olivine amygdales at 140cm and dark-crystalline mafic grains at 135cm.

IRD corrected sortable silt results show a return to more negative values peaking at 135cm with a ΔSS value of -5.354 μm. The most positive value is found at 155cm (+2.7 μm)

Unit 4 has a water content peak of 42.20g at 140cm with low point at 145cm of 13.77g; porosity peaks at 0.54 at 140cm with low point at 145cm of 0.18 while; dry bulk density peaks 1.30 at 140cm with a low point at 145cm of 0.47.

4.1 5, Unit 5 (130-65cm; Accumulation rates, 130-105cm – 5.05cm/kyr; 105-65cm – 3.9cm/yr)

A return to a fluctuating regime of grain sizes as was seen in Unit 3 but with less amplitude on the peak – trough pattern. Peaks in IRD and sand fractions at 115cm and 75cm correspond with a decrease in the wt% of clay and silt. An especially large peak is noted in the 63-100μm fraction at 70cm where the wt% increases to 11.5%. A peak in the 500μm to 1mm fraction around 100cm matches with a low point in MS of ~20 SI 10^{-5} but is not represented in the IRD count plot. MS is gradually increasing up-section reaching a peak of ~45 SI 10^{-5} by the Unit 4/5 boundary. Colour change up-section changes from 5Y 4/2 (olive grey) to 2.5Y 5/4 (light olive brown) around 100cm and then back to 5Y 4/4 (olive) by the Unit 1/2 boundary.

IRD anomalies include the appearance of chalk grains at 130cm, 125cm and 80cm, appearance of chert grains at 120cm, 115cm, 110cm, 105cm, grey volcanic lithology with amygdales and bi-valve shells at 11cm, 105cm, 100cm. It should also be noted that

the 69-70 cm 100-500μm fraction has abundant tephra shards assumed to be Vedde Ash deposits. Between 67-69cm there is a basaltic rock (3cm by 3cm) containing an olivine lathe.

IRD corrected sortable silt results shows a gradual increase to more positive values during the central part of unit 105-90cm (peak of +2.6 μm) and then reduction to negative values again with a negative peak at 70cm *(-2.7 μm).
Unit 5 has a water content peak of 46.25g at 70cm with low point at 130cm of 14.57g; porosity peaks at 0.59 at 70cm with low point at 130cm of 0.19 while; dry bulk density peaks 1.30 at 70cm with a low point at 90cm of 0.42.

4.1 6, Unit 6 (65-0cm; Accumulation rates,
65-55cm – 3.9cm/kyr; 55-0cm – 7.2cm/kyr)

Unit 1 has the most consistently high wt%s of clay and silt across the whole section. There are minor peaks in IRD and a peak of ~4% at 50cm in the 63μm-100μm size fraction wt%. Unit 1 is similar to Unit 3 but with even finer grain sizes overall. A peak in magnetic susceptibility of ~60 SI 10^{-5} at 35cm with a low point in the upper most sediments of ~20 SI 10^{-5}. The Unit is predominantly dark in colour (5Y 4/1 – dark grey) with only the surface sediments showing a change to lighter (2.5Y 4/4 – olive brown) shading.

The main anomaly in IRD in Unit 6 is the abundance of a red volcanic lithology at the 40cm depth.

IRD corrected sortable silt values are fluctuating around the mean during this period with positive peaks at 45cm (+2.1 μm) and 30cm (3.3 μm). Negative peaks occur at 55cm (-2.2 μm) and at 5cm (-2.2 μm).
Unit 6 has a water content peak of 30.36g at 50cm with low point at 65cm of 13.09g; porosity peaks at 0.39 at 50cm with low point at 65cm of 0.17 while; dry bulk density peaks 0.71 at 40cm with a low point at 20cm of 0.32.

4.2 Foraminiferal Units

Foraminiferal units were decided upon based upon changes in the flux and more especially changes in the ratios between the most abundant planktic foraminifera (*N.pachyderma)* and other species (figure 20). In the text ahead, the flux planktic and benthic peak values are followed by the number per gram, as calculated during picking of the foraminifera.

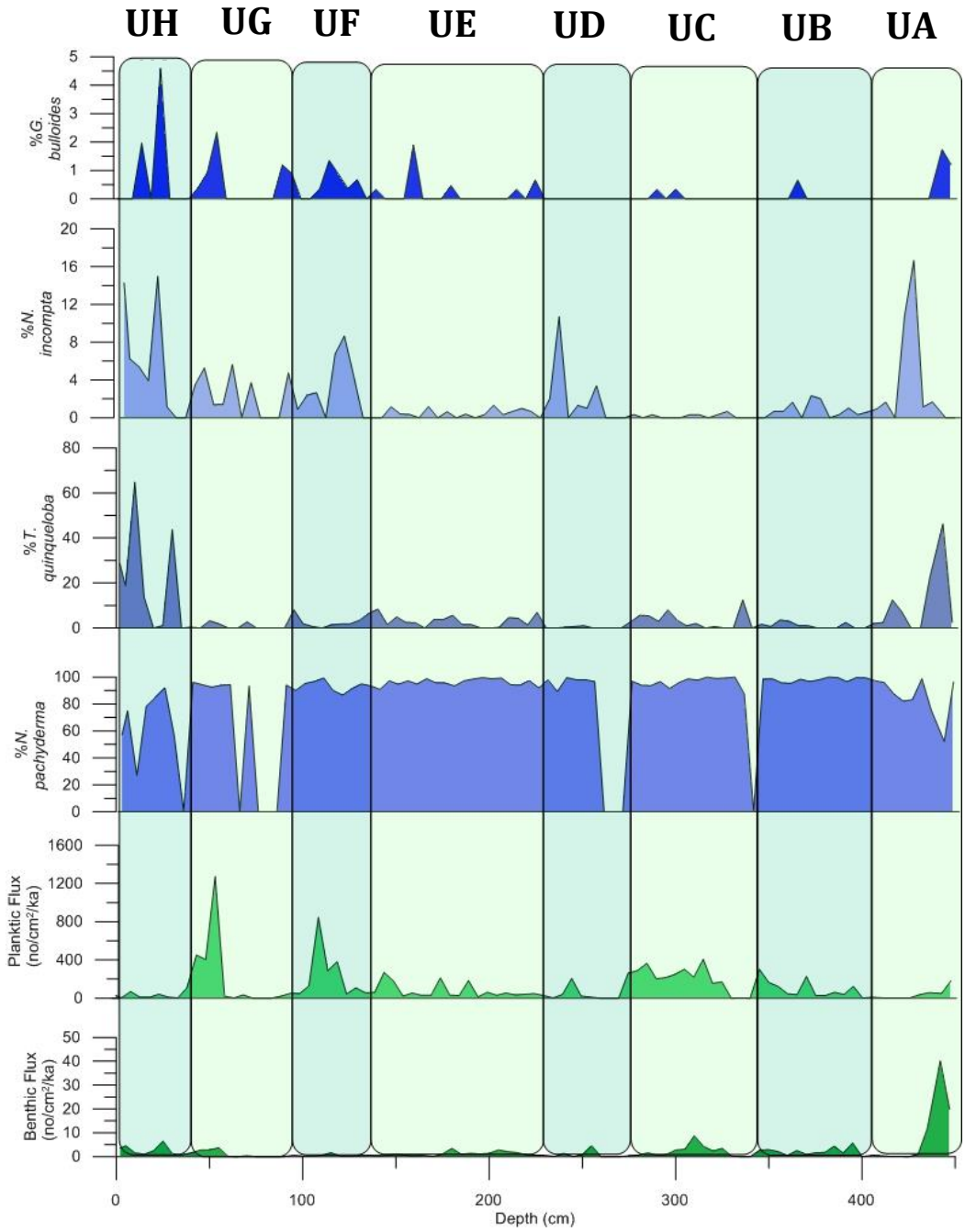

Figure 20 - Foraminiferal units as defined by changes in the flux rates and relative abundances of individual species. Falls in *N.pachyderma* values and increases in other foraminiferal forms were used as diagnostic boundaries of change.

4.2 1, Unit A (447-410cm)

Foraminiferal fluxes for planktic foraminifera are relatively low during much of Unit A, while the highest flux of benthic foraminifera in HH13-100GC is seen as a peak. A peak in planktic foraminifera flux occurs at 447cm with a value of 181.8 (no/cm^2/ka) (60 per gram) with a smaller peak occurring at 435cm with a value of 56.5 (no/cm^2/ka). Benthic fluxes peak at 442cm with a lower value than that of the planktics, 40.32 (no/cm^2/ka) (13 per gram).

%*N.pachyderma* starts with a peak of 96.4% at 447cm which then drops significantly to 52% at 442cm. There is a gradual recovery up to 98% by 430cm however then another drop occurs to 82% at 420cm.

%T.quinqueloba starts with a large peak of 46% at 442cm coinciding with the drop in %*N.pachyderma* at the same depth. Significant still at 435cm, making up 22% of the total before becoming absent at 430cm. Reappearance occurs at 415cm with a value of 12%.

%N.incompta starts with a peak of 16.7% at 425cm with another smaller peak following onto 420cm with a value of 10.7%. This coincides with a drop in %*N.pachyderma* for the same depth intervals.

A small peak of *%G.bulloides* at 442cm is noted (1.7%) coinciding with the drop in %*N.pachyderma* and high values of *%T.quinqueloba* at the same depth.

4.2 2, Unit B (410-435cm)

Unit B has overall higher planktic fluxes than in Unit A with 4 main peaks at 395cm – 123.5 (no/cm^2/ka), 385cm – 60.1 (no/cm^2/ka), 370cm – 228.1 (no/cm^2/ka) (100 per gram) and finally at the Unit B/C boundary 301.8 (no/cm^2/ka) (110 per gram) at 345cm. Smaller positive benthic fluxes occur at 395cm – 123.5 (no/cm^2/ka), 385cm – 4.4 (no/cm^2/ka) (3 per gram), at 350cm – 2.9 (no/cm^2/ka) (1 per gram).

%*N.pachyderma* has a consistent trend of >95% throughout the whole of Unit B.
%T.quinqueloba appears in peaks at 390cm – 2.4%, 360cm – 3.0% and 355cm – 3.6%.
%N.incompta appears with low peaks of 2.3% at 370cm and 2% at 375cm.
%G.bulloides values are too low to be significant in Unit B <1%.

4.2 3, Unit C (345-275cm)

Unit C has some of the most consistently high fluxes for the whole of HH13-100GC.
A complete absence of planktic foraminifera at 340cm is soon replaced by a rapid increase to a peak of 409 (no/cm^2/ka) (160 per gram) at 315cm. Benthic foraminifera are completely absent at 340 and 345cm with one small peak at 310cm of 8.8 (no/cm^2/ka) (4 per gram).

%*N.pachyderma* peaks at 100% at 330cm and is constantly high through much of Unit C. An exception is at 340cm where the value is 0%, at 335cm where the value is 87.5% and at 295cm where the value is 92%.

%T.quinqueloba peaks at 335cm with a value of 12.5% and at 295cm with a value of 8.1% both of which coincide with supressed %*N.pachyderma* values.
%N.incompta and *%G.bulloides* have values <1%.

4.2 4, Unit D (275-230cm)

Unit D has relatively low fluxes compared to Unit C with a lack of planktic and benthic foraminifera from 270-260cm. A peak in the planktic foraminifera fluxes can be seen at 245cm with a value of 207.5 (no/cm^2/ka) (75 per gram). A benthic peak of 4.6 (no/cm^2/ka) (1 per gram) can be seen at 255cm.

%*N.pachyderma* is mostly above 95% across the whole of Unit D with one exception at 235cm with a value of 89.2%.

%N.incompta appears with one peak at 235cm with a value of 10.7% coinciding with the supressed %*N.pachyderma* at the same depth interval.
%T.quinqueloba and *%G.bulloides* values are <1% through Unit D.

4.2 5, Unit E (230-140cm)

Unit E has a fluctuating serious of peaks and troughs with regards to planktic foraminifera. Benthic foraminifera flux values are too low to be considered from now through all subsequent Units (F,G and H). There are three main peaks in planktic fluxes throughout Unit E situated at 210cm – 55.2 (no/cm^2/ka), 200cm – 61.4 (no/cm^2/ka) (10 per gram), 190cm – 185 (no/cm^2/ka) (60 per gram), 175cm – 212.7 (no/cm^2/ka) (65 per gram) and 145cm – 271 (no/cm^2/ka).

%*N.pachyderma* is >90% throughout Unit E so relative negative 'peaks' are noted here. Low peaks are recognised at 225cm – 92%, 215 – 94%, 180cm – 93%, 160cm – 94%, 150cm – 94%, 140cm – 91%.

%T.quinqueloba peaks are present throughout Unit E starting with 225cm – 7%, 210,215cm – 4%, 180cm – 5.6%, 150cm – 5%, 140cm – 8%. Most of which coincide with supressed %*N.pachyderma* values.
%G.bulloides appears with a small peak of 2% at 160cm.
%N.incompta values are <1% through Unit E.

4.2 6, Unit F (140-95cm)

Unit F consists of a central peak for planktic foraminifera at ~110cm with a flux value of 857.3 (no/cm^2/ka) (180 per gram) bordered either side by trough values.
%*N.pachyderma* is >90% throughout Unit F so relative negative 'peaks' are noted here. Low peaks are recognised at 135cm – 93%, 125cm – 91%, 120cm – 87%, 115cm – 90% and 95cm – 90%.

%T.quinqueloba peaks are present at 135cm – 6.5% and 95cm – 8% coinciding with some of the suppressed %*N.pachyderma* values.
%N.incompta has a peak value of 8.7% at 120cm matching supressed %*N.pachyderma* values at this depth interval.
%G.bulloides values are <1% through Unit F.

4.2 7, Unit G (95-40cm)

Unit G starts at its base (85-75cm) with planktic flux values of ~0 (no/cm^2/ka) increasing to the largest flux value in HH13-100GC at 55cm with a value of 1274.8 (no/cm^2/ka) (270 per gram).

%*N.pachyderma* is 0% from 80-75cm and again at 65cm. Otherwise values are maintained above 90% with minor negative peaks at 90cm – 94%, 70cm – 93%, 60cm – 94% and 50cm – 92%.
%T.quinqueloba peaks occur at 70cm – 2.8%, 55cm – 2%, 50cm – 3%.
%N.incompta peaks occur at 90cm – 4%, 70cm – 3%, 60cm – 5.6% and 45cm – 5.3%.
%G.bulloides peaks occur at 70cm – 2.8% and 50cm – 3.2%.

4.2 8, Unit H (40-0cm)

Unit H has very low to near absent planktic flux values. The highest peak is present at 10cm with a value of 69.2 (no/cm^2/ka) (15 per gram).

%*N.pachyderma* is 0% at 35cm with significantly negative peaks at 30cm – 56.25, 15cm – 78% and at 10cm – 27%.

%T.quinqueloba has significant peaks in Unit H not seen since Unit A. Peaks occur at 30cm – 44%, 15cm – 14% and 10cm – 65%, corresponding with supressed.

%*N.pachyderma* values. *%N.incompta* shows peaks at 15cm – 4% and 10cm – 5.4% *%G.bulloides* peak occurs at 25cm – 4.6% and 15cm – 2%.

4.3 Isotopic Units

Isotopic units have been defined based on $\delta^{18}O$ and $\delta^{13}C$ fluctuations recorded from planktic formainifera throughout HH13-100GC and are represented in figure 21.

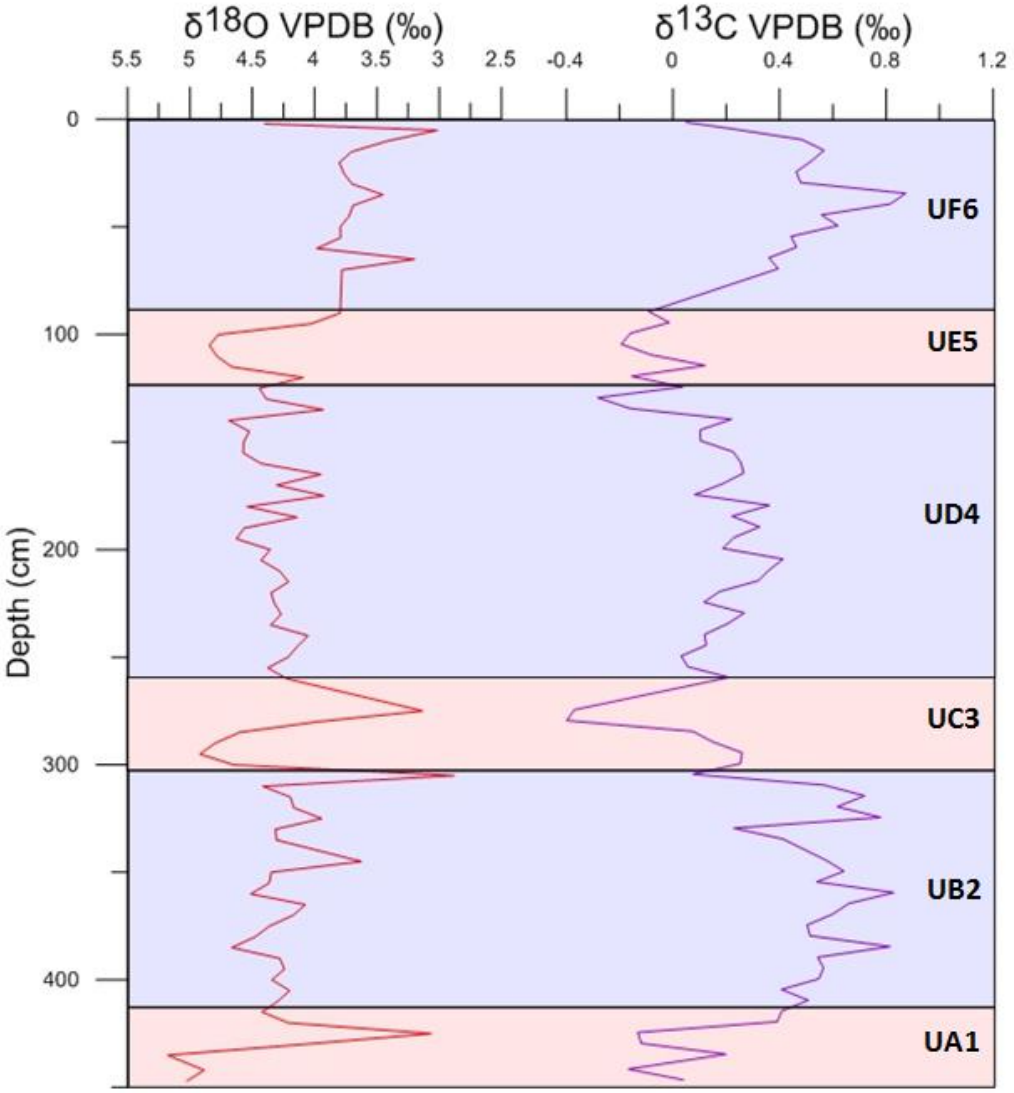

Figure 20 – The isotopic record for HH13-100GC as retrieved by isotopic analysis of foraminifera tests. Units were defined based on the major fluctuations seen in the record.

4.3 1, Unit A1 (447-415cm)

Unit A1 starts with some of the most positive δ ^{18}O values within the whole core, 447cm – 5.02‰ and 435cm – 5.18‰. There is then a significant and abrupt shift to one of the most negative values within the whole core, 425cm – 3.06‰. δ ^{13}C negative values peak at 442cm – -0.17‰, 430cm - -0.12‰ and 425cm – -0.13‰. The most positive δ ^{13}C values are located at the UA1/UB2 boundary at 415cm – 0.41‰.

The large negative anomaly at 435cm for δ ^{18}O corresponds with more negative δ ^{13}C values.

4.3 2, Unit B2 (415-300cm)

Unit B2 has moderately fluctuating (within 1‰) δ ^{18}O values until the 305cm mark where there is a sharp jump to more negative values. The most positive values for δ ^{18}O are located at 385cm – 4.66‰, 360cm – 4.51‰, 310cm – 4.41‰. While the most negative values are found at 345cm – 3.62‰, 325cm – 3.94‰ and 305cm – 2.88‰.

Unit UB2 has high δ ^{13}C values compared to all other units. Peaks are found at 385cm – 0.81‰, 360cm – 0.83‰, 325cm – 0.78‰, 315cm – 0.72‰. The most negative values are found at 330cm – 0.23‰ and 305cm – 0.07‰.

There is a lack of correlation between δ ^{18}O and δ ^{13}C until 305cm where the steep negative drop in δ ^{18}O corresponds with a sizeable drop in δ ^{13}C values.

4.3 3, Unit C3 (300-260cm)

Unit C3 is characterised by a sizeable positive – negative swing in δ ^{18}O values with a positive peak at 295cm – 4.92‰ and negative peak at 275cm – 3.13‰.

Positive δ ^{13}C values peak at 295cm – 0.26‰ and then drop significantly negative at 280,275cm - -0.40‰, -0.37‰.

There is a clear correlation between δ ^{18}O and δ ^{13}C values in Unit C3 unlike in Unit C2. The large positive swings in δ ^{18}O and δ ^{13}C values are synchronous with one another in Unit C3.

4.3 4, Unit D4 (260-120cm)

Unit D4 is characterised by a highly fluctuating plot within a small window of values for both $\delta^{18}O$ and $\delta^{13}C$. Positive $\delta^{18}O$ peaks are noted at 195cm – 4.63‰, 190cm – 4.57‰, 155,150cm – 5.47‰ and at 140cm – 4.69‰. Negative peaks are noted at 240cm – 4.05‰, 175cm – 3.93‰, 165cm – 3.95‰, 135cm, 3.93‰.

The most distinctly positive $\delta^{13}C$ value is located at 205cm – 0.41‰. The most negative values are found at 250cm – 0.03‰, 135cm - -0.16‰, 130cm - -0.28‰, 125cm – -0.04‰ and at 120cm - -0.15‰)

There is a subtle correlation between $\delta^{18}O$ and $\delta^{13}C$ in Unit D4 but it is not as evident as it was in Unit C3 or A1.

4.3 5, Unit E5 (120-85cm)

Unit E5 is characterised by a sharp increase in $\delta^{18}O$ values especially with a more subtle fall in values for $\delta^{13}C$. The most positive peak for $\delta^{18}O$ is found at 105cm – 4.84‰, while the most negative is found at 90cm – 3.80‰.

The pattern of peak and trough is more irregular than the clear drop in values seen for $\delta^{18}O$. The positive peak for $\delta^{13}C$ is found at 115cm – 0.12‰ with the most negative values being found at 105 cm - -0.19‰, 100cm - -0.16‰ and at 90cm - -0.09‰

Despite slight differences in the depth of negative value initiation there is still a good correlation between $\delta^{18}O$ and $\delta^{13}C$ positive – negative shifts.

4.3 6, Unit F6 (85-0cm)

Unit F6 is characterised by a negative $\delta^{18}O$ and $\delta^{13}C$ and more positive $\delta^{13}C$ profile. More negative peaks in $\delta^{18}O$ are noted at 60cm – 3.98‰ while the most positively valued peak occurs at 20cm – 3.80‰.

Positive $\delta^{13}C$ peaks are noted at 50cm – 0.62‰, 40cm -0.81‰ and at 35cm – 0.87‰. While the most negatively orientated peaks occur at 65cm – 0.36‰ and 5cm – 0.22‰. Much like in Unit B2 there is a lack of correlation between $\delta^{18}O$ and $\delta^{13}C$ values. More positive $\delta^{13}C$ values correlate with more negative $\delta^{18}O$ values which is the opposite of the correlations seen in Units A1, C3 and E5 where more negative $\delta^{18}O$ values correspond to more negative $\delta^{13}C$ values.

Chapter 5 - Interpretation

This section will concentrate on interpretation of the fluctuations seen throughout HH133-100GC in terms of the various proxies investigated. Particular emphasis is put on Heinrich event structure in the proxy record from start to end of each event independently. The section is divided into each MIS stage decided upon in section 4.4, meaning overlap of lithological, foraminiferal and isotopic 'units' stated in earlier parts of section 4. The depth (cm) and age (cal. BP) will be stated, constraining each MIS, in the title of each upcoming sub-section. Comparisons to other works will only be touched upon in this section; heavy focus will instead be put on this in section 6.

5.1 Construction of an age model and Marine Isotope Stage Boundaries for HH13-100GC

Using linear sedimentation rates, as described in section 2.3, an age model was created based on the assumption of consistent sedimentation rates between calibrated ages as stated in table 1 and plotted in figure 21. With no bottom age for the core, an age was assumed by using the literature and previously conducted studies on cores in the same region (figure 22) (Stein et al, 1996; Lisiecki and Raymo, 2005).

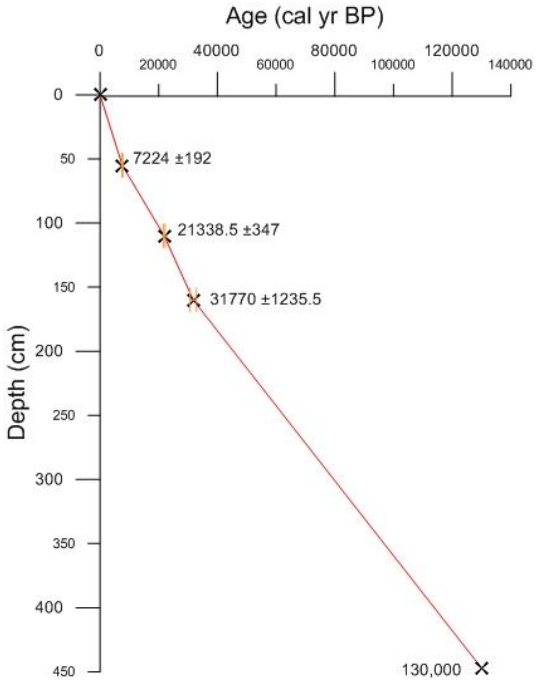

Figure 21 – Age model for HH13-100GC based on C^{14} ages calibrated using Calib 7.10 using the marine13.14 function. The calibrated ^{14}C dates are labelled at the top of the age model, with the final age of 130,000 cal. BP assumed from study of past literature and proxy evidence which suggests said age.

UBA No	Depth (cm)	Sample Type	AMS C^{14} age (BP)	Cal BP
UBA - 34426	55	*N.pachyderma tests*	8560±75	7224.5±192
UBA - 34427	110	*N.pachyderma tests*	19787±127	21338±347
UBA - 34428	160	*N.pachyderma tests*	29724±533	31170.5±1236

Table 1 – Table shows lab number, the C^{14} age and calibrated age used in the age model

MIS Boundaries	Benthic stack ages (cal BP) (Lisiecki & Raymø, 2005)	HH13-100GC ages (cal BP)
1/2	14,000	*14,541*
2/3	29,000	28,272
3/4	57,000	62,561
4/5	71,000	*79,667*
5/6	130,000	*125,854*

Table 2 – MIS boundaries from the benthic stack of Lisiecki and Raymo (2005), compared to those resolved with the age model for HH13-100GC. There are significant variations in the ages for the 3/4 and 4/5 boundary put down to local variation.

MIS 5 Sub-Stages	Benthic stack ages (cal BP) (Lisiecki & Raymø, 2005)	HH13-100GC ages (cal BP)
5a	82,000	*81,378*
5b	87,000	88,220
5c	96,000	95,063
5d	109,000	*108,748*
5e (Eemian)	130,000	*122,433*

Table 3 – MIS sub-stage 5 comparisons between benthic stack ages and ages calculated in HH13-100GC. The Eemian peak has an age 7000 years younger in HH13-100GC but all other sub-stage peaks match near perfectly with the benthic stack.

With a bottom age decided upon (130,000yr BP) and assuming a surface age of ~0yr BP (~1950AD), construction of marine isotope stage boundaries could be undertaken. The isotopic data ($\delta^{18}O$ and $\delta^{13}C$) was reviewed and compared to previous work (Stein et al, 1996) and more importantly the stage boundaries as defined by the benthic stack from Lisiecki and Raymo (2005) (refer to section 1.2). The isotope stage boundaries for HH13-100GC are stated in table 2 and 3 with comparison to the benthic stack boundary ages and peaks of MIS 5 sub-stages. These boundaries are very close to the units defined in section 4.3. With MISs defined, a full lithostratigraphic section for HH13-100GC could be contructed (figure 23).

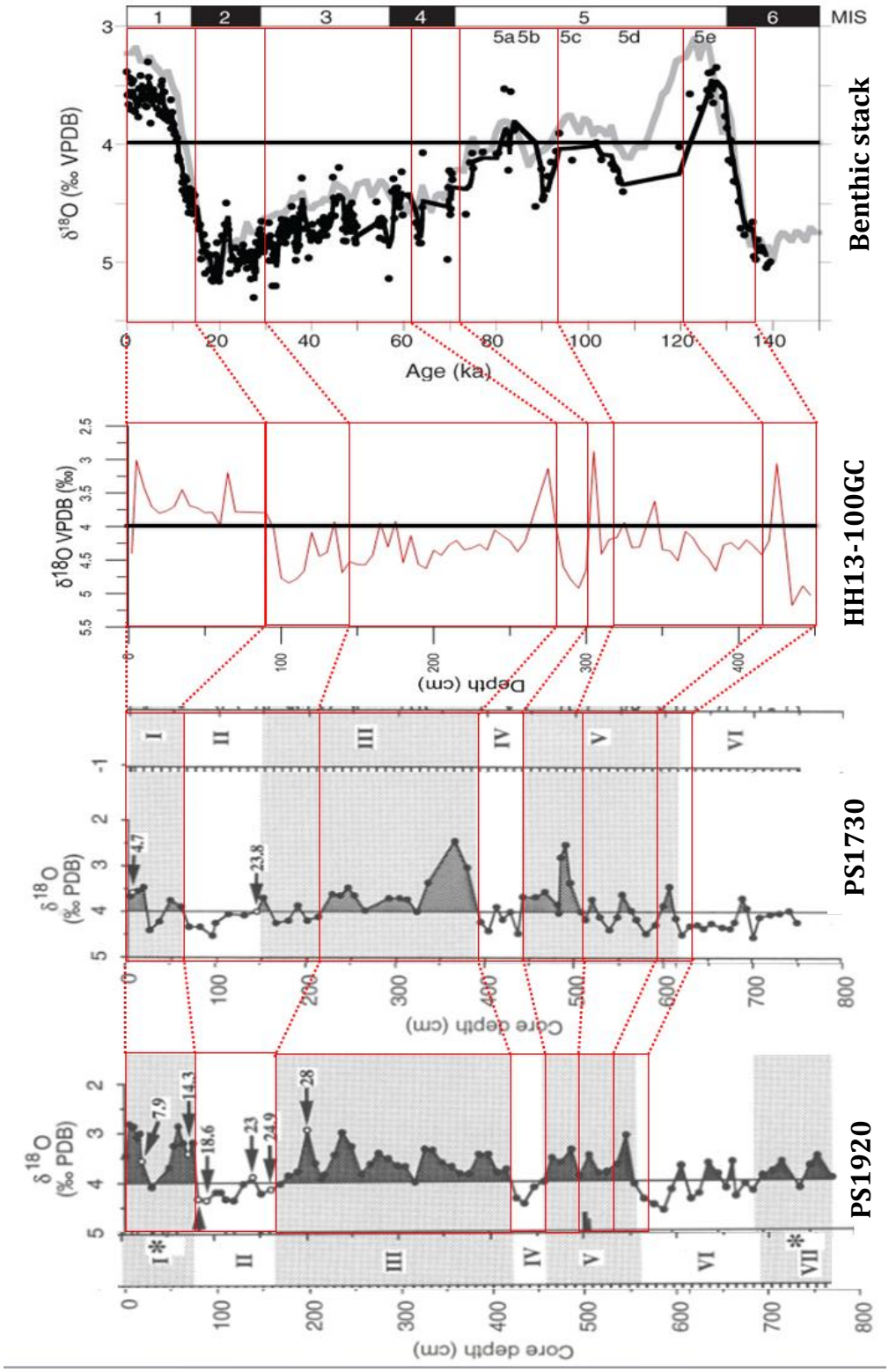

Figure 22 – The $\delta^{18}O$ signal for HH13-100GC compared with that of two other cores from Stein et al (1996) (left) and the benthic stack of Lisiecki and Raymo (2005). Correlation between cores was used to refine the age model and establish a base age.

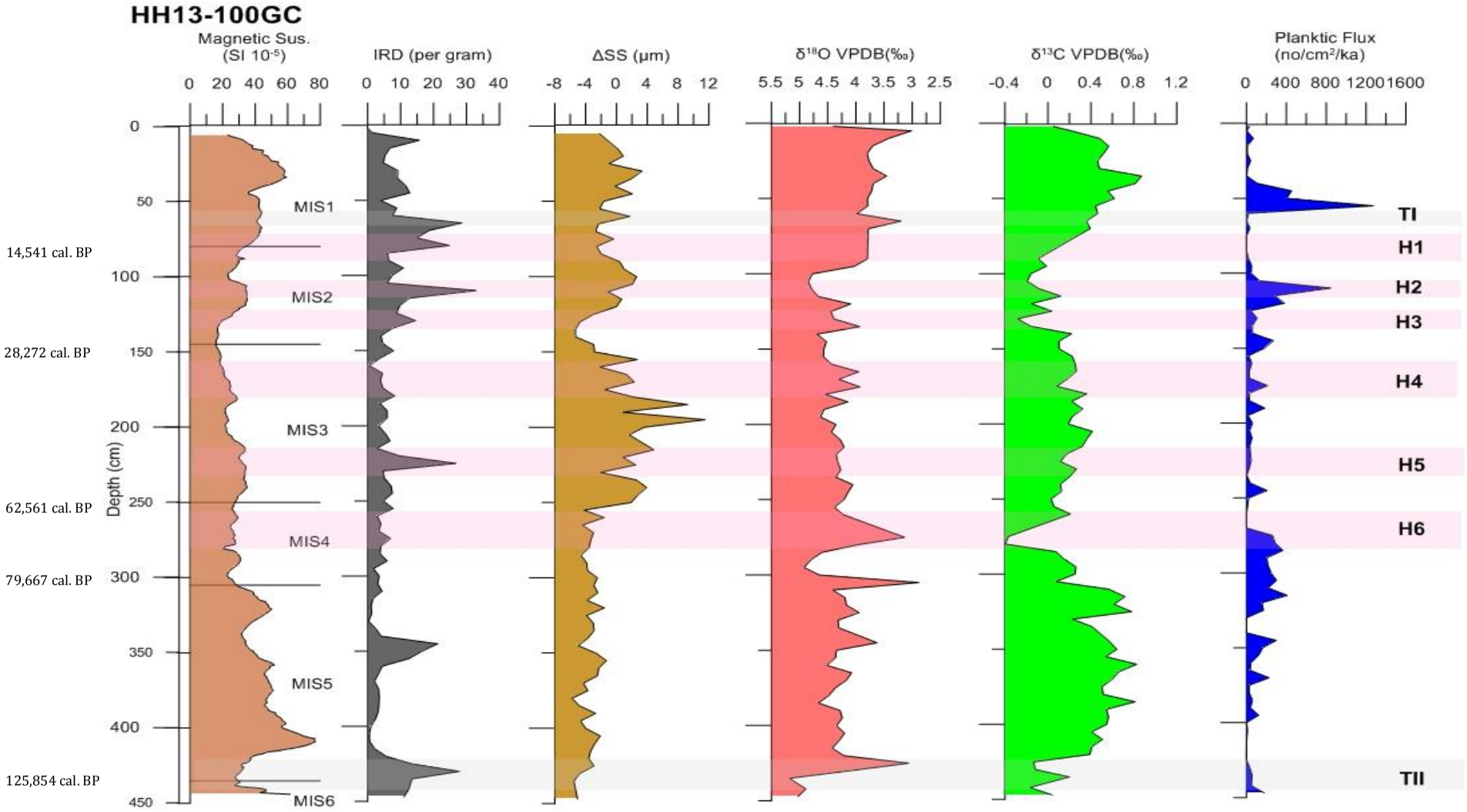

Figure 23 – Graph comparison of proxy data from HH13-100GC with MISs assigned with ages noted to the left. Heinrich events are also defined by the faded pink boxes and glacial termination events are marked by faded grey boxes. Please refer to subsequent sections for more detailed age v data comparisons.

5.2 MIS6 – Late Saalian glacial (~130,000-125,854 cal. BP; 447-435cm)

During this period, $\delta^{18}O$ values are consistently heavy, this corresponds to a lack of freshwater input, low melt rates and the likelihood of land based ice being high (Nam et al, 1995). Generally light $\delta^{13}C$ values indicate a fairly poorly ventilated ocean structure with stratification of the water column likely (Oppo et al, 2006). This is supported by a significant percentage (~30%) of *T.quinqueloba* (temperate species) compared with supressed values of *N.pachyderma* (~70%) (Polar species). This indicates a heavy presence of Atlantic water beneath an assumed ice shelf cover with a layer of polar waters sitting on top with little mixing. This would mean a reduction in the formation of NADW and slowdown of the AMOC during this late stage of the Saalian glacial. This lack of mixing is the likely culprit behind such low planktic flux, as the increased carbon storage in the ocean would have led to more acidic (carbonic) waters meaning a shallower calcite compensation depth and therefore lack of foraminiferal tests reaching the sea floor (Nam et al, 1995). The highest benthic flux for the whole of HH13-100GC are seen during MIS6 and are an indicator for productivity, although weak.

The ΔSS values show a shift from slightly positive to slightly negative values indicating a gradual slowdown in the speed of the EGC velocity.

Moderate and increasing IRD levels with decreasing magnetic susceptibility, are an indicator that perhaps the warmer Atlantic waters were starting to shallow and reach the base of the ice periodically, as you would expect with a decreased AMOC; build-up of Atlantic water (indicated by temperate *T,quinqueloba* appearing abundantly around 127,500 cal. BP).

The light and laminated sediments as seen in the core XRF images are concurrent with glacial sedimentation lacking in organic content.

The main trends of MIS6 are summed up in graph form in figure 24.

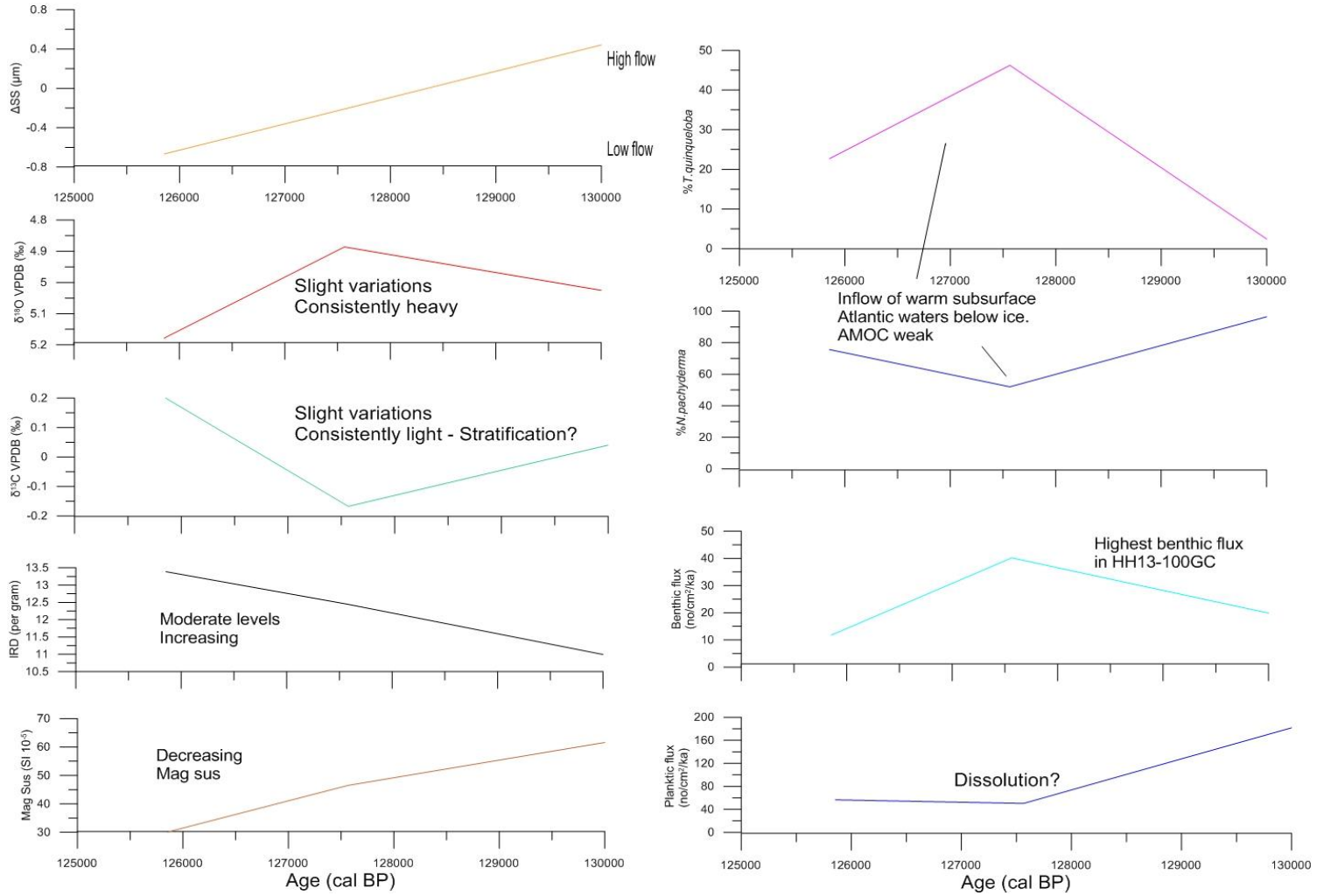

Figure 24 – MIS6 time constrained analysis of proxy data. The main inferences made are labelled on the corresponding graph in question. All ages are in cal. BP.

5.3 MIS5 – Eemian and Early Weichselian (125,854-79,667 cal. BP; 435-300cm)

One of the most striking aspects of MIS 5 is the signal for consistently heavy $\delta^{13}C$ values indicating good ventilation and increased surface water productivity. However low ΔSS values indicate that despite good ventilation the EGC was reduced, with speeds fluctuation from low to high values ~ every 8000 cal. BP. Proxy data indicates MIS5 was a turbulent time for climate and oceanographical change.

The main trends of MIS5 are summed up in graph form in figure 25 (Eemian) and 26.

5.3 1, Saalian glacial termination (TII) (Peak ~125,000 cal. BP; 435cm)

MIS5 initiates with significant IRD values and low magnetic susceptibility indicating a mass wasting event from land and shelf ice systems around 122,433 cal. BP. This marks the termination of the Saalian glacial (TII) and transition into MIS5. Values for $\delta^{13}C$ during this transition are light due to the mass input of freshwater causing stratification of the water column, lack of productivity and a shutdown of the AMOC due to a reduction in deep water formation. Low ΔSS values indicate a significantly reduced EGC flow during this time, consistent with a lack of deep water formation reducing overflow rates of deep water to the deep Atlantic.

5.3 2, Eemain (Peak ~122,433 cal. BP; 425cm)

TII is followed rapidly (~ 200 years) by a significant shift to lighter $\delta^{18}O$ with initiation of increasing $\delta^{13}C$ and lowering of IRD levels. This looks to imply a significant warming period, where initial termination of the glacial is replaced by rapid warming and continued wasting of ice sheets to the extent that IRD values fall as icebergs fail to reach the region or are melted out. After 500 years post event IRD levels fall to 0 indicating both a lack of icebergs or even sea ice in the period 117,000 and 115,000 cal. BP. This can be assumed to be as a result of the well published sub-stage 5e or Eemian warm spike resulting from insolation processes (Van de Berg, 2011, Lohmann et al, 2015 and Pedersen et al, 2016).

The Eemian is also characterized by increased levels of the temperate foraminifera *N.incompta* and *T.quinqueloba* and supressed levels of the polar *N.pachyderma*. This suggests advancement of the Atlantic front and greater influence of Atlantic waters. However, planktic fluxes are very low for this period, potentially due to the massive input of meltwater during TII which would have reduced vertical mixing between surface and deep waters, creating nutrient enriched, less oxygenated conditions causing carbonate dissolution much like was seen during MIS6. This also suggests a weakened AMOC during the Eemian, until ice exhaustion would have led to a return of a stronger AMOC by a shift to more ventilated waters with a greater degree of mixing and deep water formation as indicated by a shift to heavier $\delta^{13}C$ values. This process however, takes ~5000 cal. BP before a return of higher planktic fluxes at 114,000 cal. BP.

XRF imagery of the core shows a significant darker band at the Eemian transition, separating the lighter coloured glacial sediments from darker sediments down-core. This dark banding indicates high organic content during the Eemian, probably as a result of increased temperatures leading to greater productivity of marine organisms in the region supported by a shift to heavier $\delta^{13}C$ values.

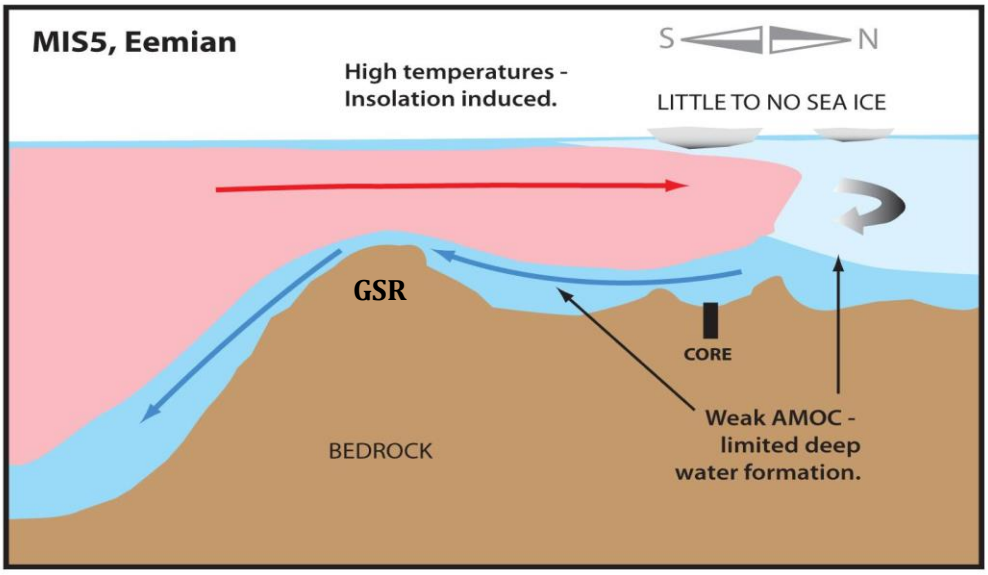

Figure 25 – A schematic representation of oceanographic and surface conditions during the Eemian based on proxy data from HH13-100GC. A significant lack of IRD indicates low sea ice, even ice free conditions during this time. Insolation induced high temepratures combined with lack of sea ice made for inefficient creation of deep water and a more prevelant pushing northward warm Atlantic Intermediate water over the Greenland Scotland ridge (GSR) to the south of the core site. This is only a schematic as warmer Atlantic waters would likely have intruded from the south east, not direct south as the diagram portrays.

5.3 3, Sub-stage 5d (Peak ~108,748 cal. BP; 385cm)

At 108,748 cal. BP there is a slight (~0.2‰) shift to heavier values in both $\delta^{18}O$ and $\delta^{13}C$ indicating a return to cooler conditions with less meltwater input and therefore an assumed increase in land based ice (therefore assigned sub-stage 5d). Planktic foraminifera fluxes start to build again (supported by $\delta^{13}C$ peak; increased productivity) and the influence of Atlantic water, indicated by temperate species, is negligible. A general plateau of IRD (per gram) around 4 and increase in the 100-500μm wt% to around 4% indicates likely seasonal sea ice conditions with only a small increase in ice-rafting of material to the area compared to the ice free conditions apparent ~5000 years prior to sub-stage 5d.

Despite a likely increase in land based ice, ice sheet recovery (post-Eemian) would have required significant time to build an ice sheet capable of producing an ice shelf from Greenland to Jan Mayen, or to support year round sea ice cover. Therefore, sub-stage 5d can be considered to be a stepping stone on the road to ice sheet re-development. Levels of near 100% *N.pachyderma,* a heavy shift in $\delta^{13}C$ values and $\delta^{18}O$ values indicate at least periodic ice cover. The small increase in coarser sediment is seen in the XRF imagery as a lighter band which is distinct but not as distinct as the glacial laminations as seen in MI6. A slightly lighter colouration indicates an increase in the amount of sea ice based detritus falling to the sea floor.

Post sub-stage 5d a shift back to lighter $\delta^{13}C$ values with increasingly lighter $\delta^{18}O$ values match with a significant reduction in the flow of the EGC as indicated by low (~-6) ΔSS values. This may be due to a small increase in meltwater impacting an already weakened EGC.

5.3 4, Sub-stage 5c (Peak 95,063 cal. BP; 345cm)

This sub-stage was decided upon due to a large IRD peak (~23 per gram) and shift in $\delta^{18}O$ of -~0.8‰ and increasingly lighter $\delta^{13}C$. All these factors indicate a large ice sheet collapse episode with reductions in land based ice (probably built up during the colder sub-stage 5d) and input of freshwater into the ocean. This IRD spike coincides with a drop in magnetic susceptibility indicating more than just sea ice influx of material as was likely during sub-stage 5d.

Around 2500 years post IRD/ $\delta^{18}O$ shift there is a peak in lighter $\delta^{13}C$ values and large increase in the occurrence of *T.quinqueloba,* brief disappearance of *N.pachyderma* and low flat-line of planktics fluxes to 90,000 cal. BP. During this time there is also a drop to IRD values of ~1 per gram. This indicates advancement of the Atlantic front and infiltration of Atlantic waters post meltwater peak (sub-stage 5c). This indicates a slowdown in the AMOC and close to surface Atlantic waters in the region. This is supported by a distinct drop in ΔSS values indicting slow-down of the EGC. This appears to be a significant warming event during MIS5 and is recognized in the XRF imagery as series of fine laminations light in colour until ~90,000 cal. BP (reduction in organic content of sediment).

5.3 5, Sub-stage 5b (Peak 88,220 cal. BP; 325cm)

Sub-stage 5b is very similar in characteristics to sub-stage 5d; shift to heavier $\delta^{13}C$ (+0.6‰) and $\delta^{18}O$ (shift degree -0.2‰) values, recovery of planktic foraminiferal fluxes, lack of temperate foraminiferal species and dominance of *N.pachyderma*. All of these factors indicate good ventilation of the water column and high productivity with little influence of meltwater; an efficient AMOC. Supported by a positive spike in ΔSS values indicating increased EGC flow.

One difference is that IRD levels are around 1 per gram for this sub-stage, indicating even less iceberg activity in the region than in sub-stage 5d, and instead, steady seasonal sea ice indicated by a small peak in the 100-500μm grain fraction. The high magnetic susceptibility values (~60SI 10^{-5}) combined with low IRD values are testament to the

lack of ice rafted material reaching the region. The XRF imagery shows a darker band around this time indicating higher productivity (organic content) and less input of IRD.

5.3 6, Sub-stage 5a (Peak 81,378 cal. BP; 305cm)

Sub-stage 5a was identified by significant shifts to lighter values of $\delta^{18}O$ (-1.5‰) and $\delta^{13}C$ (-0.6‰). These indicate a large input of freshwater into the ocean via land based ice loss and a decrease in the ventilation and productivity in the region. Although this only appears to correlate with a slight reduction in planktic fluxes reaching a minimum at 78,000 cal. BP (refer to figure (MIS4)) where a peak in *T.quinqueloba* is seen. This ~3000yr lag is similar to the lag seen post sub-stage 5c with regards to lowering planktic foraminifera fluxes and inflow of Atlantic water/ slowdown of the AMOC indicated by a reduction in the ΔSS values indicating slowdown of the EGC. IRD values are maintained at low levels but magnetic susceptibility shifts (-15SI 10^{-5}) indicate a source region change of the material with a small spike in the 100-500μm there is enough evidence to assume icebergs were drifting and depositing IRD over the region at this time. XRF imagery shows shift to lighter colouration indicating increased IRD levels and decreased organic content (a result of lower productivity).

The reason for the lag between meltwater influx and increasing influx of Atlantic water is a difficult one to decipher. A simple explanation could be simply that once iceberg exhaustion occurs, a return to deep water formation pulls Atlantic water northwards. This is unlikely though, as a shift to heavy $\delta^{18}O$ values in MIS4 would indicate creation, not exhaustion of seasonal ice over the region. The reason for Sub-stage 5c and 5a initiation is difficult to quantify as there is no real indication of Atlantic water influx prior to these 'events' which could destabilize ice sheets and facilitate iceberg generation (Broecker et al, 1992 Bond et al, 2001).

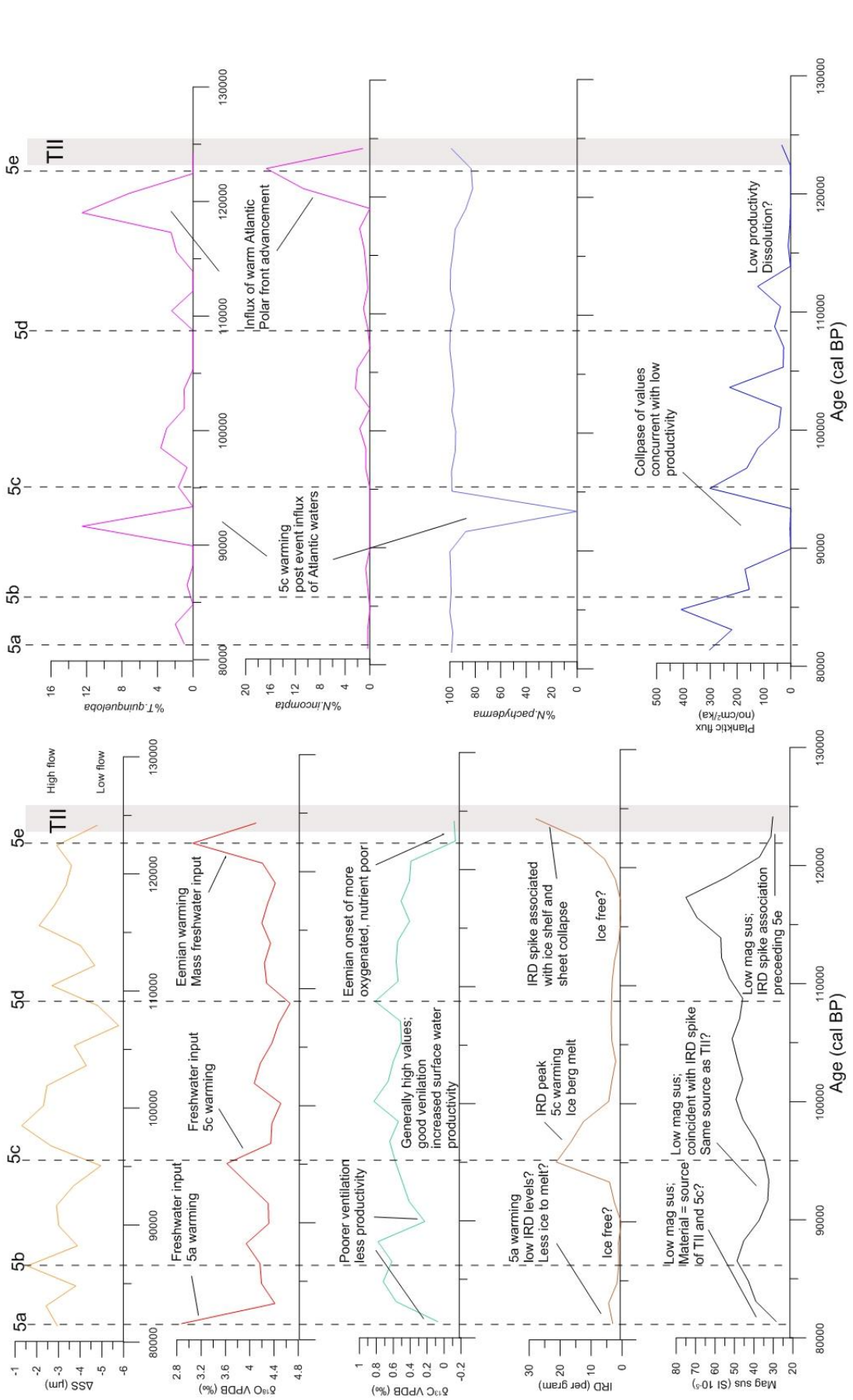

Figure 26 – MIS5 time constrained analysis of proxy data. The main inferences made are labelled on the corresponding graph in question. All ages are in cal. BP.

5.4 MIS4 & Heinrich Event 6 – Upper Mid-Weichselian (79,667-62,561 cal. BP; 300-250cm)

MIS4 starts with a positive shift in $\delta^{18}O$ (+2‰) and maintenance of low $\delta^{13}C$ values peaking around 78,000 cal. BP. This would indicate initiation of ice formation at the surface with a lack of meltwater and a poorly ventilated subsurface with stratification developing. This is supported by a consistent abundance of *T.quinqueloba* indicating a layer of sub-surface Atlantic water which appears to periodically reach the base of the ice, indicated by heightened IRD counts ~76,000 cal. BP. Sustained low ΔSS values indicate an inefficient flow of the EGC and therefore an indication of a lack of deep water formation until the very end of MIS 4 ~ 63,000 cal. BP. The sediment colour in the XRF images for the period 80,000-74,000 (300-280cm) is very light in nature, an indication of colder, low organic production sedimentation.

The main trends of MIS4 are summed up in graph form in figure 27.

5.4 1, Heinrich event 6 (H6) (Peak – 71,500 cal. BP; 275cm)

Heinrich event 6 is identified by a rapid shift to lighter isotope values; $\delta^{18}O$ (-2‰) and $\delta^{13}C$ (-1‰). A small peak in IRD (+3 per gram), low mag sus values (~28SI 10^{-5}) and a collapse of foraminiferal fluxes to 0 by 69,000 cal. BP all indicate a major freshwater impulse event, resulting in a highly stratified water column, poorly ventilated subsurface, low productivity and near shutdown of the AMOC with lack of mixing/ deep water formation. Values for ΔSS stay negative during this event indicating low EGC flow as has been a consistent feature throughout MIS6, 5 and now 4. A rapid decrease in land based ice, as suggested by the significant $\delta^{18}O$ shift, indicates ice sheet collapse on mega-scale within a window of only ~300 years. A large, heavy dropstone (4cm width, 2cm height) with metamorphic properties is present in the core at ~275cm and is likely connected to H6 along with abundant dolomite seen in the 500µm->1mm size fractions. There are indications that the rock texture could be of microbial mat origin. This would require the rock to be of significant age, potentially even Archaen which is concurrent with the base rock type of the upper margins of Scorsbysund fjord on the Eastern Greenland coastline due west of HH13-100GC (Henricksen, 2008). The XRF images show

a clear shift from the light sediments to darker laminated sediments likely due to an increase in terrigenous input into the system.

What is significant is the pre-mentioned prevalence of *T.quinqueloba* as an indicator of Atlantic water in the subsurface prior to the H6. A stronger AMOC pulling in significant sub surface Atlantic water levels prior to the event may have resulted in a shallowing of the Atlantic water, enough to melt the basal regions of ice shelves on the continental slope, potentially resulting in irreversible ice stream speed up and ice sheet collapse.

Post H6 sees a recovery to heavier isotopic values within 500 years, but maintenance of low planktic flux values and sustained high IRD levels indicate that icebergs were present and shedding material over the region many centuries after the main event.

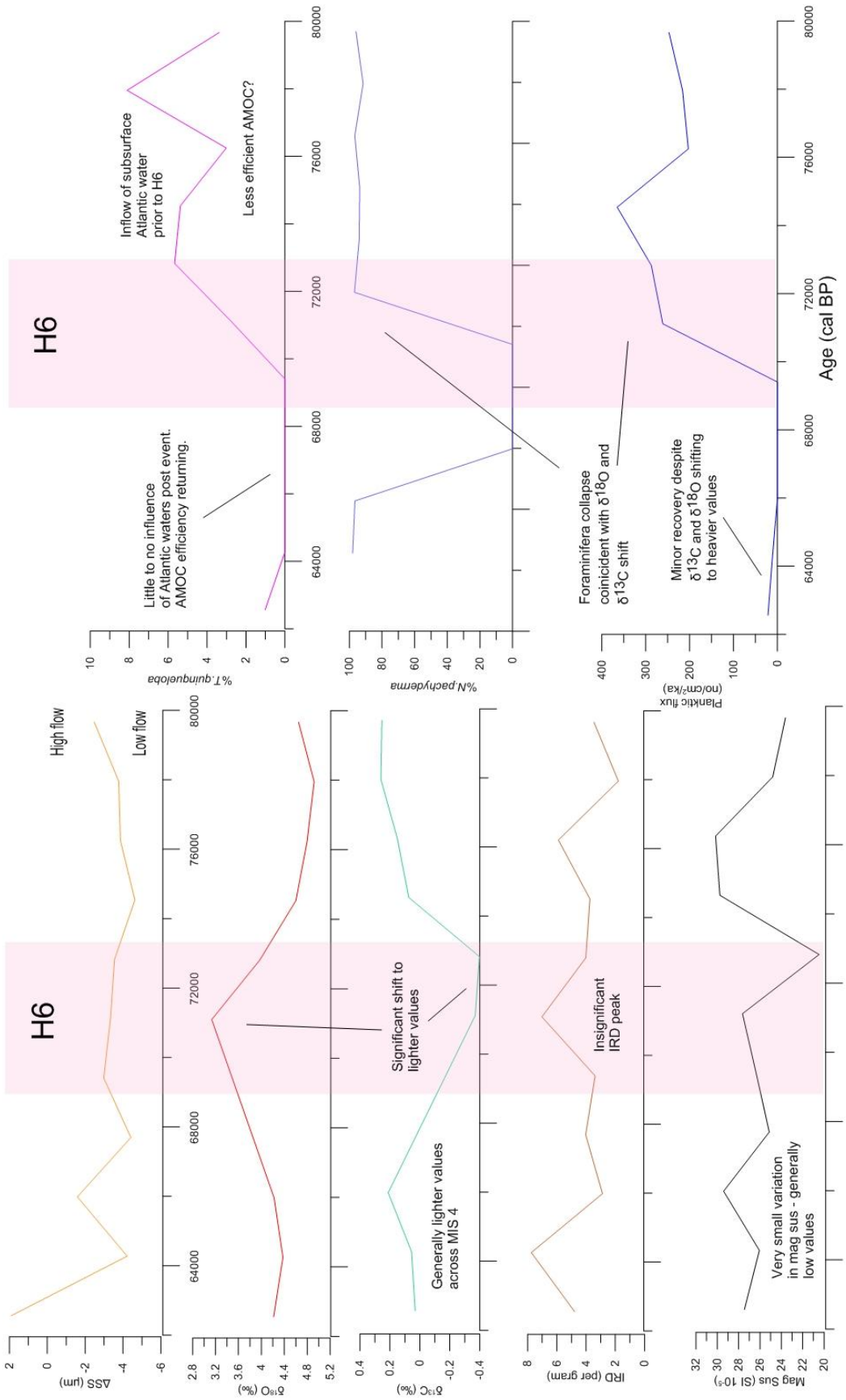

Figure 27 – MIS4 time constrained analysis of proxy data. The main inferences made are labelled on the corresponding graph in question. All ages are in cal. BP.

5.5 MIS3 & Heinrich events 5, unknown and 4 (62,561-28,272 cal. BP; 250-145cm)

MIS3 is characterised by chaotic shifts in isotope values and generally low planktic fluxes, including indications of periodic Atlantic front advancement and retreat. The most efficient way to interpret the MIS3 record is to discuss it in terms of two evident Heinrich events and another third possible event between H4 and H5. Laminated sediments are present throughout MIS in XRF imagery indicating fluctuating environmental conditions.

The main trends of MIS3 are summed up in graph form in figure 28.

5.5 1, Heinrich event 5 (H5) (Peak – 55,000 cal. BP; 230cm)

Onset of Heinrich event 5 was difficult to constrain due to a weak isotopic signal for the event but significant IRD peak. Another curiosity is collapse of planktic flux values around 2000 cal, BP years prior to the IRD spike.

Starting with isotopic data, $\delta^{18}O$ shows very little change, fluctuating between 4.2‰ and 4.4‰, meanwhile $\delta^{13}C$ shows a slight shift to lighter values (-0.15‰). Therefore, the signal for increased meltwater is fairly muted, and only slight reductions in productivity/ a slight increase in stratification is indicated by $\delta^{13}C$. A low ΔSS shift indicates that the EGC did suffer a significant slowdown during this event (change of ~-6μ). An IRD peak and very low planktic values during this period are markers for the H5 more than the isotopic proxies. Perhaps lower iceberg levels were present at this time, meaning less meltwater, but an increase in the IRD content of the icebergs themselves occurred. The anomalous abundance of a red, possibly volcanic, lithology in the record at this time period in the 500μm to >1mm size fraction is further weight behind the argument that this was not an insignificant event. A change in lithology from the abundant grey carbonates which dominate nearly every section of HH13-100GC signifies a change in the source region and magnitude of ice transport to the region. This is an unknown and could be an anomaly as all other proxies suggest a meltwater event during H5.

Like H6, H5 is preceded by an increase in the abundance of a temperate foraminifera species, *N.incompta* suggesting, just like in H6, a build-up and shallowing warmer Atlantic water indicating a stronger AMOC prior to H5. A peak in *T.quiqueloba* occurs simultaneously with the IRD peak, again an indication of shallow Atlantic waters causing basal buttress failure of ice streams along the Greenland margin. Therefore it can be concluded that H5 initiated while a high efficiency AMOC was in place.

5.5 2, Unknown event (H?) (Peak - 46,000 cal. BP; 200cm)

Around 9000 cal. BP, a significant shift to lighter $\delta^{13}C$ values (-0.2‰) occurs again with little change in $\delta^{18}O$ values. This period is simultaneous with a lowering of planktic fluxes and is preceded by a peak in the percentage of *T.quinqueloba.* Following the trends of H6 and H5. Although no peak in IRD is present, there is a significant shift in the magnetic susceptibility to lower values (-10SI 10^{-5}) indicating a change in the source region of iceberg delivery (Robinson et al, 1995). Indeed, the 500μm->1mm grain size fraction shows an increase in red and pink lithologies at this time interval. It is possible that H5 was a two staged event, with initial large ice sheet collapse followed by a second event in response to a seriously weakened AMOC which did not recover post the initial H5 event. This is indicated by a continued presence of *T.quinqueloba* right up to ~500 years prior to this shift to lighter $\delta^{13}C$ values.

5.5 3, Heinrich event 4 (H4) (Peak - 34,000 cal. BP; 165-170cm)

Heinrich event 4 is more of a classical event compared to H5 with regards to its isotopic signature. A large shift to lighter $\delta^{18}O$ (+1.2‰) indicates an impulse of freshwater and reduction of land based ice, while a shift to lighter $\delta^{13}C$ (-0.3‰) values indicates lower productivity and an increase in stratification. This interpretation is backed up by the collapse of planktic values, consistent with the onset of H4 ~37,000 cal. BP. ΔSS value fall is also an indicator of a lack of deep-water formation and a slowing EGC. IRD levels are fairly low ~6 grains per gram with a gradually decreasing magnetic susceptibility.

Yet again, there is a peak in *T.quinqueloba* around 100 years prior to shifts in $\delta^{18}O$ and $\delta^{13}C$. An apparent consistent theme, an efficient AMOC with northward flow of warm subsurface Atlantic waters prior to the event and gradual return of efficiency post or even in the late stages of the event, indicated by a fairly rapid (+0.2‰) return to heavier $\delta^{13}C$ within a 1000 year time frame, can be used as an explanation for the onset of H4 as was the case for H5 and H6.

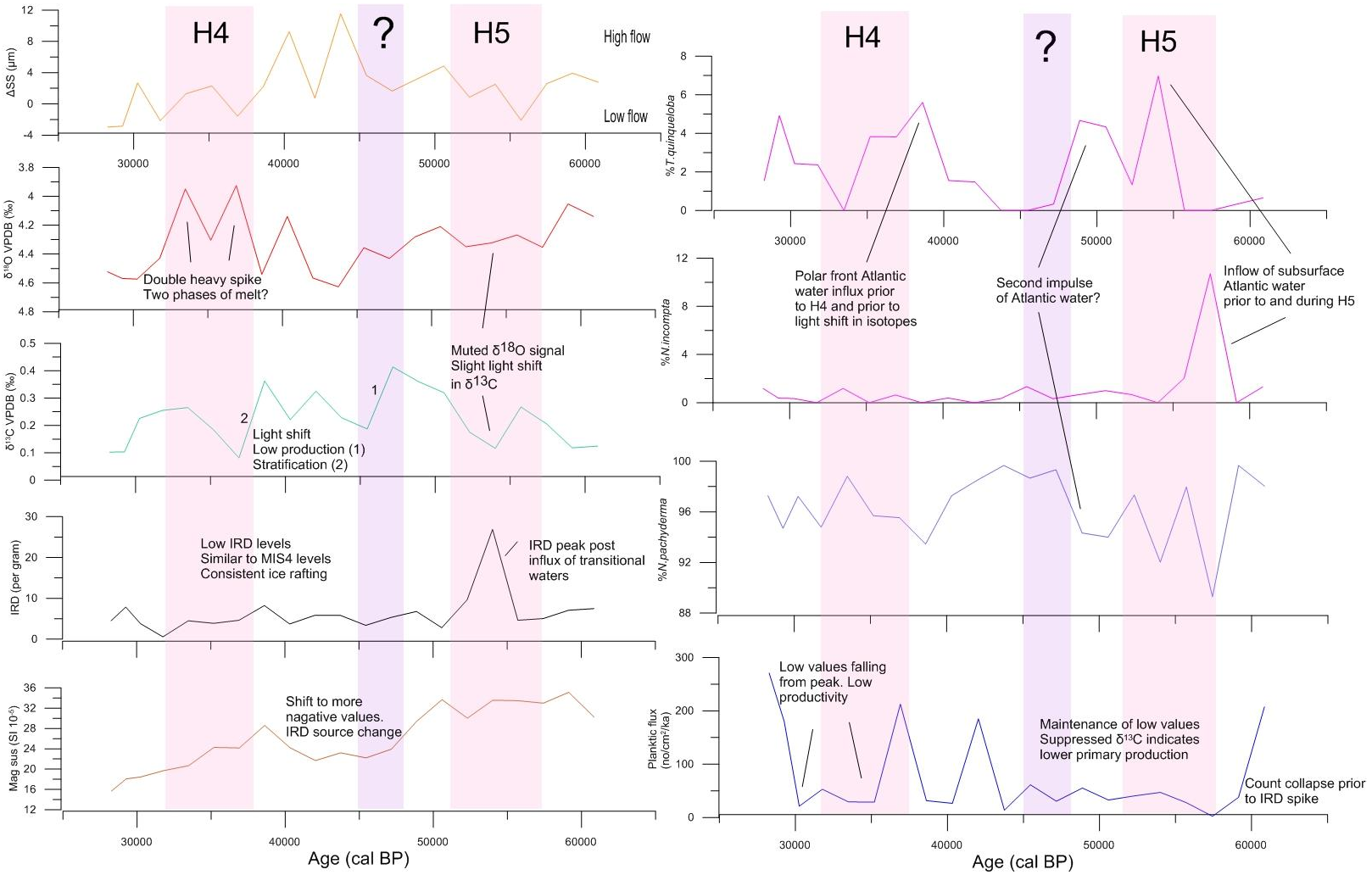

Figure 28 – MIS3 time constrained analysis of proxy data. The main inferences made are labelled on the corresponding graph in question. All ages are in cal. BP.

5.6 MIS2 & Heinrich events 3, 2 and 1 (28,272-14,541 cal. BP; 145-80cm)

MIS2 is characterized by generally light $\delta^{13}C$ values and heavy $\delta^{18}O$ values indicating periodic ice cover during much of this period with a stratified water column and generally low productivity and weakened AMOC. The sediments in the XRF imagery appear much lighter than the sediments in MIS3 and are more closely connected into the colour shades seen in MIS4 and MIS6, indicating that MIS2 was a cold, ice cover dominated period.

The main trends of MIS2 are summed up in graph form in figure 29.

5.6 1, Heinrich event 3 (H3) (Peak – 27,000 cal. BP; 140cm)

Heinrich event 3 occurs at the MIS3/2 boundary with the classic shift of $\delta^{18}O$ to lighter values (-0.8‰) with a delay of ~900 years before peak light $\delta^{13}C$ (-1.2‰) occurs. This indicates an increase in freshwater and reduction of land based ice with reduced AMOC efficiency. This is supported by low planktic fluxes and elevated percentages of *T.quinqueloba* which indicates the northward movement of the Atlantic front and shallowing of the intermediate Atlantic waters as discussed in previous Heinrich event sections. Slowdown of the EGC is also indicated very low ΔSS values. A significantly low magnetic susceptibility value of ~16SI 10^{-5} is noted during this event and correlated with an abundance of dark coloured volcanic rocks noted in the 500μm-1mm grain size fraction. These may be connected to the basaltic rocks on the southern mouth of the Scorsbysund fjord, a paleo-ice stream channel (Vanneste et al, 1995).

5.6 2, Chalk and chert appearance (25,300-22,232 cal. BP; 130-115cm)

The IRD size fraction (500μm->1mm) shows a significant abundance of chert and chalk grains between H3 and H2. With a small shift to lighter $\delta^{18}O$ and $\delta^{13}C$ values and generally elevated IRD levels there is evidence here of a small meltwater event. However, chalk and chert are not a lithology associated with the East Greenland coast and are instead associated commonly with North Sea sourced Heinrich layer deposition

(Hebbeln et al, 1994). An increase in the flow of the EGC indicated by increasing ΔSS values could indicate that post H3 increased northerly flow of Atlantic water pulled northeward by AMOC reassertion, carried icebergs from the North Sea region as indicated by heightened levels of *N.incompta.*

5.6 3, Heinrich event 2 (Peak – 21,500 cal. BP; 110cm)

Heinrich event 2 is indicated by a shift to lighter $\delta^{13}C$ values (-0.6‰) and maximum IRD peak (34 per gram) around 21,500 cal. BP. The $\delta^{18}O$ signal is muted with a minor shift to heavier values, indicating a reduction in the amount of meltwater addition. A collapse in planktic fluxes at the time of IRD peak levels and the pre-stated fall in $\delta^{13}C$ values do indicate that productivity fell and a reduction in mixing of surface to deep water masses (stratification) was occurring at this interval. A small low peak in the ΔSS values could also indicate increased stratification with a lowering of EGC velocities and lack of deep-water formation. An increase in the presence of the temperate species *N.incompta* just prior (within 300 years) to H2 is akin to the previously mentioned hypothesis for subsurface intrusion of Atlantic water prior to Heinrich events 6,5,4 and 3.

The lack of a signal in the $\delta^{18}O$ values could indicate that meltwater rates were low but content of terrigenous material in the ice above was high. No significant shift signal could suggest that complete ice break up did not occur during this Heinrich event, and that only basal regions of an existing extensive surface ice were melted. After all, this period is noted as the last glacial maximum, so temperatures were likely low, even with a sub-surface upward projection of warmer Atlantic intermediate waters. Perhaps the location was within a zone of ice stream projection from the Greenland coast. An increase in the IRD content matches a dramatic increase in magnetic susceptibility values (+18SI 10^{-5}), indicating a shift in the source area of IRD material compared to the low values for H3. The material within the 500μm->1mm was noted as red, beige and grey carbonate material. These lithologies match the base-rock in the area Jameson Land, Scorsbysund, Eastern Greenland identified by numerous authors such as Piasecki et al, 1984 and Wignall et al (2002) where ice stream activity is said to have been significant.

5.6 4, Heinrich event 1 (Peak – 15,000 cal. BP; 85-80cm)

At 17,000 cal, BP. there is complete loss of planktic foraminifera, not recovering from the collapse in values at the end of H2. Although abundances of *T.quinqueloba* and *N.incompta*do increase prior to this collapse, suggesting again, northward progression of the Atlantic front prior to the Heinrich event.

Due to the absence of foraminifera, isotopic data is not available for the period 17,000 to 12,100 cal. BP. Therefore a significant IRD spike and reduction in the EGC flow as suggested by decreasing ΔSS values, along with the collapse in foraminifera fluxes are used to indicate Heinrich event 1 here. A shift to higher values of magnetic susceptibility also indicate a return to the IRD source region of H2, although investigation of the IRD grain sizes reveals, if anything, darker, more volcanic material amongst the grey carbonate limestone constant.

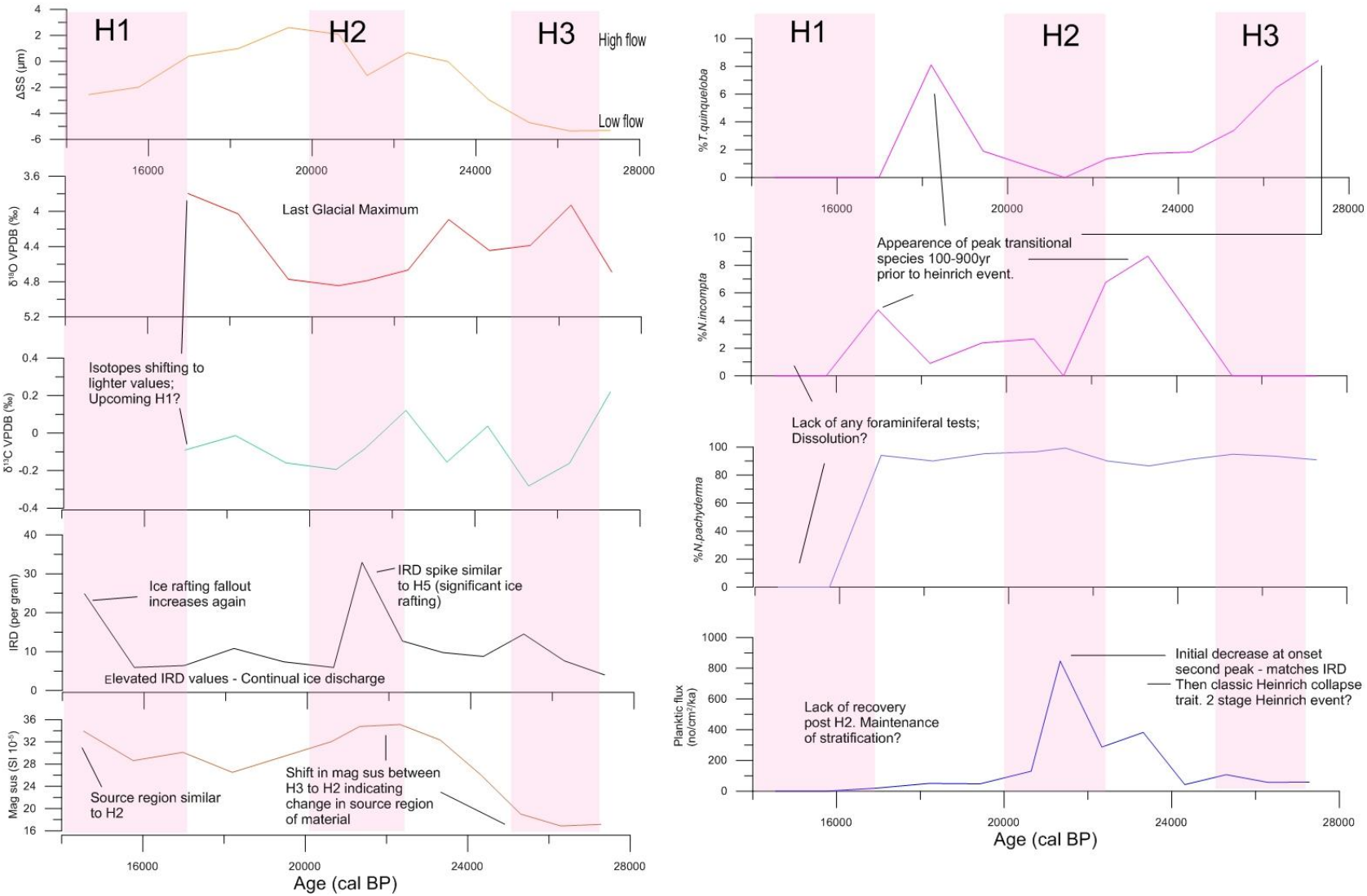

Figure 29 – MIS2 time constrained analysis of proxy data. The main inferences made are labelled on the corresponding graph in question. All ages are in cal. BP.

5.7 MIS1 – Holocene (14,541-~0 cal. BP; 80-0cm)

The transition between MIS2 and MIS1 is usually marked by the appearance of the Bølling-Allerød warming (Broecker, 1998). However with a lack of isotopic data during and either side of this event in the stratigraphy, based on previously published dates, along with a poor proxy record for the transition, it would be unwise to draw conclusions about the conditions during this event in HH13-100GC. The following Younger Dryas period (Fairbanks, 1989) is represented by heavier $\delta^{18}O$ becoming lighter towards the end of the event, with a consistently low $\delta^{13}C$ value indicating low levels of deep water formation rates by lack of mixing. This is supported by a shift to lower ΔSS values as the event progressed, meaning a reduction in the EGC speed. An IRD peak around ~10,200 cal. BP indicates the end of the Younger Dryas with wasting of land based ice break up/ ice-berg delivery to the region. Post Younger Dryas planktic (per gram) values recover significantly around 8000 years timed with returned flow of the EGC indicated by rapidly increasing ΔSS values.

The Holocene era is dominated by relatively light $\delta^{18}O$ levels indicating a consistent supply of meltwater to the area and sustained loss of land based ice. Generally heavy $\delta^{13}C$ values, similar in trend to MIS5 indicate good ventilation and good productivity especially around the 6000-4000 cal. BP period. This matches with values of ~0 for ΔSS which indicate a moderate efficiency intensity of the EGC at this time. Elevated IRD values support the interpretation that wasting of land based ice and melting of icebergs was a persistent feature of the Holocene.

A minor melt event looks to have taken place around the 5000 cal. BP time, with a low spike in magnetic susceptibility values and a small shift to lighter $\delta^{18}O$ (-0.2‰) followed by a lightening of $\delta^{13}C$ values (0.4‰). At this time the planktic fluxes collapse to near 0 after the post YD peak. A consistent signal for Atlantic water influence in the region is indicated by the presence of *N.incompta*, *T.quinqueloba* and for the first time in HH13-100GC; *G.bulloides.*

End values for the Holocene indicate a significant shift to lighter $\delta^{18}O$ and $\delta^{13}C$ values and decreased flow of the EGC. This could potentially represent the 'little ice age' period, with lower magnetic susceptibility values indicating a change in sediment input as opposed to the large spike at 3500 cal. BP (~60SI 10^{-5})

The main trends of MIS1 are summed up in graph form in figure 30.

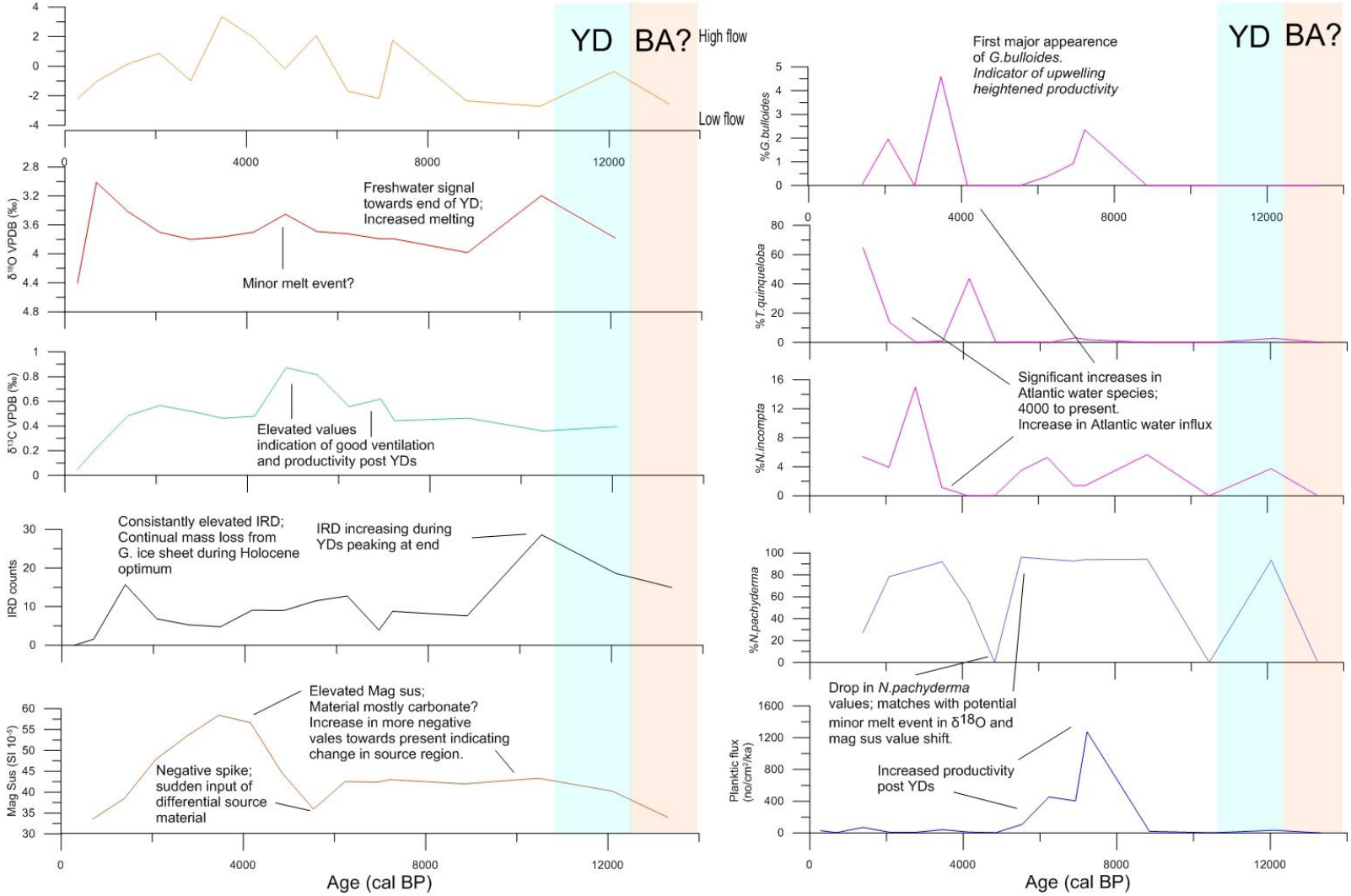

Figure 30 – MIS1 time constrained analysis of proxy data. The main inferences made are labelled on the corresponding graph in question. All ages are in cal. BP. The Bølling Allerød (BA?) is placed in the location that previous works have dated the time period, meanwhile evidence for the Younger Dryas (YD) can be seen in the section.

5.8 Summary of Heinrich event morphology

There are three persistent themes prior to and during Heinrich events identified in HH13-100GC. These are the appearance of temperate foraminifera forms peaking just prior to the Heinrich event, a near complete drop in planktic fluxes and evidence of a slowdown in the EGC based on ΔSS values during the event. These trends are present in all Heinrich events identified in this core, summarized in figure 31a and b.

Isotopic trends are clear in Heinrich events 6,4,3 and 1 with a shift to lighter values of $\delta^{18}O$ and $\delta^{13}C$ indicating meltwater and lowering productivity. However H5 and H2 show little variation in isotopic signature. This could be an indication that meltwater injection was less during these events, although this is strange, as peak IRD levels are found in both these Heinrich events. Lesser IRD levels are found in all other Heinrich events In HH13-100GC. A potential explanation for this could be that there were higher IRD content of the icebergs themselves during these Heinrich events resulting in greater fallout despite lesser meltwater outflow. Heinrich event H5 and H2 hold lithological components (red and coloured limestones) in far higher abundances than during H6,4,3 and 1 where differing lithologies were found. Heinrich events 5 and 2 may therefore have had a much closer source region for iceberg development than all other Heinrich events in this region. Meaning a shorter residence time for icebergs in the ocean and thereofre higher material fallout despite less icebergs as suggested by the lack of change in the isotopic signature. This is why it is important to consider lithological investigation when looking into Heinrich layers, not only in this region but also elsewhere, in order to build a lithological framework of source material. From this, it is possible to connect source regions and ice stream collapse zones for each event, although this would be a goliath task.

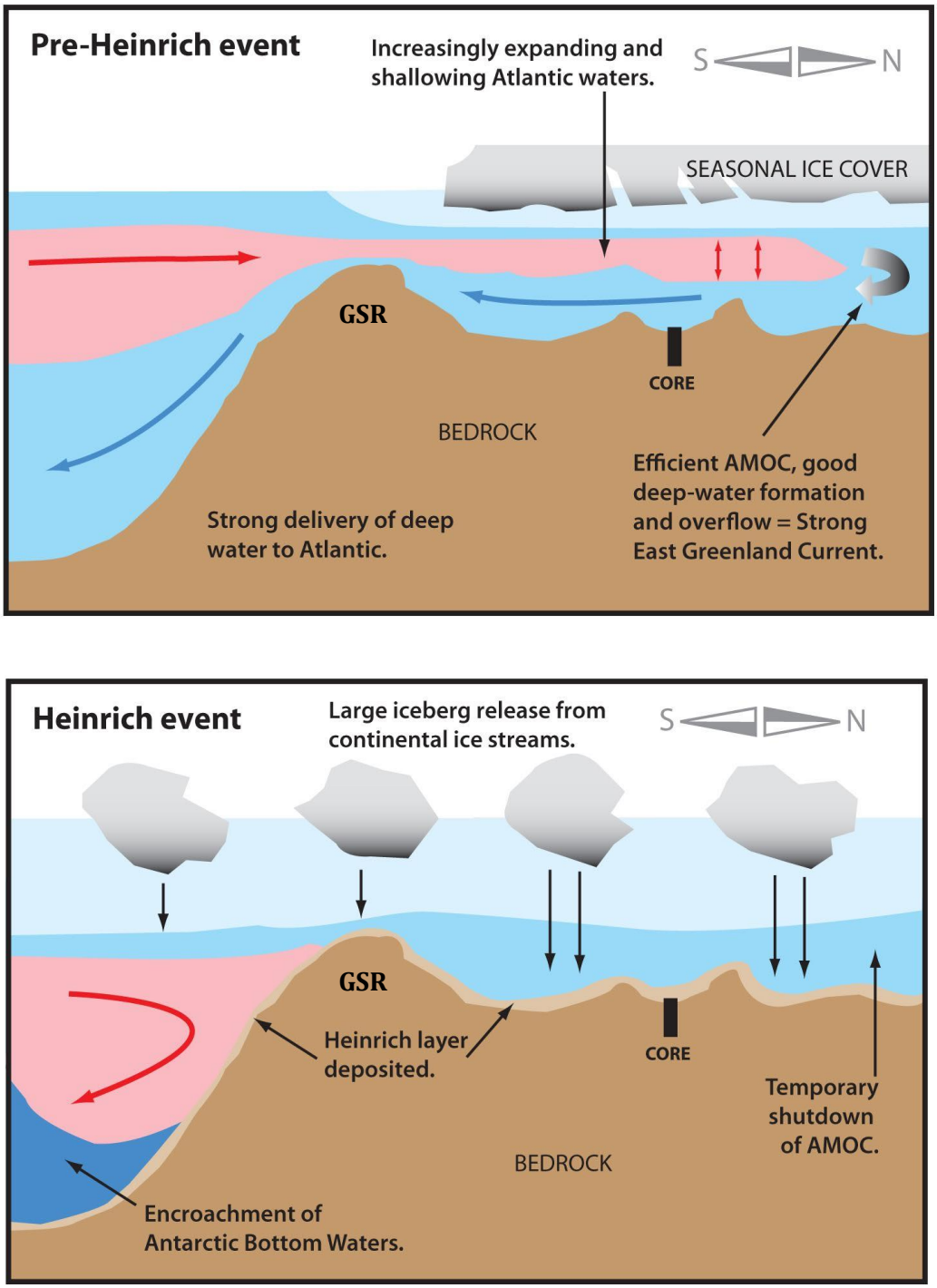

Figure 31a, b – Schematic diagrams of pre and peak Heinrich event modes of water column structure. Pre-Heinrich event (a) has an efficient AMOC pulling in warm Atlantic Intermediate Waters northward into the Greenland seas beneath the ice cover and assumed ice shelves on the Greenland coast starting the process of melt. During Heinrich events mass ice shelf collapse resulted in large armadas of icebergs dropping IRD onto the sea floor creating a Heinrich layer. The massive input of freshwater shuts down or significantly weakens the AMOC restricting inflow of Atlantic waters to the Greenland Sea.

Chapter 6 - Discussion

This chapter is split into four sub chapters. The first chapter will be concerned with the comparisons of HH13-100GC with previously conducted work in the region. The second sub chapter will focus on comparisons with the NGRIP core from Greenland. The third sub chapter will primarily concentrate on MIS 4, 3 and 2 with regards to Heinrich event initiation and the effects not only on regional but also global scale inferred from HH13-100GC proxies. The final sub chapter will try to draw parallels with Heinrich event initiation in the past and the present day mass collapse of ice shelves and sheets globally. One is referred to chapter 1, sub-chapter 1.2 for the comprehensive history of the area in question, this will not be repeated here.

6.1 Comparisons to previous sediment core records

HH13-100GC is one of the first deep sea sediment cores to have been taken and investigated thoroughly within such close proximity to Jan Mayen, on the transition region between the EGC and northward movement of Atlantic waters. The closest, and Fram Strait based, deep sea sediment and shelf edge cores were taken during the R.V. Polarstern ARK V/3 in 1988 (Figure 32) (Nam et al, 1995; Stein et al, 1996). Two of these cores (PS 1730 to the west and PS1726 on the shelf slope west of PS 1730) will be used in conjunction with HH13-100GC to quantify the interpretations made in chapter 5 (figure 33).

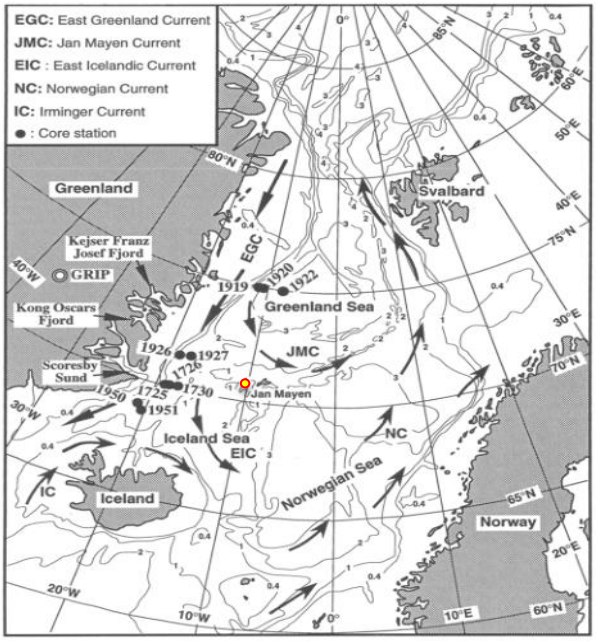

Figure 32 – (From Stein et al, 1996) shwoing the positions of the cores used in this study (PS1730 and PS1726 for comparison to HH13-100GC. The position of HH13-100GC is noted by the yellow marker with red border.

Magnetic susceptibility records are only available for the shelf slope (PS1726) but show remarkable similarities to the record in HH13-100GC albeit with more elevated values. Nam et al (1995) argues that these fluctuations in magnetic susceptibility are due to changing source regions of material delivery, an argument confirmed by the changing lithologies seen during peak and troughs in the HH13-100GC record. However, IRD spikes in the PS1726 are not consistent with the spikes seen in HH13-100GC and are more closely related to those seen in PS1730. This would appear to suggest that deposition of IRD occurred to different extents and perhaps also at different time intervals than it did in shelf regions. This is supported by Nam et al (1995) who argues that more frequent events would occur in shelf regions due to closer proximity of ice shelf collapse and retreat compared to more distal locations that would be affected significantly less. With such close links to the magnetic susceptibility records of HH13-100GC and PS1726 Nam et al's (1995) argument is tested, as the striking similarity in both cores would lead one to assume that shelf to deep sea events were synchronous and occurring during the same timeframe.

The darker volcanic material noted in Heinrich event 3 in HH13-100GC may have instead originated from further north on Greenland's east coast as suggested by Hebbeln et al, 1998. Icebergs moving down from the north, would bypass the densly packed icefield of the shelf region and flow further out where cores HH13-100GC and PS1730 are located. Although this cannot be independently confirmed by observations in this work alone, and would need extensive lithological investigation of IRD grains in sediment cores across the Fram Strait and farther afield regions.

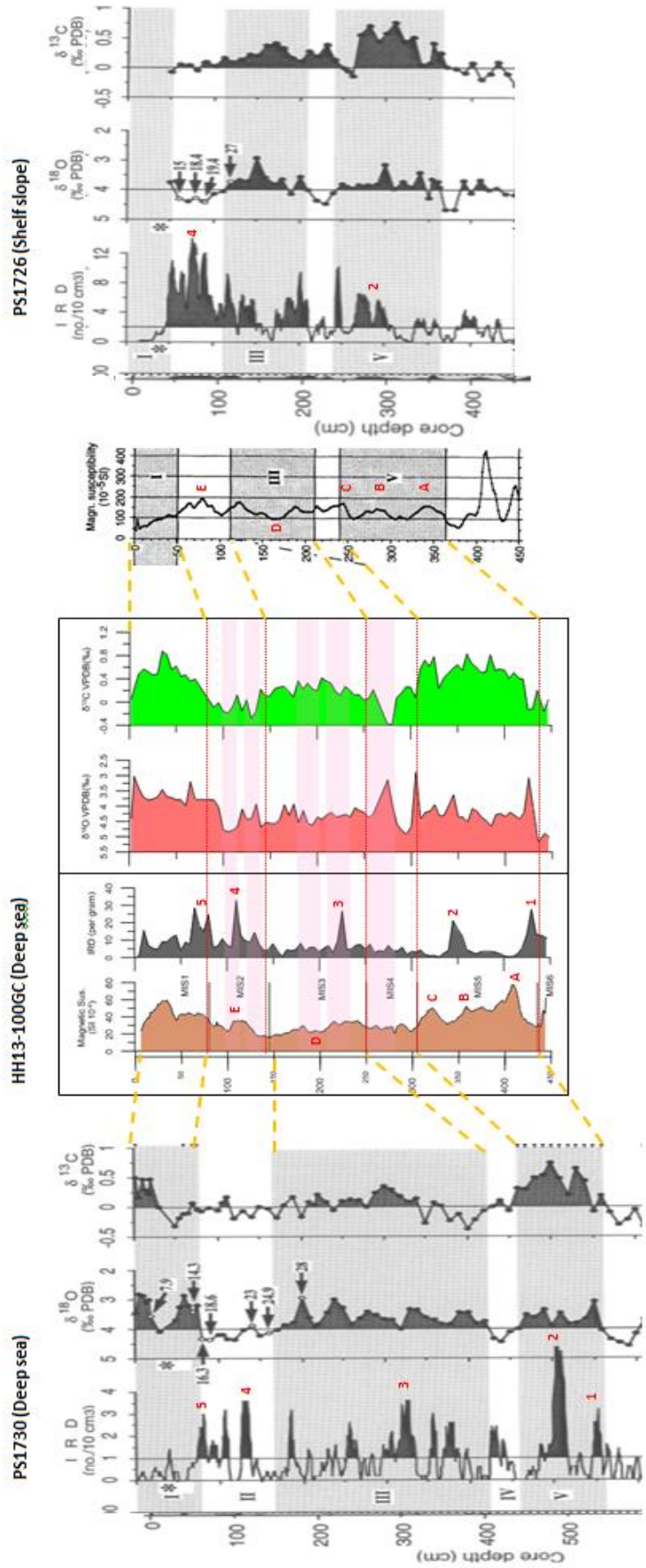

Figure 33 – A comparison of cores PS1730, HH13-100GC and PS1726 in that order from left to right. IRD peaks in HH13-100GC are correlated to the other two cores in the form of red numbers. The magnetic susceptibility records are correlated from PS1726 to HH13-100GC in the form of red letters with A,B,C and E representing high peaks and D represeting a low peak.

The isotopic similarities between PS1730, PS1726 and HH13-100GC are uniform with only two areas of contention. The first comes at the end of MIS5, where HH13-100GC shows a strong signal for meltwater (light $\delta^{18}O$) at the sub-stage 5a 'event'. Both PS1730 and PS1726 show a much more flat-line trend with PS1726 barely showing any signal at all. HH13-100GC is the farthest from the shelf of all 3 cores, therefore it is assumed that the large peak seen in HH13-100GC is more evident due to being located in an area where higher melt rates would be assumed. As in this region greater influence of Atlantic water from the east would likely be present compared to the western cores.

The second area of contention comes after MIS 4, where recovery of $\delta^{13}C$ values is seen in HH13-100GC and PS1726 but remains significantly light in PS1730. Nam et al (1995) argues that these lighter $\delta^{13}C$ values in PS1730 are due to reduced atmosphere-ocean CO^2 exchange as a result of meltwater discharge. This is challenged by the rapid recovery of $\delta^{13}C$ values seen in HH13-100GC immediately post MIS4. In the region of HH13-100GC mixing may have started to occur more rapidly than areas further west still suffering from iceberg calving and melting. However this isn't supported for by the return in $\delta^{13}C$ values in the shelf core PS1726 at the same time as recovery in HH13-100GC. Therefore, it is an unknown as to why $\delta^{13}C$ values were so light in the area of PS1730, while locations to the west and east saw recovery to heavier values.

6.2 Comparisons to NGRIP ice core

By the use of comparison between sediment and ice cores we can look not only at conditions within the oceans, but also the climate fluctuations above the surface (Oppo et al, 2012). In figure 34 a connection is established between Heinrich events identified in HH13-100GC, by culmination of sediment proxy data, compared with the $\delta^{18}O$ signal within the NGRIP ice core (Andersen et al, (2004).

Previous works have allowed for the ages of Heinrich events to be transposed onto the Greenland ice core record (Stein et al, 1996; Rasmussen et al, 2014). As would be expected, an a-symmetric relationship is seen between increasingly light (heavy) $\delta^{18}O$ shifts in sediment compared to a shift to heavier (lighter) values in the ice core record. This is due to the Rayleigh fractionation explained and described in chapter 1.1 sub section 4. This is a powerful tool in validating changes we see in ocean sediments to climate fluctuations and allows us to make inferences as to what was occurring on a global scale in terms of climate shifts. However, despite Heinrich events being evident in the record of NGRIP there are also evidently many more climate shifts taking place between Heinrich events with similar signatures. This is potentially the reason we see subtle signatures in the sediment record for other smaller Heinrich like events such as described in chapter 5.4 sub chapter 2. Other authors have also studied the possibility for more than the 6 main Heinrich events most prevalent during the last glacial (Rashid, 2003).

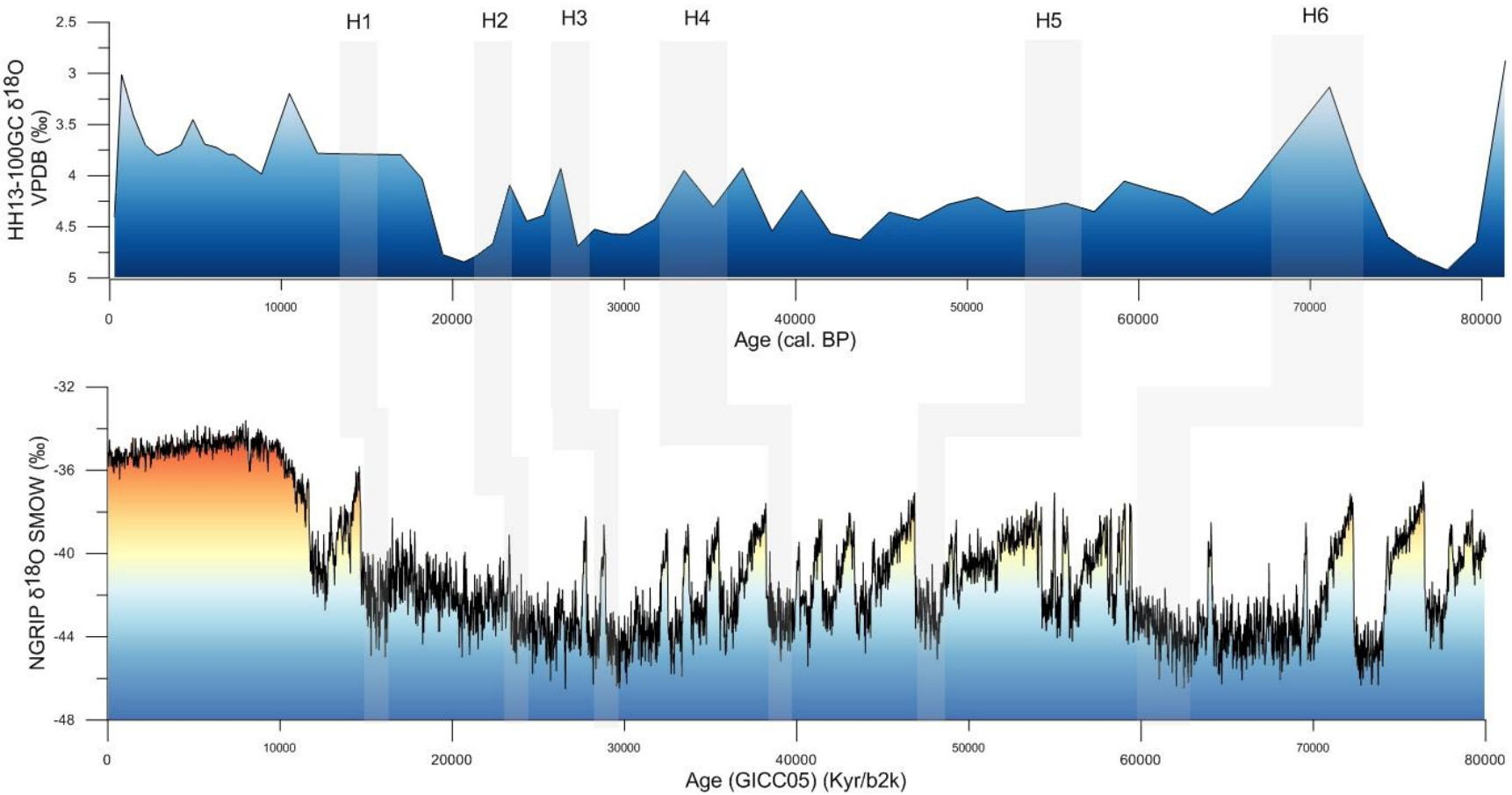

Figure 34 - (Plotted raw NGRIP data, North Greenland Core project members) A comparison between Heinrich events seen in HH13-100GC and the NGRIP $\delta^{18}O$ record. Clear shift can be seen to colder conditions during Heinrich events in the NGRIP record with a rapid recovery to warmer temperature spikes (Dansgaard Oeschger events). Correlation of Heinrich events to the NGRIP was carried out using the comparison work of Rasmussen et al, 2014.

6.3 Heinrich events during MIS 4, 3 and 2 in HH13-100GC – The bipolar see-saw?

Despite numerous investigations into the processes leading to Heinrich event occurrence, there is still controversy surrounding the topic (Marcot et al, 2011; Bassis et al, 2017). HH13-100GC can offer a significant resource of information in the quest to solve the puzzle in our understanding of these massive ice sheet collapse events.
It has been identified through foraminiferal, IRD, isotopic and grain size analysis in HH13-100GC that during Heinrich events the East Greenland Current slowed down, indicating a reduction in deep water formation and therefore reduction in flow over the Greenland-Scotland Ridge. This is an interpretation proposed in numerous studies from North Atlantic and south Nordic Sea cores (Rasmussen et al, 1996; Shackleton et al, 2000; Ezat et al, 2017; Jessen and Rasmussen, 2015).

During the stadial period MIS 6, there is an evidently reduced EGC flow indicated by sortable silt analysis in HH13-100GC. Yet ocean waters below the ice were evidently Atlantic based with temperate foraminiferal assemblage, meaning the AMOC model of push and pull highlighted by Rasmussen et al, 2016 was efficient. With a lack of overflow the pull effect (barotropic pressure gradient) was reduced meaning Atlantic waters pushed northward from the northern Atlantic into the Nordic seas pooling near the surface and creating a stratified water column (Charles et al, 1996; Broecker, 1998). This is also indicated by the heavily supressed $\delta^{13}C$ and heavy $\delta^{18}O$ values during the late part of MIS6 as seen in HH13-100GC during this time. Although the presence of high planktic fluxes (especially benthic in relation to the remaining down core HH13-100GC) suggests at least periodic ice free conditions at the surface, a theory supported by Nam et al (1995).

Heinrich events on the other hand, are characterized by preceding efficient flow of the EGC as indicated by more positive ΔSS values in HH13-100GC. This would indicate good flow over the Greenland Scotland Ridge activating the pull state of Rasmussen et al's (2016) thinking where down flow of deep water over the Greenland-Scotland Ridge southward causes Atlantic water to be pulled into the Nordic and Greenland Seas. However it is at this stage where controversy arises. Marcott et al (2011), notes a 2^0C increase in sub-surface temperatures in the North Atlantic region 1-2kyr prior to

Heinrich events. This would transpire to increased heat transport into the Nordic and Greenland seas via the North Atlantic drift, pushing the Atlantic front northward in this region (Rasmussen et al, 2016). This is seen in HH13-100GC with the occurrence of peaks in temperate planktic foraminifera forms in the few thousand years prior to Heinrich event initiation. However, with an efficient AMOC, a build-up of heat in the region seems difficult to quantify, unless factors farther afield were having on effect on the ocean heat transport system (Barker et al, 2009). This brings us to the idea of a bi-polar see-saw between northern and southern Polar Regions with regards to heat transport in the oceans (figure 35) (Seidov and Maslin, 2001; Knutti et al, 2004; Oppo et al, 2012).

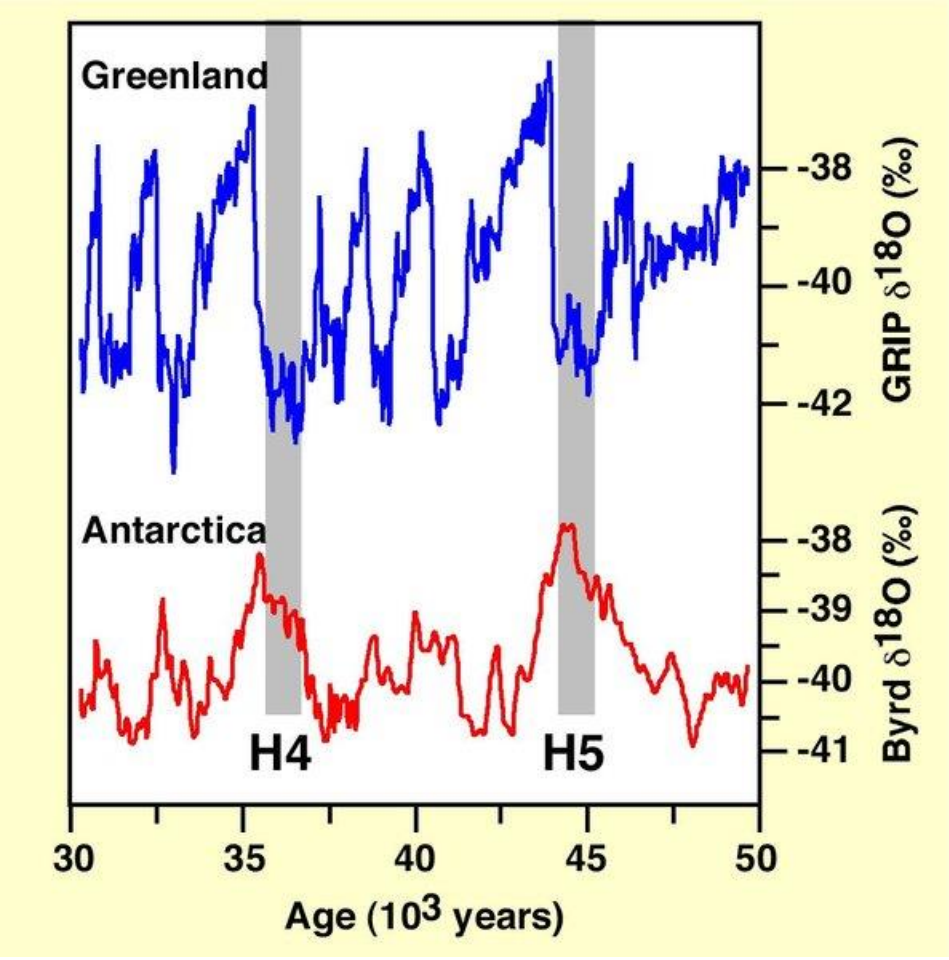

Figure 35 – (From Knutti et al, 2004) A comparison of Heinrich event morphology of the GRIP $\delta^{18}O$ record compared to that of the Byrd Antarctic core. There is clearly a shift to warmer conditions in Antarctica during periods of Heinrich event cooling in the NGRIP record.

Figure 35 shows the asymmetric nature of Antarctic and northern Greenland $\delta^{18}O$ (‰) and therefore inferred temperature fluctuations during the last glacial (Blunier et al, 1998). This asymmetry is significant as it offers clues as to the changing conditions of the thermohaline circulation prior to and during Heinrich events (Broecker, 1998; Pedro et al, 2011). Most research, centres on the major impacts of changing input of deep waters from the Arctic or Polar origins and more especially the important role of the AMOC in those changes (Stocker and Johnsen, 2003; Stouffer et al, 2006).

The theory suggests that during stadial periods in the northern Hemisphere, an efficient AMOC delivered deep water to the Atlantic which then shallowed as it moved south towards the Antarctic area. A build-up of heat developed in the Antarctic until increasing subsurface water temperatures led to freshwater input from melting ice-streams and glaicers. This in turn reduced the production of Antarctic Bottom water (AABW) leading to a positive feedback loop of continued warming in the Antarctic region causing mass collapse of ice shelves. Once ice melt exhaustion took place in Antarctica a return to Antarctic Bottom water development and lower temperatures could occur, allowing flow northward to start warming the North Atlantic region, as indicated by sub-surface temperature increases (Marcott et al, 2011). Meanwhile the increasingly warm sub-surface of the Nordic and Greenland seas would start to cause melt and freshwater influence slowing down the AMOC and promoting collapse of ice sheets in the northern Atlantic region due to halocline instabilities. A release of massive heat energy from the ocean to atmosphere likely resulted in the well know Dansgaard Oeschger warming events (Rasmussen et al, 2004; Vettoretti and Peltier, 2016). A delay in the development of Antarctic sea ice and reintroduction of AMOC efficiency post Heinrich event could possibly be the reason for such dramatic warming episodes (EPICA Community Members, 2006).

As mass ice collapse occurred during Heinrich events in the North Atlantic and polar seas, temperatures fell as indicated by a heavy shift in $\delta^{18}O$ in the NGRIP record. Meanwhile in Antarctic, in ice records such as the Byrd core, warming was inferred by lightening of $\delta^{18}O$ values (Oppo et al, 2012). This is because a reduction in North Atlantic deep water meant that less heat was transported northward from the central Atlantic increasing heat storage in the Southern Hemisphere. It must be noted that an out of

phase relationship is see in the record due to the isolation effect of Antarctica from the global circulation pattern due to the effect caused by the Circumpolar current (Stocker and Johnsen, 2003).

6.4 The wind effect

The record from HH13-100GC supports the bi-polar seesaw model but still leaves the question unanswered as to why such a rapid destabilisation of the halocline occurred to initiate Heinrich events. Something seemingly ignored by many authors is the impact of wind and the potential of Ekman transport of sub-surface warm waters onto the Greenland shelf. Ice sheets tend to be dry features with high pressure systems centred on top of them just like the modern day Greenland ice sheet (Fairbridge, 1987). With an increasing temperature of the Atlantic waters leading up to Heinrich events low pressure systems may have increased in intensity and moved with a more northerly trajectory into the Greenland region. This could result in more southerly wind events along the East Greenland Coastline resulting in Ekman transport due to the Coriolis effect of the ever increasing intermediate Atlantic waters under the ice shelves resulting in loss of buttressing and ice stream velocity increase. Polyna development would have greatly enhanced this effect close to ice shelves off the Greenland coast as is the case today in western Antarctica (Kim et al, 2017). However this is a spurious argument as we have a distinct lack of data with regards to past weather, however, it is a hypothesis applied to many of the present day marine terminating ice streams in western Antarctica (Kim et al, 2017; Thoma at el, 2008) and could have significance to Heinrich event development.

6.5 Heinrich events as an analogue to the modern day mass wasting of ice sheets

Heinrich event mass ice sheet collapses has been linked to the modern day rapid retreat of and thinning of global ice sheets (Bassis 2017). Sub surface warming as a catalyst for both Greenland's (Nick et al, 2009; Rignot et al, 2010) and Antarctic ice streams (Jacobs et al, 2011; Thoma et al, 2008) has been proposed, drawing direct comparisons to what we observe in HH13-100GC just prior to each Heinrich event during the last glacial.

Taking the example of a modern day Antarctic glacier, we can see that sub-surface warming is having a significant effect on the thinning and potential eventual collapse. Pine Island Glacier situated in the Western Antarctic ice sheet has a bedrock below sea level and has seen an increase in overall velocity of 75% since 1973 with an increasing mass loss from ~3.9 Gt/yr from 1992-1999 to ~46.0 Gt/yr by 2007. Thinning rates at the grounding line rapidly increased from ~2m/yr between 1992-2000 to 10m/yr by 2006 (Turner et al, 2017). The rapid nature of changes at PIG, and the similar changes at the neighbouring Thwaits glacier, cannot be explained by changes in force balance alone (gravitational stress v the sum of resistances) with the lack of change in the lateral extent of PIG gives further weight to this argument. This damages the binge-purge hypothesis for Heinrich formation proposed by MacAyeal (1993). Scott et al. (2009) found that rates of inland acceleration could be over 200km per decade. Such rapid rates must be due to a melting factor at the downstream end of the glacier. There is now unequivocal evidence that the warmer Circumpolar Deep Water (CDW) is flowing toward the base of the ASE glaciers via palaeo troughs (Nitsch et al, 2007; Turner et al, 2017). Anthropogenically induced warming increases the risk of more extreme climatic events such as more frequent and severe El Nino events which in turn increases the temperature of the CDW directly (Turner et al, 2017). Meanwhile variations in the position of the Amundsen Sea Low is causing greater Ekman transport of warmer subsurface waters to the base of the ice shelf intensifying melt rates and therefore surface velocities (Kim et al, 2017).

If we apply the above situation to a pre Heinrich event state one can draw very clear parallels. In HH13-100GC we saw an increase in the temperate foraminifera forms leading up to each Heinrich event. This indicates a gradually warming sub-surface as previously stated. The delivery of this warmer sub-surface water onto the Greenland shelf ice shelf foundations was likely a complex process involving Ekman transport and atmospheric controls that we cannot model at this time. An unquantified hypothesis of simple halocline destabilisation seems too simplistic if we consider the modern day situation of basally melting ice shelves.

During the last glacial, ice levels were likely much higher than they are today, with increased isostatic push down on the landmasses (Peltier, 2004). Bassis et al, 2017 uses this as an argument for a model of sub surface warming which is then cut off as isostatic uplift occurs post ice sheet collapse. This uplift raises sub surface 'pinning points' high enough to act as a barrier to warmer surface waters from accessing the ice shelf base. Several thousand year intervals between each event as seen in HH13-100GC is enough time according to uplift models from Paulson et al, 2007 to result in this isostatic change (up to 6mm a year). Although with a reduced AMOC already occurring as a result of the huge freshwater input it would appear that mixing out of the warmer sub surface waters would have occurred anyway regardless of isostasy changes. This is confirmed by more negative ΔSS values and a disappearance of temperate foraminiferal forms during the event as seen in HH13-100GC challenging Bassis et al (2017) who concentrates on the purely physical processes of isostatic change without relation to changing ocean conditions.

Chapter 7 - Summary and conclusions

The deep sea sediment core HH13-100GC constitutes a high precision record of climate and oceanographic fluctuation from the termination of the Saalian glacial to the present day. All 6 marine isotope stages were defined by use of isotopic signatures in relation to the published benthic stack of Lisiecki and Raymo (2005).

During the late Saalian, extensive sea ice cover over the region was underlain by sub-surface warm Atlantic waters as indicated by the heavy presence of *T.quinqueloba.* The negative ΔSS values indicate that the EGC and therefore the AMOC was significantly reduced during this time. Heavy $\delta^{18}O$ values are testament to the lack of meltwater and prevalence of significant land based ice levels during this time.

Marine isotope stage 5's sub stages are all represented well in HH13-100GC, especially the last interglacial (Eemian 5e) indicated by significantly light $\delta^{18}O$ values and a very dark band in the XRF imagery at this depth interval separating the light glacial sediments from the darker colours of the remaining down core sections. Major meltwater is also indicated for sub stage 5a, more so than is seen in other core sections in the region, likely a result of more the more distal nature of this core than others closer to Greenland.

Marine isotope stage 4 is dominated by a cooling period with heavier $\delta^{18}O$ values interrupted by a major meltwater injection, interpreted as Heinrich event 6. This sets the stage for a sequence of 5 more Heinrich events during marine isotope stages 3 and 2 until ceasing post Younger Dryas and start of the Holocene. Heinrich events 6, 4, 3 and 2 are well represented in the isotopic record with clear shifts to lighter $\delta^{18}O$ and $\delta^{13}C$ indicating high meltwater rates and a drop in productivity. While Heinrich events 5 and 2 are not well represented in the isotopic record but can be identified by anomalously high IRD spikes and reductions in the EGC as interpreted from ΔSS value falls. Falls in the %*N.pachyderma* and increases in the %*T.quinqueloba* and or *N.incompta* just prior to all interpreted Heinrich events has been suggested here as evidence for influx of warmer subsurface water just prior to Heinrich events which is the likely reason for basal ice melt and eventual ice sheet collapse. One aspect of interest in interpretation of

individual Heinrich events in HH13-100GC was the lithological component change of each event. It appears that source regions for iceberg rafted material were not synchronous over each event. Instead a clear distinction was found between them, for example, the H2 layer contained abundant coloured sedimentary grains, while H6 was dominated by dolomite based material.

The Holocene transition then took place around 11,000 (cal. BP), post Younger Dryas with a shift to more abundant temperate foraminifera forms, increased productivity and continual ice rafting of material to the sea floor caused by an increase in temperature indicated by light $\delta^{18}O$ values and elevated IRD counts.

Analogues have been made to present day ice sheet collapse, especially in the Antarctic region, with regards to Heinrich event development. Currently, mass ice loss and thinning of glaciers is occurring in both Greenland and Western Antarctica in response to sub surface warming of the basal ice shelf/ glacier terminus regions. The same characteristics are identified just prior to Heinrich events of the last glacial as seen in HH13-100GC, indicating a possible Heinrich style event, albeit on a lesser scale, for the present day ice sheets. Increased warming of the oceans by anthropogenic forcing will only serve to increase the risk of greater subsurface melting beneath marine terminating glaciers in the future, resulting in a Heinrich event style demise.

References

Alley, R.B. and Ágústsdóttir, A.M., 2005. The 8k event: cause and consequences of a major Holocene abrupt climate change. *Quaternary Science Reviews*, *24*(10), pp.1123-1149.

Alley, R.B., Andrews, J.T., Brigham-Grette, J., Clarke, G.K.C., Cuffey, K.M., Fitzpatrick, J.J., Funder, S., Marshall, S.J., Miller, G.H., Mitrovica, J.X. and Muhs, D.R., 2010. History of the Greenland Ice Sheet: paleoclimatic insights. *Quaternary Science Reviews*, *29*(15), pp.1728-1756.

Alley, R.B., Andrews, J.T., Brigham-Grette, J., Clarke, G.K.C., Cuffey, K.M., Fitzpatrick, J.J., Funder, S., Marshall, S.J., Miller, G.H., Mitrovica, J.X. and Muhs, D.R., 2010. History of the Greenland Ice Sheet: paleoclimatic insights. *Quaternary Science Reviews*, *29*(15), pp.1728-1756.

Andersen, K.K., Azuma, N., Barnola, J.M., Bigler, M., Biscaye, P., Caillon, N., Chappellaz, J., Clausen, H.B., Dahl-Jensen, D., Fischer, H. and Flückiger, J., 2004. High-resolution record of Northern Hemisphere climate extending into the last interglacial period. *Nature*, *431*(7005), pp.147-151.

Andrews, J.T. and Dunhill, G., 2004. Early to mid-Holocene Atlantic water influx and deglacial meltwater events, Beaufort Sea slope, Arctic Ocean. *Quaternary Research*, *61*(1), pp.14-21.

Anker Pedersen, R., Thejll, P., Mottram, R., Davies, S. and Lamb, H., 2016, April. Can an Earth System Model Reproduce the Palaeo-Climate Proxy Record in eastern Africa during the Eemian?. In *EGU General Assembly Conference Abstracts* (Vol. 18, p. 15088).

Bagniewski, W., Meissner, K.J. and Menviel, L., 2017. Exploring the oxygen isotope fingerprint of Dansgaard-Oeschger variability and Heinrich events. *Quaternary Science Reviews*, *159*, pp.1-14.

Bamber, J., den Broeke, M., Ettema, J., Lenaerts, J. and Rignot, E., 2012. Recent large increases in freshwater fluxes from Greenland into the North Atlantic. *Geophysical Research Letters*, *39*(19).

Barbante, C., Barnola, J.M., Becagli, S., Beer, J., Bigler, M., Boutron, C., Blunier, T., Castellano, E., Cattani, O., Chappellaz, J. and Dahl-Jensen, D., 2006. One-to-one coupling of glacial climate variability in Greenland and Antarctica. *Nature*, *444*(7116), pp.195-198.

Barker, S., Chen, J., Gong, X., Jonkers, L., Knorr, G. and Thornalley, D., 2015. Icebergs not the trigger for North Atlantic cold events. *Nature*, *520*(7547), pp.333-336.

Bassis, J.N., Petersen, S.V. and Mac Cathles, L., 2017. Heinrich events triggered by ocean forcing and modulated by isostatic adjustment. *Nature*, *542*(7641), pp.332-334.

Bauch, H.A., 1994. Significance of variability in Turborotalita quinqueloba (Natland) test size and abundance for paleoceanographic interpretations in the Norwegian-Greenland Sea. *Marine Geology*, *121*(1-2), pp.129-141.

BBC news. (2007). *Neogloboquadrina pachyderma.* Available: http://scienceblogs.com/grrlscientist/2007/05/06/neoloboquadrina-pachyderma/. Last accessed 14/05/2017.
Berger, A. and Loutre, M.F., 2002. An exceptionally long interglacial ahead?. *Science*, *297*(5585), pp.1287-1288.

Berger, A., 1978. Long-term variations of daily insolation and Quaternary climatic changes. *Journal of the Atmospheric Sciences*, *35*(12), pp.2362-2367.

Blunier, T., Chappellaz, J., Schwander, J., Dällenbach, A., Stauffer, B., Stocker, T.F., Raynaud, D., Jouzel, J., Clausen, H.L., Hammer, C.U. and Johnsen, S.J., 1998. Asynchrony of Antarctic and Greenland climate change during the last glacial period. *Nature*, *394*(6695), pp.739-743.

Bond, G., Broecker, W., Johnsen, S., McManus, J., Labeyrie, L., Jouzel, J. and Bonani, G., 1993. Correlations between climate records from North Atlantic sediments and Greenland ice. *Nature*, *365*(6442), pp.143-147.

Bond, G., Kromer, B., Beer, J., Muscheler, R., Evans, M.N., Showers, W., Hoffmann, S., Lotti-Bond, R., Hajdas, I. and Bonani, G., 2001. Persistent solar influence on North Atlantic climate during the Holocene. *Science*, *294*(5549), pp.2130-2136.

Bond, G., Showers, W., Cheseby, M., Lotti, R., Almasi, P., Priore, P., Cullen, H., Hajdas, I. and Bonani, G., 1997. A pervasive millennial-scale cycle in North Atlantic Holocene and glacial climates. *science*, *278*(5341), pp.1257-1266.

Bond, G.C., Showers, W., Elliot, M., Evans, M., Lotti, R., Hajdas, I., Bonani, G. and Johnson, S., 1999. The North Atlantic's 1-2 Kyr Climate Rhythm: Relation to Heinrich Events, Dansgaard/Oeschger Cycles and the Little Ice Age. *Mechanisms of global climate change at millennial time scales*, pp.35-58.

Brock, J.C., McClain, C.R., Anderson, D.M., Prell, W.L. and Hay, W.W., 1992. Southwest monsoon circulation and environments of recent planktonic foraminifera in the northwestern Arabian Sea. *Paleoceanography*, *7*(6), pp.799-813.

Broecker, W., Bond, G., Klas, M., Clark, E. and McManus, J., 1992. Origin of the northern Atlantic's Heinrich events. *Climate Dynamics*, *6*(3-4), pp.265-273.

Carstens, J. and Wefer, G., 1992. Recent distribution of planktonic foraminifera in the Nansen Basin, Arctic Ocean. *Deep Sea Research Part A. Oceanographic Research Papers*, *39*(2), pp.S507-S524.

Carstens, J., Hebbeln, D. and Wefer, G., 1997. Distribution of planktic foraminifera at the ice margin in the Arctic (Fram Strait). *Marine Micropaleontology*, *29*(3-4), pp.257-269.

Charles, C.D., Lynch-Stieglitz, J., Ninnemann, U.S. and Fairbanks, R.G., 1996. Climate connections between the hemisphere revealed by deep sea sediment core/ice core correlations. *Earth and Planetary Science Letters*, *142*(1-2), pp.19-27.

Coplen, T.B., 1996. New guidelines for reporting stable hydrogen, carbon, and oxygen isotope-ratio data. *Geochimica et Cosmochimica Acta*, *60*(17), pp.3359-3360.

Crucifix, M. and Loutre, F.M., 2002. Transient simulations over the last interglacial period (126-115 kyr BP): feedback and forcing analysis. *Climate Dynamics*, *19*(5), pp.417-433.

Crutzen, P.J., 2006. The "anthropocene". In *Earth system science in the anthropocene*. Springer Berlin Heidelberg. (pp. 13-18)

Cuffey, K.M. and Marshall, S.J., 2000. Substantial contribution to sea-level rise during the last interglacial from the Greenland ice sheet. *Nature*, *404*(6778), pp.591-594.

Dansgaard, W., Johnsen, S.J., Clausen, H.B., Hvidberg, C.S. and Steffensen, J.P., 1993. Evidence for general instability of past climate from a 250-kyr. *Nature*, *364*, p.15.
Dearing, J., 1999. Magnetic susceptibility. *Environmental magnetism: A practical guide*, *6*, pp.35-62.

Denton, G.H., Alley, R.B., Comer, G.C. and Broecker, W.S., 2005. The role of seasonality in abrupt climate change. *Quaternary Science Reviews*, *24*(10), pp.1159-1182.

Duprat, J., Pujol, C. and Labeyrie, L.D., 1996. SIMMAX: A modern analog technique to deduce Atlantic sea surface temperatures from planktonic foraminifera in deep-sea sediments. *Paleoceanography*, *11*(1), pp.15-35.

Epstein, S. and Mayeda, T., 1953. Variation of O18 content of waters from natural sources. *Geochimica et cosmochimica acta*, *4*(5), pp.213-224.

Epstein, S. and Mayeda, T.K., 1953. Variations of the 18O/16O ratio in natural waters. *Geochim. Cosmochim. Acta*, *4*(213), pp.1702-1703.

Ezat, M.M., Rasmussen, T.L., Thornalley, D.J., Olsen, J., Skinner, L.C., Hönisch, B. and Groeneveld, J., 2017. Ventilation history of Nordic Seas overflows during the last (de) glacial period revealed by species-specific benthic foraminiferal 14C dates. *Paleoceanography*, *32*(2), pp.172-181.

Fairbanks, R.G., 1989. A 17, 000-year glacio-eustatic sea level record: influence of glacial melting rates on the Younger Dryas event and deep-ocean circulation. *Nature*, *342*(6250), pp.637-642.

Fairbridge, R.W., 1987. GLACIAL ANTICYCLONE THEORYGlacial anticyclone theory. In *Climatology*. Springer US. (pp. 463-463)

Fronval, T. and Jansen, E., 1996. Rapid changes in ocean circulation and heat flux in the Nordic seas during the last interglacial period. *Nature*, *383*(6603), p.806.

Funder, S., Hjort, C., Landvik, J.Y., Nam, S.I., Reeh, N. and Stein, R., 1998. History of a stable ice margin—East Greenland during the middle and upper Pleistocene. *Quaternary Science Reviews*, *17*(1-3), pp.77-123.
Geosystems, *8*(10).

Gornitz, V., 2012. Glacial Isostasy, Sea Level and Mantle Rheology edited by R. Sabadini, K. Lambert, and E. Boschi. *Journal of Coastal Research*, *10*(2).

Hass, H.C., 2002. A method to reduce the influence of ice-rafted debris on a grain size record from northern Fram Strait, Arctic Ocean. *Polar research*, *21*(2), pp.299-306.

Hebbeln, D. and Wefer, G., 1997. Late Quaternary paleoceanography in the Fram Strait. *Paleoceanography*, *12*(1), pp.65-78.

Hebbeln, D., Dokken, T., Andersen, E.S., Hald, M. and Elverhøi, A., 1994. Moisture supply for northern ice-sheet growth during the Last Glacial Maximum.

Heinrich, H., 1988. Origin and consequences of cyclic ice rafting in the northeast Atlantic Ocean during the past 130,000 years. *Quaternary research*, *29*(2), pp.142-152.

Hemleben, C., Spindler, M., & Anderson, O. R. (1989). *Modern planktonic foraminifera* New York: Springer. (p. 363).

Hemming, S.R., 2004. Heinrich events: Massive late Pleistocene detritus layers of the North Atlantic and their global climate imprint. *Reviews of Geophysics*, *42*(1).

Henderson, G.M., 2002. New oceanic proxies for paleoclimate. *Earth and Planetary Science Letters*, *203*(1), pp.1-13.

Henriksen, N., Higgins, A.K., Gilotti, J.A. and Smith, M.P., 2008. Introduction—The Caledonides of Greenland. *Geological Society of America Memoirs*, *202*, pp.v-xv.

Jacobs, S.S., Jenkins, A., Giulivi, C.F. and Dutrieux, P., 2011. Stronger ocean circulation and increased melting under Pine Island Glacier ice shelf. *Nature Geoscience*, *4*(8), pp.519-523.

Jansen, E., Overpeck, J., Briffa, K.R., Duplessy, J.C., Joos, F., Masson-Delmotte, V., Olago, D., Otto-Bliesner, B., Peltier, W.R., Rahmstorf, S. and Ramesh, R., 2007. Paleoclimate. *Climate Change 2007: The Physical Science Basis. Working Contribution of Working Group I to the Fourth Assessment Report of the Intergovernmental Panel on Climate Change*.

Jessen, S.P. and Rasmussen, T.L., 2015. Sortable silt cycles in Svalbard slope sediments 74–0 ka. *Journal of Quaternary Science*, *30*(8), pp.743-753.

Johannessen, T., Jansen, E., Flatøy, A. and Ravelo, A.C., 1994. The relationship between surface water masses, oceanographic fronts and paleoclimatic proxies in surface sediments of the Greenland, Iceland, Norwegian Seas. In *Carbon cycling in the glacial ocean: constraints on the ocean's role in global change*. Springer Berlin Heidelberg. (pp. 61-85)
John g. (2010). *Eemian orbital forcing.* Available:

http://brightstarswildomar.blogspot.no/2010/09/eemian-orbital-forcing.html. Last accessed 14/05/2017.

K. Kris Hurst. (2017). *Marine Isotope Stages (MIS) - Tracing the Climate of Our World .* Available: https://www.thoughtco.com/marine-isotope-stages-climate-world-171568. Last accessed 14/05/2017.

Katz, M.E., Cramer, B.S., Franzese, A., Hönisch, B., Miller, K.G., Rosenthal, Y. and Wright, J.D., 2010. Traditional and emerging geochemical proxies in foraminifera. *Journal of Foraminiferal Research*, *40*(2), pp.165-192.

Kennett, J.P. and Srinivasan, M.S., 1983. *Neogene planktonic foraminifera: a phylogenetic atlas*. Hutchinson Ross.

Kim, T.W., Ha, H.K., Wåhlin, A.K., Lee, S.H., Kim, C.S., Lee, J.H. and Cho, Y.K., 2017. Is Ekman pumping responsible for the seasonal variation of warm circumpolar deep water in the Amundsen Sea?. *Continental Shelf Research*, *132*, pp.38-48.

Kissel, C., Mazaud, A., Channell, J.E. and Beer, J., 2000. North Atlantic palaeointensity stack since 75ka (NAPIS–75) and the duration of the Laschamp event. *Philosophical Transactions of the Royal Society of London A: Mathematical, Physical and Engineering Sciences*, *358*(1768), pp.1009-1025.

Knutti, R., Flückiger, J., Stocker, T.F. and Timmermann, A., 2004. Strong hemispheric coupling of glacial climate through freshwater discharge and ocean circulation. *Nature*, *430*(7002), pp.851-856.

Kopp, R.E., Simons, F.J., Mitrovica, J.X., Maloof, A.C. and Oppenheimer, M., 2009. Probabilistic assessment of sea level during the last interglacial stage. *Nature*, *462*(7275), pp.863-867.

Kucera, M. and Darling, K.F., 2002. Cryptic species of planktonic foraminifera: their effect on palaeoceanographic reconstructions. *Philosophical Transactions of the Royal Society of London A: Mathematical, Physical and Engineering Sciences*, *360*(1793), pp.695-718.

Kucera, M., 2007. Chapter six planktonic foraminifera as tracers of past oceanic environments. *Developments in marine geology*, *1*, pp.213-262.

Kucera, M., Weinelt, M., Kiefer, T., Pflaumann, U., Hayes, A., Weinelt, M., Chen, M.T., Mix, A.C., Barrows, T.T., Cortijo, E. and Duprat, J., 2005. Reconstruction of sea-surface temperatures from assemblages of planktonic foraminifera: multi-technique approach based

on geographically constrained calibration data sets and its application to glacial Atlantic and Pacific Oceans. *Quaternary Science Reviews*, *24*(7), pp.951-998.

Lisiecki, L.E. and Raymo, M.E., 2005. A Pliocene-Pleistocene stack of 57 globally distributed benthic δ18O records. *Paleoceanography*, *20*(1).

Lohmann, G., Schneider, R., Jungclaus, J.H., Leduc, G., Fischer, N., Pfeiffer, M. and Laepple, T., 2015. Evaluation of Eemian and Holocene Climate Trends: Combining Marine Archives with Climate Modelling. In *Integrated Analysis of Interglacial Climate Dynamics (INTERDYNAMIC)*. Springer International Publishing. (pp. 31-35)

Lopes, R.P., Kinoshita, A., Baffa, O., Figueiredo, A.M.G., Dillenburg, S.R., Schultz, C.L. and Pereira, J.C., 2014. ESR dating of Pleistocene mammals and marine shells from the coastal plain of Rio Grande do Sul state, southern Brazil. *Quaternary International*, *352*, pp.124-134.

Lowe, J.J. and Walker, M.J., 2014. *Reconstructing quaternary environments*. Routledge.
MacAyeal, D.R., 1993. Binge/purge oscillations of the Laurentide ice sheet as a cause of the North Atlantic's Heinrich events. *Paleoceanography*, *8*(6), pp.775-784.

Mangerud, J.A.N., Dokken, T., Hebbeln, D., Heggen, B., Ingolfsson, O., Landvik, J.Y., Mejdahl, V., Svendsen, J.I. and Vorren, T.O., 1998. Fluctuations of the Svalbard–Barents Sea Ice Sheet during the last 150 000 years. *Quaternary Science Reviews*, *17*(1), pp.11-42.

Marcott, S.A., Clark, P.U., Padman, L., Klinkhammer, G.P., Springer, S.R., Liu, Z., Otto-Bliesner, B.L., Carlson, A.E., Ungerer, A., Padman, J. and He, F., 2011. Ice-shelf collapse from subsurface warming as a trigger for Heinrich events. *Proceedings of the National Academy of Sciences*, *108*(33), pp.13415-13419.

McCave, I.N., 2008. Size sorting during transport and deposition of fine sediments: sortable silt and flow speed. *Developments in Sedimentology*, *60*, pp.121-142.
McIntyre, A. and Ruddiman, W.F., 1972. Northeast Atlantic post-Eemian paleooceanography: a predictive analog of the future. *Quaternary Research*, *2*(3), pp.350-354.

Menviel, L., Yu, J., Joos, F., Mouchet, A., Meissner, K.J. and England, M.H., 2016. Poorly ventilated deep ocean at the Last Glacial Maximum inferred from carbon isotopes: A data-model comparison study. *Paleoceanography*.

Morey, A.E., Mix, A.C. and Pisias, N.G., 2005. Planktonic foraminiferal assemblages preserved in surface sediments correspond to multiple environment variables. *Quaternary Science Reviews*, *24*(7), pp.925-950.

Moros, M., Lemke, W., Kuijpers, A., Endler, R., Jensen, J.B., Bennike, O. and Gingele, F., 2002. Regressions and transgressions of the Baltic basin reflected by a new high-resolution deglacial and postglacial lithostratigraphy for Arkona Basin sediments (western Baltic Sea). *Boreas*, *31*(2), pp.151-162.

Muhs, D.R., 2002. Evidence for the timing and duration of the last interglacial period from high-precision uranium-series ages of corals on tectonically stable coastlines. *Quaternary Research*, *58*(1), pp.36-40.

Nam, S.I., Stein, R., Grobe, H. and Hubberten, H., 1995. Late Quaternary glacial-interglacial changes in sediment composition at the East Greenland continental margin and their paleoceanographic implications. *Marine Geology*, *122*(3), pp.243-262.

NASA. (2017). *Rapid response satellite imagery.* Available: https://earthdata.nasa.gov/earth-observation-data/near-real-time/rapid-response. Last accessed 14/05/2017.

Nick, F.M., Vieli, A., Howat, I.M. and Joughin, I., 2009. Large-scale changes in Greenland outlet glacier dynamics triggered at the terminus. *Nature Geoscience*, *2*(2), pp.110-114.

Nitsche, F.O. Jacobs, S.S. Larter, R.D. Gohl, K. (2007). Bathymetry of the Amundsen Sea continental shelf: implications for geology, oceanography, and glaciology. *Geochemistry, Geophysics,*

North Greenland Ice Core Project members, 2004. North Greenland ice core project oxygen isotope data. *IGBP PAGES/World Data Center for Paleoclimatology Data Contribution Series*, *59*.

Oppo, D.W., McManus, J.F. and Cullen, J.L., 2006. Evolution and demise of the Last Interglacial warmth in the subpolar North Atlantic. *Quaternary Science Reviews*, *25*(23), pp.3268-3277.

ORHEIM, O., 1993. GLACIERS OF EUROPE-GLACIERS OF JAN MA YEN, NORWAY. *US Geological Survey Professional Paper*, p.153.

Paulson, A., Zhong, S. and Wahr, J., 2007. Inference of mantle viscosity from GRACE and relative sea level data. *Geophysical Journal International*, *171*(2), pp.497-508.

Pedro, J.B., Rasmussen, S.O., van Ommen, T.D., Morgan, V.I., Chappellaz, J., Moy, A.D., Masson-Delmotte, V. and Delmotte, M., 2011. The last deglaciation: timing the bipolar seesaw. *Climate of the Past*, *7*.

Peltier, W.R., 2004. Global glacial isostasy and the surface of the ice-age Earth: the ICE-5G (VM2) model and GRACE. *Annu. Rev. Earth Planet. Sci.*, *32*, pp.111-149.

Pfleger, F.B. 1948. Foraminifera of a submarine core from the Caribbean Sea Göteborgs Kungliga Vetenskaps-och Vitterhets-samhälles Handlingar, 6B, 5 pp. 3–9

Piasecki, S.T.E.F.A.N., 1984. Preliminary palynostratigraphy of the Permian–Lower Triassic sediments in Jameson Land and Scoresby Land, East Greenland. *Bulletin of the Geological Society of Denmark*, *32*, pp.139-144.

Praetorius, S., Mix, A., Jensen, B., Froese, D., Milne, G., Wolhowe, M., Addison, J. and Prahl, F., 2016. Interaction between climate, volcanism, and isostatic rebound in Southeast Alaska during the last deglaciation. *Earth and Planetary Science Letters*, *452*, pp.79-89.

Railsback, L.B., Gibbard, P.L., Head, M.J., Voarintsoa, N.R.G. and Toucanne, S., 2015. An optimized scheme of lettered marine isotope substages for the last 1.0 million years, and the climatostratigraphic nature of isotope stages and substages. *Quaternary Science Reviews*, *111*, pp.94-106.

Rasmussen, T.L. and Thomsen, E., 2004. The role of the North Atlantic Drift in the millennial timescale glacial climate fluctuations. *Palaeogeography, Palaeoclimatology, Palaeoecology*, *210*(1), pp.101-116.

Rasmussen, T.L., Thomsen, E. and Moros, M., 2016. North Atlantic warming during Dansgaard-Oeschger events synchronous with Antarctic warming and out-of-phase with Greenland climate. *Scientific reports*, *6*.

Rasmussen, T.L., Thomsen, E., Skirbekk, K., Ślubowska-Woldengen, M., Kristensen, D.K. and Koç, N., 2014. Spatial and temporal distribution of Holocene temperature maxima in the northern Nordic seas: interplay of Atlantic-, Arctic-and polar water masses. *Quaternary Science Reviews*, *92*, pp.280-291.

Rasmussen, T.L., Thomsen, E., Ślubowska, M.A., Jessen, S., Solheim, A. and Koç, N., 2007. Paleoceanographic evolution of the SW Svalbard margin (76 N) since 20,000 14 C yr BP. *Quaternary Research*, *67*(1), pp.100-114.

Rasmussen, T.L., Thomsen, E., Weering, T.C. and Labeyrie, L., 1996. Rapid changes in surface and deep water conditions at the Faeroe Margin during the last 58,000 years. *Paleoceanography*, *11*(6), pp.757-771.

Reimer, P.J., Baillie, M.G., Bard, E., Bayliss, A., Beck, J.W., Blackwell, P.G., Ramsey, C.B., Buck, C.E., Burr, G.S., Edwards, R.L. and Friedrich, M., 2009. IntCal09 and Marine09 radiocarbon age calibration curves, 0–50,000 years cal BP. *Radiocarbon*, *51*(04), pp.1111-1150.

Reimer, P.J., Bard, E., Bayliss, A., Beck, J.W., Blackwell, P.G., Ramsey, C.B., Buck, C.E., Cheng, H., Edwards, R.L., Friedrich, M. and Grootes, P.M., 2013. IntCal13 and Marine13 radiocarbon age calibration curves 0–50,000 years cal BP. *Radiocarbon*, *55*(4), pp.1869-1887.

Rignot, E. and Kanagaratnam, P., 2006. Changes in the velocity structure of the Greenland Ice Sheet. *Science*, *311*(5763), pp.986-990.

Rignot, E., Koppes, M. and Velicogna, I., 2010. Rapid submarine melting of the calving faces of West Greenland glaciers. *Nature Geoscience*, *3*(3), pp.187-191.

Robinson, S.G., Maslin, M.A. and McCave, I.N., 1995. Magnetic susceptibility variations in Upper Pleistocene deep-sea sediments of the NE Atlantic: Implications for ice rafting and paleocirculation at the last glacial maximum. *Paleoceanography*, *10*(2), pp.221-250.

Rozanski, K., Araguás-Araguás, L. and Gonfiantini, R., 1993. Isotopic patterns in modern global precipitation. *Climate change in continental isotopic records*, pp.1-36.

Rudels, B., 2012. Arctic Ocean circulation and variability-advection and external forcing encounter constraints and local processes. *Ocean Science*, *8*(2), p.261.

Ryan, W.B.F., S.M. Carbotte, J.O. Coplan, S. O'Hara, A. Melkonian, R. Arko, R.A. Weissel, V. Ferrini, A. Goodwillie, F. Nitsche, J. Bonczkowski, and R. Zemsky (2009), Global Multi-Resolution Topography synthesis, Geochem. Geophys. Geosyst., 10, Q03014, doi:10.1029/2008GC002332. http://www.geomapapp.org

Schiebel, R. Hemleben C., Extant planktic foraminifera: A brief review, Paläontogische Zeitschrift, 79 (2005), pp. 135–148

Schmidt, D.N., Renaud, S., Bollmann, J., Schiebel, R. and Thierstein, H.R., 2004. Size distribution of Holocene planktic foraminifer assemblages: biogeography, ecology and adaptation. *Marine Micropaleontology*, *50*(3), pp.319-338.

Scott, J. Gudmundsson, H. Smith, A. Bingham, R. Pritchard, H. Vaughan, D. (2009). Increased rate of acceleration on Pine Island Glacier strongly coupled to changes in gravitational driving stress. *The Cryosphere*, *3*, 125-131.

Seidov, D. and Maslin, M., 2001. Atlantic ocean heat piracy and the bipolar climate see-saw during Heinrich and Dansgaard–Oeschger events. *Journal of Quaternary Science*, *16*(4), pp.321-328.

Shackleton, N.J. and Opdyke, N.D., 1973. Oxygen isotope and palaeomagnetic stratigraphy of Equatorial Pacific core V28-238: Oxygen isotope temperatures and ice volumes on a 105 year and 106 year scale. *Quaternary research*, *3*(1), pp.39-55.

Shackleton, N.J., 1969. The last interglacial in the marine and terrestrial records. *Proceedings of the Royal Society of London B: Biological Sciences*, *174*(1034), pp.135-154.

Shackleton, N.J., 2000. The 100,000-year ice-age cycle identified and found to lag temperature, carbon dioxide, and orbital eccentricity. *Science*, *289*(5486), pp.1897-1902.

Shackleton, N.J., Lamb, H.H., Worssam, B.C., Hodgson, J.M., Lord, A.R., Shotton, F.W., Schove, D.J. and Cooper, L.H.N., 1977. The oxygen isotope stratigraphic record of the late pleistocene [and discussion]. *Philosophical Transactions of the Royal Society of London B: Biological Sciences*, *280*(972), pp.169-182.

Sigman, D.M. and Boyle, E.A., 2000. Glacial/interglacial variations in atmospheric carbon dioxide. *Nature*, *407*(6806), pp.859-869.

Simstich, J., Sarnthein, M. and Erlenkeuser, H., 2003. Paired δ 18 O signals of Neogloboquadrina pachyderma (s) and Turborotalita quinqueloba show thermal stratification structure in Nordic Seas. *Marine Micropaleontology*, *48*(1), pp.107-125.

Spielhagen, R.F. and Erlenkeuser, H., 1994. Stable oxygen and carbon isotopes in planktic foraminifers from Arctic Ocean surface sediments: Reflection of the low salinity surface water layer. *Marine Geology*, *119*(3-4), pp.227-250.

Stein, R., Nam, S.I., Grobe, H. and Hubberten, H., 1996. Late Quaternary glacial history and short-term ice-rafted debris fluctuations along the East Greenland continental margin. *Geological Society, London, Special Publications*, *111*(1), pp.135-151.

Stenni, B., Buiron, D., Frezzotti, M., Albani, S., Barbante, C., Bard, E., Barnola, J.M., Baroni, M., Baumgartner, M., Bonazza, M. and Capron, E., 2011. Expression of the bipolar see-saw in Antarctic climate records during the last deglaciation. *Nature Geoscience*, *4*(1), pp.46-49.

Stocker, T.F. and Johnsen, S.J., 2003. A minimum thermodynamic model for the bipolar seesaw. *Paleoceanography*, *18*(4).

Stoner, J.S., Channell, J.E.T. and Hillaire-Marcel, C., 1995. Late Pleistocene relative geomagnetic paleointensity from the deep Labrador Sea: Regional and global correlations. *Earth and Planetary Science Letters*, *134*(3-4), pp.237-252.

Stouffer, R.J., Yin, J., Gregory, J.M., Dixon, K.W., Spelman, M.J., Hurlin, W., Weaver, A.J., Eby, M., Flato, G.M., Hasumi, H. and Hu, A., 2006. Investigating the causes of the response of the thermohaline circulation to past and future climate changes. *Journal of Climate*, *19*(8), pp.1365-1387.

Stuiver, M. and Reimer, P.J., 1993. Extended 14 C data base and revised CALIB 3.0 14 C age calibration program. *Radiocarbon*, *35*(01), pp.215-230.

Toscano, M.A. and Lundberg, J., 1999. Submerged Late Pleistocene reefs on the tectonically-stable SE Florida margin: high-precision geochronology, stratigraphy, resolution of Substage 5a sea-level elevation, and orbital forcing. *Quaternary Science Reviews*, *18*(6), pp.753-767.

Tschumi, T., Joos, F., Gehlen, M. and Heinze, C., 2011. Deep ocean ventilation, carbon isotopes, marine sedimentation and the deglacial CO2 rise. *Climate of the Past*, *7*(3), pp.771-800.

Turner, J., Orr, A., Gudmundsson, G.H., Jenkins, A., Bingham, R.G., Hillenbrand, C.D. and Bracegirdle, T.J., 2017. Atmosphere-ocean-ice interactions in the Amundsen Sea Embayment, West Antarctica. *Reviews of Geophysics*.

Unknown. *Neogloboquadrina pachyderma.* Available: https://taxonomic.aad.gov.au/keys/incertae/key/Incertae%20Sedis/Media/Html/Neogloboquadrina_pachyderma.htm. Last accessed 14/05/2017.

Van de Berg, W.J., Van Den Broeke, M., Ettema, J., Van Meijgaard, E. and Kaspar, F., 2011. Significant contribution of insolation to Eemian melting of the Greenland ice sheet. *Nature Geoscience*, *4*(10), pp.679-683.

Van der Plicht, J., Van Geel, B., Bohncke, S.J.P., Bos, J.A.A., Blaauw, M., Speranza, A.O.M., Muscheler, R. and Björck, S., 2004. The Preboreal climate reversal and a subsequent solar-forced climate shift. *Journal of Quaternary Science*, *19*(3), pp.263-269.

Vanneste, K., Uenzelmann-Neben, G. and Miller, H., 1995. Seismic evidence for long-term history of glaciation on central East Greenland shelf south of Scoresby Sund. *Geo-Marine Letters*, *15*(2), pp.63-70.

Vettoretti, G. and Peltier, W.R., 2013. Last Glacial Maximum ice sheet impacts on North Atlantic climate variability: The importance of the sea ice lid. *Geophysical Research Letters*, *40*(24), pp.6378-6383.

Watson, A.J. and Naveira Garabato, A.C., 2006. The role of Southern Ocean mixing and upwelling in glacial-interglacial atmospheric CO2 change. *Tellus B*, *58*(1), pp.73-87.

Wignall, P.B. and Twitchett, R.J., 2002. Permian–Triassic sedimentology of Jameson Land, East Greenland: incised submarine channels in an anoxic basin. *Journal of the Geological Society*, *159*(6), pp.691-703.